DISS. ETH N° 19769

A Novel Mouse Model of Demyelination

A dissertation submitted to

ETH ZURICH

for the degree of

Doctor of Sciences

presented by

HARTMUT BERND FREDERIK POHL

Dipl. Natw. ETH Zurich, Switzerland

born 08.12.1977 in Aachen, Germany

citizen of Germany

accepted on the recommendation of

Prof. Dr. Ueli Suter (examiner)

Prof. Dr. Markus Rudin (co-examiner)

2011

Table of contents

Thesis outline and objectives

Adult-onset demyelinating diseases of the central nervous system such as multiple sclerosis represent the most common neurological disorders in young adults, and are of high impact, both for the individual as well as for society. Loss of oligodendrocytes is a main feature of these diseases. Despite substantial research aiming to dissect the underlying pathogenesis, our understanding of the mechanisms involved in demyelination, subsequent damage and recovery are incomplete. This is especially the case for the complex inflammatory demyelination characteristic of multiple sclerosis, hampering our efforts to successfully treat the diseases. An overview on myelinating glia, their interaction with axons and the consequences of impairment in this interplay following demyelination as well as repair mechanisms is provided in the introduction, together with an additional outline on currently available research models. The goal of this thesis was to facilitate investigations of disease processes in demyelinating diseases and their possible alterations by providing a novel mouse model system that allows investigation of events following primary ablation of adult myelinating glia. The experimental procedures used, the mouse model based on genetically induced cell death in adult oligodendrocytes, and the resulting pathology, are described and discussed in detail throughout this work. The description of the mouse model and its magnetic resonance imaging signature compose the basis of the first two publications. Additional work on myelinating glia during my PhD thesis resulted in further publications that are not included in this work:

Pohl, H.B.F., Porcheri, C., Mueggler, T., Bachmann, L.C., Martino, G., Riethmacher, D., Franklin, R.J.M., Rudin, M., and Suter, U. (2011). Genetically Induced Adult Oligodendrocyte Cell Death Is Associated with Poor Myelin Clearance, Reduced Remyelination, and Axonal Damage. The Journal of Neuroscience 31, 1069-1080.

Mueggler, T., Pohl, H.B.F., Baltes, C., Riethmacher, D., Suter, U., and Rudin, M. (2011). MRI Signature in a Novel Mouse Model of Genetically Induced Adult Oligodendrocyte Cell Death. (submitted to NeuroImage)

Atanasoski, S., Boentert, M., De Ventura, L., Pohl, H., Baranek, C., Beier, K., Young, P., Barbacid, M., and Suter, U. (2008). Postnatal Schwann cell proliferation but not myelination is strictly and uniquely dependent on cyclin-dependent kinase 4 (cdk4). Mol Cell Neurosci 37, 519-527.

Zawadzka, M., Rivers, L.E., Fancy, S.P., Zhao, C., Tripathi, R., Jamen, F., Young, K., Goncharevich, A., Pohl, H., Rizzi, M., Rowitch, D.H., Kessaris, N., Suter, U., Richardson, W.D., and Franklin, R.J. (2010). CNS-resident glial progenitor/stem cells produce Schwann cells as well as oligodendrocytes during repair of CNS demyelination. Cell Stem Cell 6, 578-590.

The work has been presented at the following meetings (exemplary list):

2011 NCCR Neural Plasticity and Repair Symposium — Warth, Switzerland
Poster: "Genetically-induced adult oligodendrocyte cell death is associated with poor myelin clearance, reduced remyelination and axonal damage"
Pohl HBF, Porcheri C, Mueggler T, Bachmann LC, Martino G, Riethmacher D, Franklin RJM, Rudin M, Suter U

2011 Stem Cell Centre of Competence, Uni Basel — Basel, Switzerland
Oral presentation: "Removing the Glue: A Novel Model of Oligodendrogliopathy"

2009 NCCR Centre for Transgenesis Expertise Symposium — Zurich, Switzerland
Oral presentation: "Towards temporally and spatially controlled specific cell ablation in the nervous system – first implementation: a novel mouse model for demyelination"

2009 ZNZ - Neuroscience Centre Zurich Symposium — Zurich, Switzerland
Poster: "A Novel Mouse Model for Demyelination"
Pohl HBF, Mueggler T, Porcheri C, Kulstrunk M, Bachmann LC, Riethmacher D, Franklin RJM, Rudin M, Suter U

2008 Cold Spring Harbour Laboratory Meeting: — Cold Spring Harbour, NY, USA
Glia in Health & Disease
Poster: "A Novel Mouse Model for Demyelination"
Pohl HBF, Mueggler T, Kulstrunk M, Heppner F, Rudin M, Riethmacher D, Suter U

2007 Joint Meeting Swiss Society for Neuroscience – NCCR Neural — Bern, Switzerland
Plasticity and Repair – Swiss Society for Multiple Sclerosis
Poster: "A Novel Mouse Model for Demyelination"
Pohl HBF, Heppner F, Mueggler T, Riethmacher D, Suter U

2006 NCCR Centre for Transgenesis Expertise Symposium — Zurich, Switzerland
Oral presentation: "Towards temporally and spatially controlled specific cell ablation in the nervous system"

2006 D-BIOL ETH Zurich PhD Summer School — Kiental, Switzerland
Poster: "A Novel Mouse Model for Demyelination"
Pohl HBF, Heppner F, Riethmacher D, Suter U

2006 ZNZ - Neuroscience Centre Zurich PhD Retreat — Valens, Switzerland
Oral presentation: "A Novel Mouse Model for Demyelination"

Contribution of the author:

All experiments described in the Results section have been performed by the author, with the exception of the proliferative assessment of glial cells, which was performed by Cristina Porcheri (Institute of Cell Biology, ETH Zurich, Switzerland). Western blot analysis was performed in collaboration with Markus Kulstrunk (Institute of Cell Biology, ETH Zurich, Switzerland). Quantitative assessment of nodes of Ranvier was performed in collaboration with Lukas Bachmann (Institute of Cell Biology, ETH Zurich, Switzerland). Magnetic resonance imaging was performed in collaboration with Dr. Thomas Mueggler (Institute of Biomedical Engineering, ETH Zurich, Switzerland); the MRI acquisition sequences used were established by Dr. Thomas Mueggler and Dr. Christof Baltes (Institute of Biomedical Engineering, ETH Zurich, Switzerland).

Summary

The acquisition of nerve insulation by myelin was the prerequisite for the development of higher order organism with their complex nervous systems. Disruption of this insulation originating from insults on the underlying myelin-forming cells has severe impact on neuronal function. Demyelinating diseases are associated with loss of myelinating glia and nervous system damage, with the inflammatory demyelinating disease multiple sclerosis being the most prominent. Despite the serious social and individual impact of demyelinating diseases, the understanding of the involved genesis, pathology and recovery mechanisms remains incomplete. It is generally well accepted, that axons and glia, and in particular myelinating glia, are subject to complex, interdependent interactions, but it remains unclear how the loss of this interplay results in neurological damage. Loss of myelin is widely believed to contribute to axonal impairment in demyelinating diseases, which in turn is thought to be both the main disability correlate and the underlying secondary progressive disease course. Currently available animal models are often complex and inconsistent in their time course and pathology, and therefore complicate the study of the defined cellular events following demyelination and the involved disruption of axoglial interplay.

To facilitate research on events underlying demyelinating diseases and axo-glial interactions, I established and characterised a novel mouse model that allows genetic ablation of myelinating glia via triggered cell-intrinsic expression of diphtheria toxin fragment A. Induced cell death in this model leads to fast and efficient loss of oligodendrocytes and a well defined and highly reproducible disease course. Loss of myelinating glia is not accompanied by immediate loss of myelin or appearance of symptoms, but progressive myelin vacuolation due to structural decay appears with clinical progression characterised by motor deficits, tremor, and ataxia. Residual myelin and myelin debris remaining after oligodendrocyte cell death is inefficiently cleared by activated microglia but not blood-borne phagocytes. With ubiquitous debris present, remyelination remains sparse in most tissues although oligodendrocyte precursor cells are induced to proliferate and replenish oligodendroglial cell pools. The observed pathology is characterised by widespread tissue disruption and *status spongiosus* but limited vacuolation and substantial remyelination occur in some tissues. Overall, clearance and repair remain insufficient to prevent secondary axonal damage consequent to cell death of myelinating glia resulting in severe neurological impairment. Additionally, the blood-brain barrier remains undisturbed and lymphocytes are neither present within brain parenchyma nor involved in the occurring disease pathology, thereby simplifying the study of axoglial dependency in demyelination. Disease development and underlying pathology could be monitored with a multi-

methodical magnetic resonance imaging assessment using quantitative T2 mapping, phagocyte tracing with USPIO, diffusion tensor and magnetisation transfer imaging.

These results indicate that without blood-brain barrier disruption and a certain quantity and/or quality of inflammation, remyelination is insufficient, likely due to improper myelin debris clearance and results in subsequent axonal damage.

Concluding, the model provides ample novel opportunities to study the consequences of primary oligodendrogliopathy in the absence of primary confounding effects on other cell types, finally fostering our understanding of axoglial interactions, demyelination, myelin debris clearance and remyelination.

Zusammenfassung

Die Isolierung von Nerven durch Myelin war die wichtigste Voraussetzung für die Entwicklung von höheren Organismen mit ihren komplexen Nervensystemen. Die Beeinträchtigung dieser Isolierung durch schädigende Einflüsse auf die Myelin-formenden Zellen ist die Hauptursache für eine Vielfalt von Krankheiten. Schwund von myelinisierenden Gliazellen ist ein charakteristisches Merkmal demyelinisierender Erkrankungen, die oft durch schwere neurologische Störungen geprägt sind. Die prominenteste demyelinisierende Krankheit ist Multiple Sklerose, eine entzündliche Erkrankung des Zentralnervensystems. Trotz den beträchtlichen sozialen und individuellen Auswirkungen dieser Erkrankungen ist unser Verständnis der zugrunde liegenden Genese, Pathologie und Heilungsmechanismen noch unvollständig. Es ist allgemein akzeptiert, dass Axone und Gliazellen, und im besonderen Myelin-bildende Glia, auf vielfältige und komplexe Weise interagieren, aber es bleibt unklar, wie die Störung dieser Interaktionen zu neurologischem Schaden führt. Es wird generell angenommen, dass Myelinschwund zum axonalen Schaden in demyelinisierenden Erkrankungen beiträgt, welcher wiederum die Hauptursache für die neurologischen Einschränkungen ist sowie dem sekundär-progressiven Krankheitsverlauf zugrunde liegt. Momentan verfügbare Tiermodelle sind häufig Komplex und diffus im Krankheitsverlauf und der zugrunde liegenden Pathologie, wodurch die Erforschung der konkreten zellulären Abläufe und Zusammenhänge, die der Demyelinisierung folgen, verkompliziert wird.

Um die Erforschung der Geschehensabläufe, die demyelinisierenden Erkrankungen zugrunde liegen, sowie axoglialer Zusammenspiele zu fördern, habe ich ein neuartiges Mausmodell etabliert und charakterisiert, welches genetisch-gesteuerte Ablation von myelinisierenden Gliazellen mittels induzierter, zellinterner Expression von Diphtheria Toxin A Fragment erlaubt. Induzierter Zelltod führt in diesem Modell zu schneller und effizienter Beseitigung von Oligodendrozyten sowie einem sehr reproduzierbaren und definiertem Verlauf. Der Schwund von myelinformenden Gliazellen wird interessanterweise nicht durch sofortigen Myelinschwund oder umgehend eintretende Symptome begleitet, sondern führt zu verzögerter Vakuolisierung des Myelins aufgrund von Zerfall der Komponenten, parallel zu fortschreitenden Symptomen. Diese Beeinträchtigungen sind charakterisiert durch motorische Störungen, Tremor und Ataxie. Nach erfolgtem Zelltod von Oligodendrozyten verbleibendes Myelin und Myelintrümmer werden durch aktivierte Mikroglia nur ineffizient entfernt, ohne Beteiligung blutzirkulierenden Phagozyten. Mit allgegenwärtigen Myelinresten bleibt Remyelinisierung ein rares Ereignis in den meisten neuralen Geweben, obwohl Vermehrung von Oligodendrozytenvorläuferzellen induziert wird, um die Oligodendrozytenpopulation wieder aufzufüllen. Gewebsregionale Unterschiede sind offensichtlich

und reichen von ausgedehnter Gewebezersetzung und *Status Spongiosus* in den Faserbündeln der weißen Substanzen bis zu schwacher Vakuolisierung mit erheblicher Remyelinisierung im Corpus Callosum. Im Großen und Ganzen bleibt die Beseitigung von Myelin und Gewebeheilung unzureichend, um sekundäre Schädigung von Axonen, die zu schwerwiedender neurologischer Beeinträchtigung führt, zu verhindern. Zusätzlich bleibt die Blut-Hirn-Schranke intakt und Lymphozyten sind weder präsent noch an dem auftretenden pathologischen Schaden beteiligt. Krankheitsentwicklung und zugrunde liegende Pathologie konnten mittels multimethodologischer Magnetresonanztomografie unter Verwendung von T2 mapping, Phagozytenkontrastierung mittels USPIO, Diffusionstensor- und Magnetisierungstransferbildgebung überwacht werden.

Diese Resultate weisen darauf hin, dass ohne eine Störung der Blut-Hirn-Schranke und eine Entzündung nötiger Quantität und/oder Qualität Remyelinisierung unzureichend bleibt, vermutlich aufgrund unzulänglicher Entfernung von Myelinresten, und somit axonale Schädigung die Folge ist.

Das hier vorgestellte Mausmodell bietet schlussfolgernd beträchtliche neue Möglichkeiten um die Konsequenzen von primärer Oligodendrogliopathie in der Abwesenheit von irritierenden Primäreffekten auf andere Zelltypen zu studieren, und wird schlussendlich unser Verständnis von axoglialen Wechselwirkungen, Demyelinisierung, Beseitigung von Myelintrümmern und Remyelinisierung fördern.

Introduction

The vertebrate nervous system is a highly complex organ and probably the most marvellous achievement of evolutionary development. It derives its name from the nerves, cylindrical fibre bundles that exit the brain and spinal cord, and which were already recognised by the ancient Egyptians, Greeks and Romans.

The nervous system and its cell types

The brain and spinal cord together comprise the central nervous system (CNS), while the nerves that sprout out from it and form a widespread network throughout the body, comprise the peripheral nervous system (PNS). Despite its both structural and functional complexity, the nervous system is composed of very few cell types that are classically divided into two groups: neurons and glial cells.

Neurons

Neurons are cells with a rather voluminous cytoplasm and a protruding network of cellular processes, of which one, the axis-cylinder appendix –nowadays termed axon– is dominant. They were recognised as the wiring cells of the nervous system by the work of Cajal and Golgi and are today known for their importance in signal transduction and network formation (for further insight, refer to: Glickstein, 2006). They fulfil this function via electrical excitability and combined electrical and chemical signal transduction through an extensive network. The neuron's cell body and its processes, the dendrites, are electrically excitable, and signal conduction along the axon –the axon potential– triggers chemical cell-cell transmission at the terminal synapses, where also signal processing takes place.

Glia

Whilst neurons were early on well recognised for their function, and are subject to detailed studies since centuries, glial cells were scientifically disregarded for decades. This neglect was both causing in and consequent to poor understanding of their role and relevance for the nervous system, reflected by their appellation as the brain's glue. This lack of attention was highly unjust, given that glial cells not only outnumber neurons almost tenfold in the mammalian brain (Hyden & Pigon, 1960), but also fulfil manifold functions in tissue homeostasis, nervous system operations and their alterations, repair and control of pathogens –some of which roles were just recently discovered and are still emerging.

Glial cells are historically divided into macroglia and microglia. While the former consist of astroglia and oligodendroglia, both named after their cellular morphology, the latter consist only of one cell type. Microglia do not originate from the nervous system, but are blood-borne cells of monocytic origin dispersed in the nervous parenchyma. They therefore are phagocytes and comprise the brain's innate immune system. Astroglia are star-shaped cells that fulfil manifold functions in the nervous system, of which only a part is presently known and understood. They are involved in trophic support of neural cells, form the blood-brain barrier (BBB), maintain extracellular ion balance, modulate signal transmission, and are involved in repair and scarring of nervous tissue following injury. Glia also were a fundamental prerequisite for the development of higher order organisms, dependent on a complex nervous systems and long distance signal transmission.

Myelinating glia

Although invertebrates already feature glial cells in intimate contact with neurons, the ultimate driving force of increased body size and evolution, offering improved muscle control and behaviour, was the acquisition of myelination of axons. This structure –termed myelin by Virchow in 1846 (Virchow, 1846)– is a unique specialisation of the vertebrate's myelinating glia, the oligodendrocyte in the CNS and the Schwann cell in the PNS. It is achieved by enwrapping axons with a structure composed of multilayered cell membranes, which are densely packed, rich in lipids, poorly hydrated and tightly sealing the axon's surface (reviews on myelin: Baumann & Pham-Dinh, 2001; Sherman & Brophy, 2005; Schweigreiter et al., 2006; Simons & Trotter, 2007). This insulation of the axon is organized longitudinally in regular intervals along its axis, thereby clustering the ion channels to the gaps in between –termed the nodes of Ranvier– (see Fig. 1-1) (Salzer et al., 2008). The resulting speed up of signal transmission by saltatory impulse propagation from node to node therefore allowed tremendous increase in axon signal conduction without the need of size augmentation of nerve fibres, and was first understood long before myelin was recognised as a specialized outgrowth of glia (Geren & Raskind, 1953). Only this achievement allowed body size increment of vertebrates, despite the spatial limitations implicated by a nervous system located within bones (Zalc et al., 2008).

Schwann cells

Interestingly, myelination in the PNS by Schwann cells differs substantially from myelination in the CNS. The former cells restrict myelination to a single axonal segment –termed internode– and the cell is spatiality restricted to this one segment, whereas oligodendrocytes myelinate multiple axons with membrane protrusions that emerge from a distantly located cell body (Bunge et al., 1962). Besides the comparable task, which both cell types fulfil with overlapping but not similar molecular

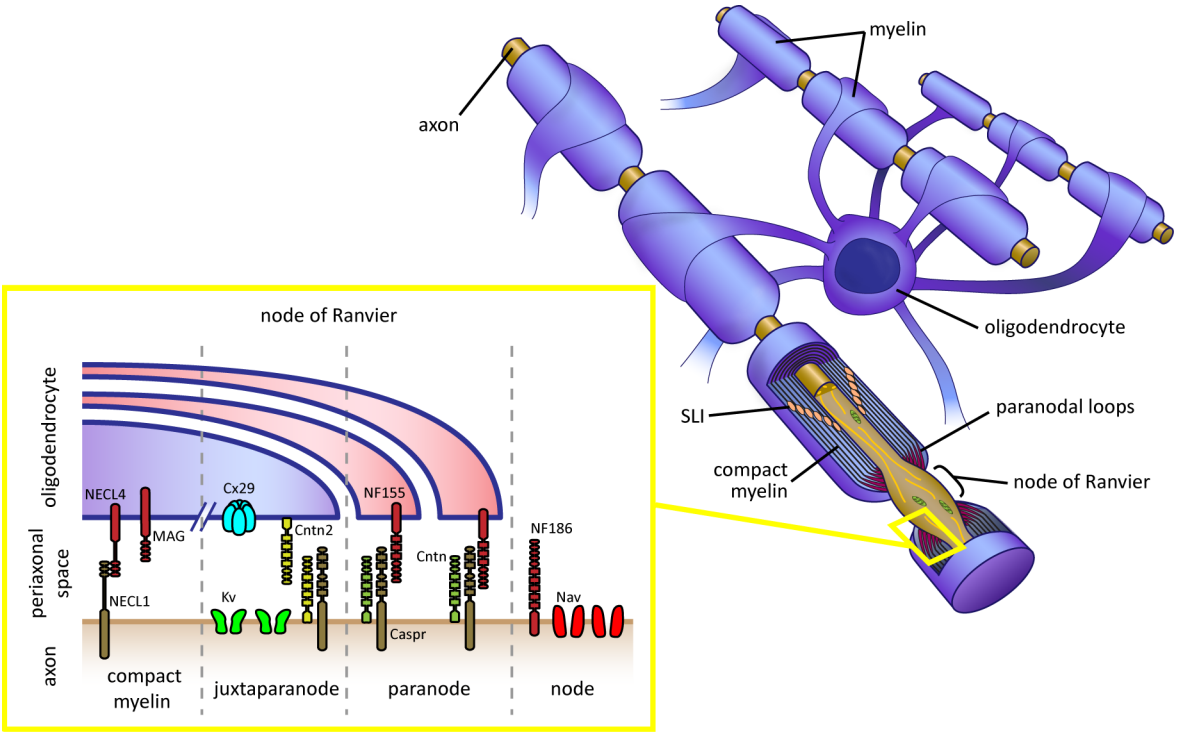

Fig. 1-1: Myelin and the axoglial junction.

One oligodendrocyte enwraps several axons to form myelin internodes. This compact myelin is formed by densely packed membranes with very little cytoplasm and only interrupted by Schmidt-Lantermann-incisures (SLI) (see also Fig. 1-2). Besides these, only the inner and outer cytoplasmic tonque and the paranodal loops comprise the non-compacted myelin containing cytoplasmic cavities. The internodal segments separate gaps of free axonal surface, the nodes of Ranvier. At these sites, voltage-gated sodium channels (Nav) are clustered and action potentials are generated and transmitted in a saltatory manner; while the voltage-gated potassium channels (Kv) are located at the juxtaparanodal axonal surface below the compact myelin. The paranodal loops formed at the lateral ends of the myelin wraps are the location of the axoglial junction, which forms a seal between the periaxonal space and the outside milieu at the node. The axoglial junction also prevents lateral diffusion of axonal membrane components and is therefore essential for axonal compartmentalization. Caspr, contactin-associated protein; Cntn, contactin; Cx29, connexin 29kDa; MAG, myelin-associated glycoprotein; NECL, nectin-like protein/synCAM; NF155/186, neurofascin 155kDa/186kDa. (*Adapted from Nave, 2010a)*

strategies, the developmental and evolutionary origins of Schwann cells and oligodendrocytes differ, with both coexisting since 300 million years (Yoshida & Colman, 1996). PNS Schwann cells originate during embryonic development from migrating neural crest cells that transform into immature Schwann cells before birth, and further on depend in their development on the diameter of the associated axon. While Schwann cells contacting large calibre axons will differentiate into mature myelinating Schwann cells and form myelinated internodes, those associated with small-calibre C-fibre axons will form Remak bundles by engulfing multiple axons without myelinating them (Jessen & Mirsky, 2005).

Oligodendrocytes

In contrast, oligodendrocyte precursors arise from pluripotent neuroepithelial cells in the ventricular zones of the neural tube very early during embryonic life (Curtis et al., 1988; Warf et al., 1991). They proliferate and migrate outwards into the subventricular zone to form committed oligodendrocyte precursor cell (OPC) populations at longitudinally distributed foci along the neuroaxis, from where they distribute into the CNS parenchyma in successive waves (Luskin et al., 1988; Price & Thurlow, 1988; Colognato & ffrench-Constant, 2004; Kessaris et al., 2006; Richardson et al., 2006). Here they migrate and constantly scan the axonal network to define their ultimate positions (Kirby et al., 2006), where they finally differentiate into mature oligodendrocytes and with their extensive branching network myelinate multiple internodes, with one oligodendrocyte being capable of myelinating up to 100 different axonal segments (Bjartmar et al., 1994).

Myelination

To myelinate axons in their vicinity, OPCs rapidly remodel their numerous filopodium-like processes, to scan for vacant axons and repel each other while competing for space –a mechanism thought to both modulate equal distribution of oligodendrocytes as well as equidistant internodal spacing (Kessaris et al., 2006; Kirby et al., 2006). The processes then enlarge their membrane surface while they both wind around the axon and expand laterally along it, probably until they encounter axonal surface occupied by another process, be it from the same or a different cell, from when on they start to compete for space finally leading to equally long internodes along an axon, normally reaching internodal lengths between 150 and 200 µm (Butt & Ransom, 1989). Concurrently, the cytoplasm trapped in the membrane wraps compacts and the inside surfaces of the membranes fuse to form the major dense line, with the exception of the very edges –the inner and outer cytoplasmic tongue (Fig. 1-2). During the first few wraps, this loose central myelin sheath consists of a spiral of major dense lines and has not compacted completely. With more wraps, myelin compacts while the outer membrane surfaces fuse to form the intraperiod lines to reach a final constant periodicity of the membrane lamella of 12 nm (Caley & Butler, 1974; Baumann & Pham-Dinh, 2001). Longitudinally, this compacted myelin is interrupted by cytoplasmic bridges that are connected via gap junctions and span the myelin sheath from the inner, adaxonal side towards the outer abaxonal surface. These cytoplasmic channels are termed Schmidt-Lanterman incisures and are rare in CNS but frequent in PNS myelin. Myelin compaction is also incomplete at the lateral ends, where the myelin loops are filled with cytoplasm and are in tight contact with the axonal membranes forming the paranodal loops (Fig. 1-1). Spiral membrane enwrapping of the axon continues and can reach to over 100 wraps of the oligodendrocytes membrane around large calibre axons.

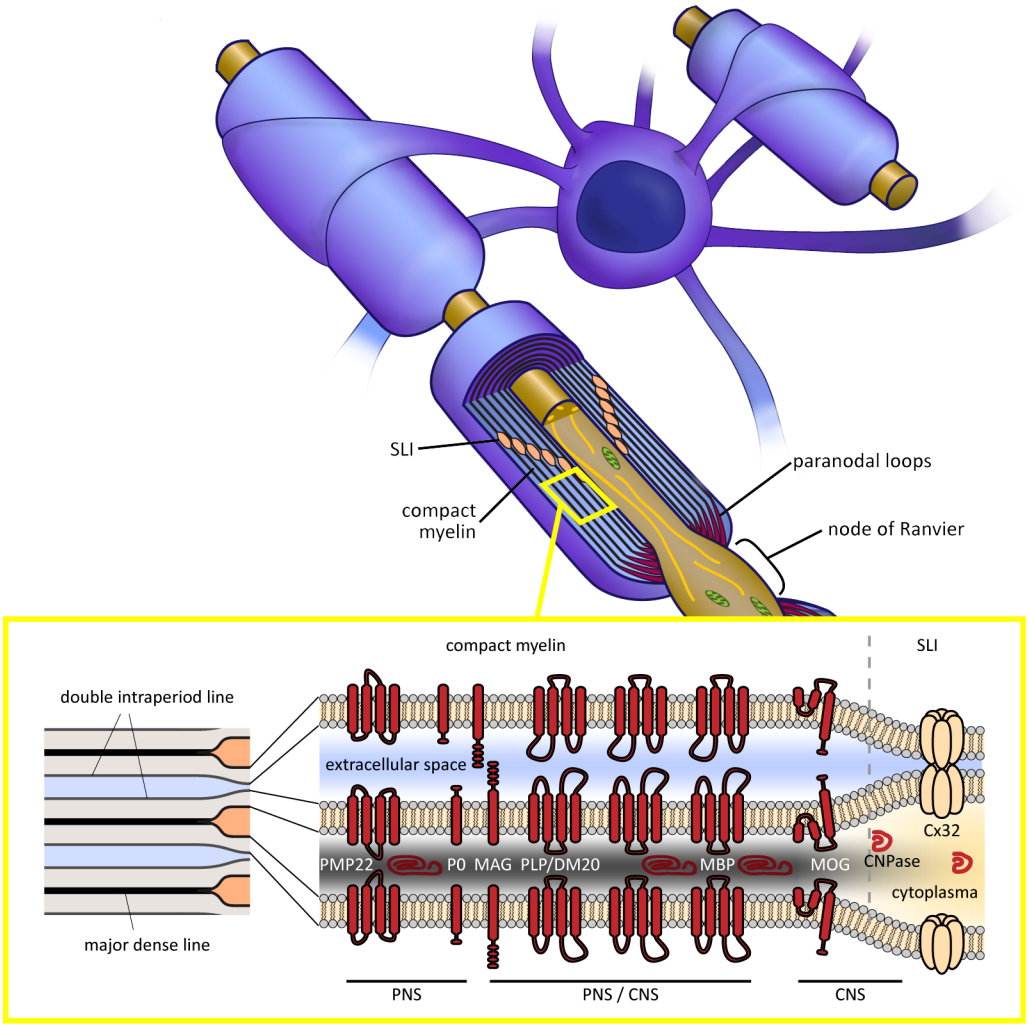

Fig. 1-2: Myelin structure and composition.

Myelin is a structure of densely packed membrane wraps with a periodic ultrastructure. While the Schwann cells of the peripheral nervous system's (PNS) myelinate only one internodal segment of an axon, the oligodendrocytes of the central nervous system's (CNS) form multiple myelin internodes. The majority of an internode is composed of compact myelin, with very little non-compacted myelin in the Schmidt-Lantermann incisures (SLI). The SLI form cytoplasmic bridges that connect inner and outer myelin layers via gap-junctions, and are frequent in PNS myelin but rare in the CNS. Myelin compaction is achieved by the apposition of the external faces of the membranes of myelinating glia, thereby forming the double intraperiod line seen in ultrasctrutural examinations of myelin. The apposition of the external membrane faces is followed by exclusion of the cytoplasm and compaction of the cytoplasmic space, thereby forming the major dense line. The cytoplasm of compact myelin therefore contains only little liquid and densely packed proteins. PMP22, peripheral myelin protein 22kDa; P0, myelin protein zero; MAG, myelin-associated glycoprotein; PLP/DM20, proteolipid protein or its splice variant DM20; MBP, myelin basic protein, MOG, myelin oligodendrocyte glycoprotein; CNPase, cytosolic 2'3'-cyclic nucleotide 3'-phosphodiesterase; Cx32, connexin 32kDa. (Adapted from Baumann & Pham-Dinh, 2001)

Myelin

Thus, myelin enwrapping the neuron's axon ultimately forms the essential constituent of the nervous system's white matter, a structure composed of densely packed and mostly myelinated fibre bundle tracts, by representing approximately 50% of its dry weight (Norton & Poduslo, 1973). Myelin is poorly hydrated, with a water content of only 40%, and its dry weight apportions into 70% lipids and 30% proteins. This ratio of lipids and proteins is rather the reverse compared to most cellular membrane compositions, and is peculiar to myelin membranes. This high fat content makes these structures appear white and enables even macroscopic discrimination against the CNS' grey matter, which is poorly myelinated and constituted mostly of the neurons' cell bodies. Also the lipid composition of myelin membranes is very specific, with cholesterol, phospholipids, and glycolipids represented in molar ratios ranging from 4:3:2 to 4:4:2, with a peculiar richness in glycosphingolipids, in particular GalC (reviewed in: Morell et al., 1994).

Myelin proteins

Myelin protein composition is also extraordinary, with the vast majority of the proteins being exclusive to myelin and myelinating glia (Fig. 1-2). The major CNS myelin proteins myelin basic protein (MBP) and proteolipid protein (PLP) or its isoform DM-20 constitute alone 80% of the total proteins. Less frequent but comparably specific myelin components are the gap-junction protein Connexin 32 (Cx32) and the glycoproteins myelin-associated glycoprotein (MAG) and myelin oligodendrocyte glycoprotein (MOG) as well as the cytosolic 2'3'-cyclic nucleotide 3'-phosphodiesterase (CNPase). In contrast, in PNS Schwann cells the major myelin proteins are myelin protein zero (P0), peripheral myelin protein 22 (PMP22), MBP and (Baumann & Pham-Dinh, 2001; Jessen & Mirsky, 2005). While the latter two are minor components of PNS myelin, especially compared to their abundance in CNS myelin, they additionally fulfil altered roles. MBP for instance is, in contrast to its role in the CNS, not needed for PNS myelin compaction (Kirschner & Ganser, 1980), but can function interchangeably if P0 is lacking (Martini et al., 1995). This variation in component use illustrates again the interesting differences by which two independent cell types use comparable but not identical tools to develop the unique structure of myelin.

Myelin plasticity

Although myelin formation is an early event, starting in most mammals perinatally and most fibres being associated with compact myelin in early postnatal development, myelination continues into late adolescence and myelin thickness may increase in some CNS regions, such as cortical fibres in associative areas throughout much of adulthood (Yakovlev & Lecours, 1967; Benes et al., 1994; Paus

et al., 1999). Myelination was long thought to be non-recurring and irrevocable, but it is much more dynamic than often considered. During postnatal development and body growth, some axons – especially those of certain peripheral nerves but also CNS-resident ones– will grow remarkably in length, which naturally raises the question of what happens to the internodal myelin segments, when the axon elongates (Sherman & Brophy, 2005). Although lengthening is known to happen and to rely on Periaxin-DRP2-dystroglycan complex-dependent formation of Cajal bands (Sherman et al., 2001; Court et al., 2004), it is not entirely clear whether the necessary elongation of myelin coverage is achieved entirely by internodal elongation or whether also *de novo* formation of myelin segments occurs. The latter is likely to appear, given that some nerves elongate as much as four times after myelination has already begun and impulse propagation velocity is highly dependent on nodal separation distance (Brill et al., 1977).

In addition, an increase in myelination was suspected to underlie learning and practicing processes in the human adult brain as assessed by magnetic resonance imaging (MRI) findings (Bengtsson et al., 2005; Scholz et al., 2009) and in environmental enrichment studies in rodents (Juraska & Kopcik, 1988). These findings even led to proposals that neural plasticity comprises, besides network and connection plasticity, activity-related changes of myelin to strengthen or synchronise specific connections (Fields, 2005), suggesting that *de novo* myelin formation is a continuous process in adult brains. This idea is well supported by the findings that OPCs both react to electrical activity within axonal tracts (Li et al., 2010), and also continuously differentiate into myelinating oligodendrocytes within the adult CNS (Rivers et al., 2008), indicating that myelination is not definite but underlies substantial dynamic processes.

Axon-glia interactions

To precisely establish and maintain the complex architecture of myelinated fibres, and to organise the detailed functional and structural cellular interplay that is required to establish the structure, a well defined and precisely timed cascade of signals is vital. Although myelination is an intrinsic property of myelinating glia (Temple & Raff, 1986), their maturation and survival as well as initiation and regulation of myelination depends on a variety of signals and factors, both cell-intrinsic as well as -extrinsic determinants (Baumann & Pham-Dinh, 2001; Kessaris et al., 2006).

Axonal signals towards oligodendroglia

Besides a fine tuned, cell internal regulatory program necessary for the initiation of the indispensable changes in cell metabolism and morphology involved in the dramatic cellular development from a progenitor cell via very active OPCs towards myelinating glia (for further insight see reviews: Baumann & Pham-Dinh, 2001; Sherman & Brophy, 2005; Richardson et al., 2006; Emery, 2010), a well timed and tuned interaction with the developing neural environment is crucial. Thus myelinating glia sense and interact with the axonal component of the CNS through a variety of communicative means, of which not all are known and some are only partially understood.

For instance, OPCs react to axonal electric activity with proliferation to fine tune the necessary amount of myelinating glia (Barres & Raff, 1993), but impulse activity is also suggested to influence not only proliferation of OPCs but also myelination. Myelination efficacy of the optic nerve for example is highly dependent on visual system activity (Gyllensten & Malmfors, 1963; Omlin, 1997) (Tauber et al., 1980), and electrical activity-mediated extra-synaptic release of adenosine may promote OPC differentiation and myelination (Stevens et al., 2002). Additionally, astrocytes release promyelinating factors in response to electrical impulses (Ishibashi et al., 2006). Surface expression of axonal ligands or cytokines involved in axo-glial signalling have been suggested to be influenced by certain patterns of neuronal impulse activity (Itoh et al., 1995), and neural activity may also contribute to neural plasticity via the modulation of ongoing myelination in the adult CNS (see above).

Axonal signals also control the timing of glial enwrapping and myelination via a controlled switch from contact repelling cell adhesion molecules to promyelinating cell-cell interaction and adhesion. Amongst the inhibitory ligands expressed on axons are Jagged, which blocks differentiation of OPCs via Notch (Wang et al., 1998; Genoud et al., 2002), LINGO-1 (Mi et al., 2005) or the polysialated neural cell adhesion molecule (PSA-NCAM), which serves as a general negative regulator of cell-cell interaction and whose removal from the axonal surface is essential for myelination to proceed (Charles et al., 2002). Interestingly, although premyelinated neurons repress glial enwrapping, they stimulate OPC proliferation and survival simultaneously, directly or indirectly via astrocytic growth factors as well as trophic factors such as platelet-derived growth factor A (PDGF-A) or neuregulin (NRG), which is pro-proliferative for OPCs in the absence of axonal contact but its effect is switched towards OPC survival by integrin-mediated signalling (Colognato et al., 2002; Colognato et al., 2005; Simons & Trajkovic, 2006).

This is a nice example of the mechanisms necessary to fine-tune the number of oligodendrocytes required for proper white matter myelination. Overall, OPCs are greatly overproduced during

development, and only those that manage to ensheath axons will survive, while the remaining ones that fail to establish this axon-glia linkage will degenerate and undergo apoptosis (Barres et al., 1992; Trapp et al., 1997).

Neuronal signals and ligands are not only essential for oligodendrocyte survival, but also regulate myelin formation. In PNS Schwann cells, axonal surface expression levels of NRG1 type III determine whether fibre myelination or Remak bundle formation occurs, and also regulate myelin sheath thickness of myelinated axons (Michailov et al., 2004; Taveggia et al., 2005; Nave & Salzer, 2006). The number of myelin membrane wraps is precisely related to axonal diameter, resulting in a strikingly constant ratio of axon to myelinated fibre thickness, termed g-ratio (Friede, 1972). In contrast to the PNS, NRG signalling is largely dispensable in the CNS as oligodendrocytes properly myelinate even in the absence of NRG from axons. Interestingly, NRG signalling still plays a role in the regulation of oligodendroglial myelination, as its overexpression leads to hypermyelination (Brinkmann et al., 2008), but the signalling involved in CNS myelin regulation seems to be a more complex interplay of different factors such as myelination promoting laminins (Laursen et al., 2009), or the immunoglobulin-superfamily cell adhesion molecule L1 (Barbin et al., 2004), that might activate partially overlapping intracellular signalling pathways. This is another display of the fascinating differences between the two myelinating glial cell types and their usage of similar but not identical mechanisms to achieve myelination.

Glial signals towards axons

Vice versa to myelinating glia relying on axonal intervention to achieve proper myelination, axons also depend on glial interaction and signalling for proper organisation, assembly and function. Myelinated axons are organised into several distinct longitudinal domains centred around the nodes of Ranvier, the location of the clusters of voltage-gated Na^+ channels (Nav) necessary for saltatory nerve conduction (Fig. 1-1). This domain organisation is essentially depending on axo-glial interactions. Before enwrapping by glial cells has occurred, the Nav channels are diffusely distributed on the axonal surface. The diffuse distribution becomes constricted with formation of the paranodal loops by the myelinating glia and their interaction with axonal adhesion molecules to form a tight seal with the axonal surface via septate-like junctions. This region, termed paranode, forms the axo-glial junction, a tight barrier limiting diffusion of axon membrane proteins between the node and the juxtaparanode on the other side. The adjacent juxtaparanode encloses the axonal domain located under the compact myelin sheath that contains the voltage-gated K^+ channels (Kv) (for further insights, refer to: Peles & Salzer, 2000). Nodal domain organisation depends on a well orchestrated interplay between axonal and glial cell adhesion molecules and follows a distinct order: Clustering of

Nav channels is followed or mediated by restriction of lateral motility by paranodal junctions and finally the linkage of membrane protein complexes to the cytoskeleton (for further insights, refer to: Bhat, 2003; Schafer & Rasband, 2006; Simons & Trajkovic, 2006; Susuki & Rasband, 2008). Once established, the maintenance of axonal domain organisation also depends on intact glial cell interaction with the axon. Demyelination was shown to lead to nodal loss in different model and disease situations and loss of nodal morphology and domain organisation appears early in sites of artificial or disease-mediated demyelination, as for example occurring in multiple sclerosis (MS) (Craner et al., 2003; Howell et al., 2006). Additionally, mouse myelin mutants lacking key players for vesicular membrane transport or cytoskeleton dynamics in glial cells display distinct abnormalities in the nodal structure, especially the paranode, but not in compact myelin, as seen e.g. in mice lacking CNPase (Lappe-Siefke et al., 2003; Rasband et al., 2005; Simons & Trajkovic, 2006). Failure of the axo-glial junction as well as demyelination leads to a redistribution of Nav channels and a higher than normal channel density (Craner et al., 2004), and therefore to both reduction in speed as well as higher energy demands of impulse propagation (Waxman, 2006), resulting in detrimental effects on the axon.

Disruption of axo-glial junctions has also been shown to lead to cytoskeletal disorganization within the axon, accompanied by axonal swellings and degeneration similar to neurodegenerative diseases (Garcia-Fresco et al., 2006; King et al., 2009). Additionally, proper myelin formation has been suggested to be required for proper maturation of the axonal cytoskeleton (Brady et al., 1999), myelin components such as MAG are required to define mature axonal calibres (Yin et al., 1998), and demyelination of axons results in axonal calibre changes (Mason et al., 2001).

Trophic support for axons

Furthermore, there is growing evidence that normal axonal function and metabolism depend on glial support that exceeds insulation and domain organization. For instance, mice lacking PLP form normal myelin with only subtle changes in myelin compaction, but develop a late-onset axonal pathology resulting from oligodendroglial dysfunction that cannot be rescued by its isoform DM-20 (Klugmann et al., 1997; Griffiths et al., 1998; Stecca et al., 2000; Edgar et al., 2004; Rosenbluth et al., 2006). This axonal phenotype is aggravated if both PLP and CNPase are absent (Edgar et al., 2009), and might be due to dysfunctional axonal transport derived from cytoskeletal abnormalities.

Additional surprising insights came from a study of mice with peroxisomal-deficient oligodendrocytes. These mice displayed widespread axonal degeneration with late demyelination and a strong proinflammatory milieu (Kassmann et al., 2007). The normally abundant peroxisomes of oligodendrocytes therefore exhibit a neuroprotective function and seem to be involved in glial

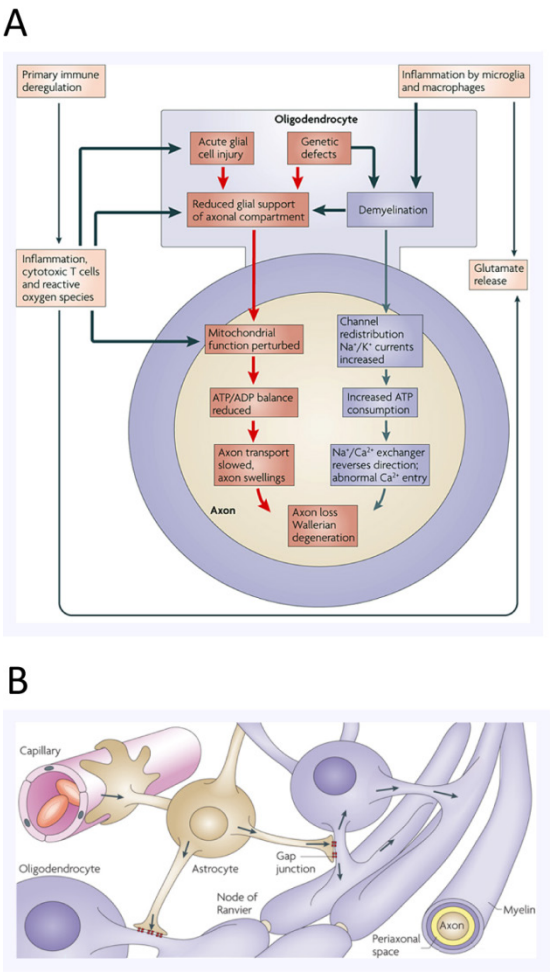

Fig. 1-3: Axon-glia interactions and consequences of their failure.

(A) Schematic representation of possible pathways to explain secondary axonal damage observed upon defects in myelinating glia. **(B)** Hypothetical metabolite shuttle of blood-borne nourishing factors via astrocytes and oligodendrocytes to the axon. (*Adapted from Nave, 2010b)*

trophic support of axons. Besides, oligodendrocytes have been found to secrete exosomes filled with myelin and stress-protective proteins that were suggested to participate in trophic support of axons (Krämer-Albers et al., 2007) and oligodendrocytes as well as Schwann cells could theoretically provide energy-rich metabolites to axons (Tachikawa et al., 2004). Additionally, astrocytes are known to be coupled to oligodendrocytes via gap-junctions, a fact that led to speculations about a lactate shuttle between these cells, similar to the one between neurons and astrocytes (Orthmann-Murphy et al., 2008; Nave, 2010b).

Theoretical observations have added to this idea. It is easily imaginable that a cell with such far-reaching processes as neurons –with some motor axons in humans being longer than one meter– depends on trophic support the distant cell body cannot provide, especially not in the expeditious manner that extremely fast reacting cells like firing neurons would require. The special constraints become even more striking when one considers that at least 99% of the plasma membrane of an axon is largely isolated from the external milieu by myelination (Edgar & Nave, 2009) and metabolic shuttling from the blood via astrocytes and oligodendrocytes to neurons has therefore recently been postulated (Nave, 2010b). This glial support might be independent of the need for myelination, as perturbation of non-myelinated Remak-bundles causes C-fibre degeneration and sensory neuropathy (Chen et al., 2003). Therefore, the idea that axons depend on complex glial metabolic support (Fig. 1-3) is indeed tempting and has deservedly become quite popular recently (Kassmann & Nave, 2008; Nave & Trapp, 2008; Edgar & Nave, 2009; Nave, 2010b, a; Piaton et al., 2010; Popko, 2010).

Demyelination

Given the important functional component of myelin in signal transmission and the intimate interplay of myelinating glia with the underlying axon, it is not a surprise that loss of myelin is strongly detrimental. Demyelination is the main and primary constituent of a variety of human diseases, some of which are viral- (Richardson-Burns et al., 2002; Hosking & Lane, 2009)or toxin-induced (Pratt & Weimer, 2005; Anyanwu & Kanu, 2007). However, the majority of demyelinating diseases result from impaired gene function or are immune-mediated.

Demyelination due to gene defects

Most common inherited myelin disorders are hereditary motor and sensory neuropathies in the PNS (Suter & Scherer, 2003) or leukodystrophies in the CNS (Schiffmann & van der Knaap, 2004) which are characterised by demyelination, myelin defects or both, resulting in often severe neural impairment. While the former are often caused by mutations in genes encoding structural myelin membrane components such as PMP22, P0 or Cx32 (Chance, 2001), underlying the latter are often functional disruptions within the lipid metabolism, due to gene defects in lipid transport, lysosomal, or peroxisomal enzymes (Faust et al., 2010), but can also result from abnormal oligodendrocyte myelinogenesis, such as in Pelizaeus-Merzbacher disease (Garbern, 2007; Gruenenfelder et al., 2011). Interestingly, CNS demyelinating diseases have also been described to originate in defects within astrocytes, and are thought to perturb their trophic support of myelinating oligodendrocytes such as in Alexander's disease and, probably, vanishing white matter disease (Boespflug-Tanguy et al., 2008).

Multiple sclerosis

The most frequent immune-mediated demyelinating disease of the CNS and most common cause of neurological deficits in young adults is the autoimmune-disease multiple sclerosis (MS), with a worldwide prevalence of approximately 120 per 100'000 and an yearly incidence of 3-5 in 100'000, varying highly with socio-geographic localisation (Compston & Coles, 2002; Pugliatti et al., 2002; Compston & Coles, 2008). Women are approximately twice as often affected as men and the disease onset is generally between 20 and 40 years. In Switzerland, it affects about 1 in 1000 people (Beer & Kesselring, 1994) and its impact on society is considerable: costs relating to this disease have been estimated to be 9 billion Euros per year within the European Union (Andlin-Sobocki et al., 2005).

An MS-like pathology was first described 1838 as a creeping paralysis thought to be mentally caused by a state of hysteria (Carswell, 1838; Cruveilhier, 1841), and the disease pathology was only in 1868 linked with the clinical appearance, scientifically documented, described and named by Charcot after

the widespread and distributed sclerotic plaques which are a main characteristic of the disease (Charcot, 1868). MS nowadays is considered to be a T-cell mediated autoimmune disease characterised by inflammatory demyelination. The cause of MS, however, remains unknown until today. Besides the unidentified mechanism(s) of triggering, it is well established that an interplay of genetic and environmental factors lies at the heart of the disease. The geographically varying prevalence indicates strong environmental factors, but the risk can only be adopted by migration early in life (Marrie, 2004). Besides correlations with stress and general health status, it has been hypothesised that exposure to Epstein-Barr virus early in life is a substantial factor of overall incidence and has been suggested to initiate autoimmunity via molecular mimicry, although other pathogens have also been suspected (Bray et al., 1992; Olson et al., 2001; Vanderlugt & Miller, 2002; Westall, 2006). Additionally, a genetic predisposition is evident in MS incidence, and was linked to specific variants of histocompatibility molecules (MHC), which are involved in antigen presentation and self-tolerance induction within the immune system (Hemmer et al., 2002; Oksenberg et al., 2004). However involvement of other genes is conceivable (Compston & Coles, 2008).

Clinical course of MS and disease heterogeneity

MS manifests as a generally non-fatal, multifocal and multiphasic disease, defined histologically by immune-mediated, inflammatory foci of demyelination, axonal impairment, damage and loss, astro- and microgliosis, and varying degrees of remyelination. Although clinically as well as pathologically heterogeneous, the majority of patients display a disease course initially characterised by repetitive episodes of varying impairment with complete recovery, the primary relapsing-remitting phase, followed by relapses with persisting deficits and finally secondary progressive impairment (Fig. 1-4). Thus, the clinical course well reflects the dominant role of distinct but related pathological processes, with inflammation and consequent transient damage being the main source of pathology early during disease progression, while chronic myelin deficiencies and axonal degeneration become more prominent as disability accumulates and the clinical course becomes progressive (Compston & Coles, 2008). Although this disease course of primary relapsing-remitting MS followed by secondary progressive MS is the most common form of symptomatic progression, a minority of patients exhibits a primary progressive form of the disease, characterised by a steady worsening with no distinct relapses/remissions; or an intermediate progressive relapsing course, where a steady worsening is accompanied by acute relapses with or without recovery (Lublin & Reingold, 1996).

This heterogeneity of MS is even further complexed on the histological level. While both spatial and temporal appearance and vanishing of lesions is very variable –although preferentially perivascular– and not necessary directly linked to the symptomatic course, the lesion's pattern of demyelination

are also discriminable into four different types which can all be present simultaneously within one patient. Both type I and II lesions exhibit clear inflammation-mediated pathology with strong infiltrates and less pronounced oligodendroglial loss, and demyelination is considered to be caused by macrophages and complement mediated lysis, respectively. In contrast, type III and IV are characterised by high oligodendroglial apoptosis. Additionally, they are thought to remyelinate less efficiently. While type III lesions are characterised by small vessel vasculitis and the damage is thought to be ischemic, type IV lesions exhibit primary oligodendrocyte damage within periplaque white matter in the absence of significant haematogenous leukocytes (Lucchinetti et al., 2000; Lassmann et al., 2001). The picture became even more complicated, when Barnett and Prineas described a freshly formed lesion that appeared within 24h before pathological analysis. These lesion types were characterised by fast and extensive oligodendroglial apoptosis followed by early microglial activation with few or no infiltrating lymphocytes (Barnett & Prineas, 2004). These findings

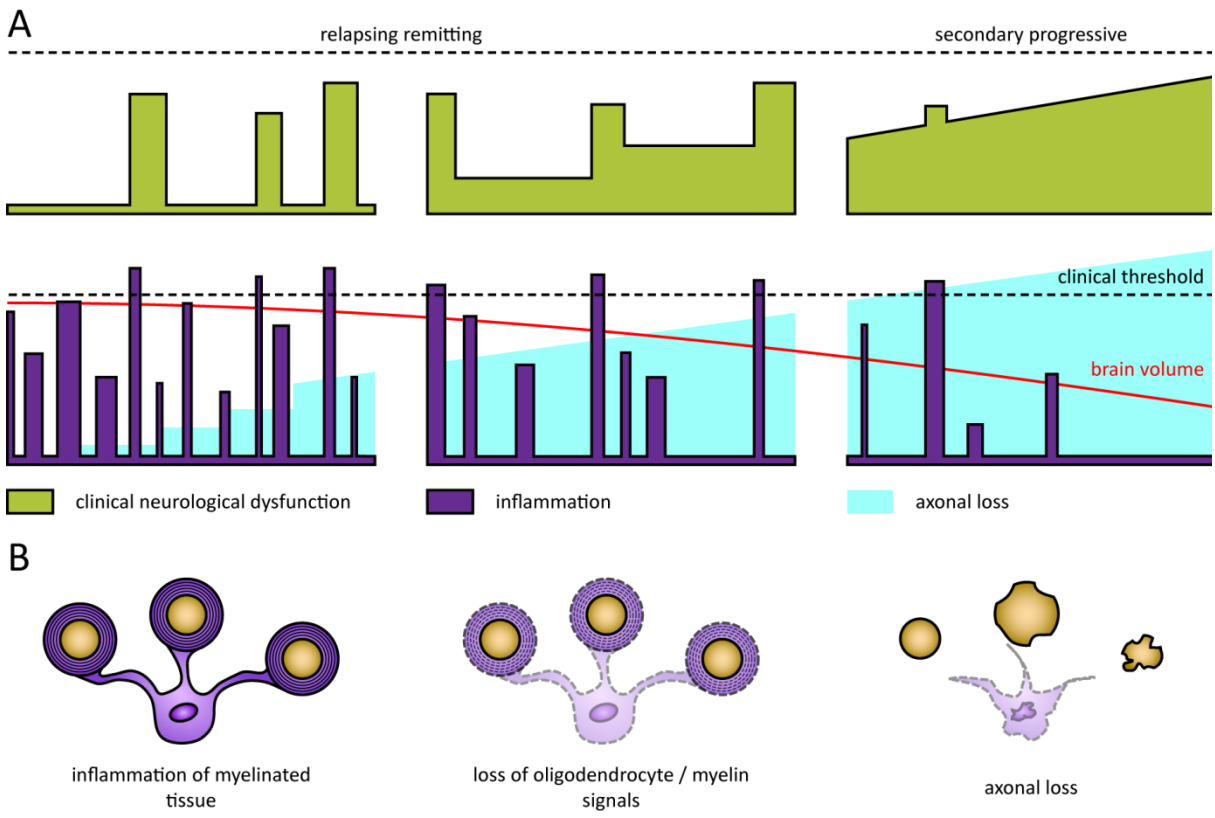

Fig. 1-4: Clinical course of Multiple Sclerosis and the underlying pathology.

(A) CNS inflammatory activity might precede clinical onset by years and single damaging events might not necessarily be reflected in acute symptomatical impairment, therefore being below a clinical threshold. However, with disease progression, damage accumulates and compensation fails, leading to persisting impairment. Besides new inflammatory events being less frequent, chronic damage facilitates ongoing disease progression. **(B)** The pathological correlate underlying the secondary progressive phase is axonal loss that can not be compensated, although damage and loss of axons also occurs early in the disease course. (*Adapted from Chandran et al., 2008; Compston & Coles, 2008)*

challenged the current view on MS lesion pathology, by indicating a rapidly changing heterogeneity of the lesions difficult to analyse with histopathology, as well as suggesting that oligodendrocyte apoptosis is the earliest change within a lesion, maybe even the primary event of the disease itself (Trapp, 2004; Barnett & Sutton, 2006; Brück, 2007). This variability of MS has currently led to the question of whether it is really one disease or is the observed pathological heterogeneity instead a temporal one based on lesion evolution (Barnett et al., 2009). Additionally, autoimmunity as a primary event has been questioned (Martino et al., 2000; Trapp, 2004).

Axonal damage in demyelination

Although MS is considered to be an autoimmune-mediated inflammatory disease, it is nowadays generally believed, that axonal/neuronal damage is the major correlate of neurological dysfunction (Chandran et al., 2008; Trapp & Nave, 2008; Edgar & Nave, 2009). Although both the importance and the degree of axonal damage has been disputed since the early histological descriptions of MS, evolution of imaging techniques led to a resurgence of interest in the role of axonal injury in MS. Axonal damage and transection, as well as neuronal injury, has meanwhile been well described to be a cardinal component of MS lesions (Ferguson et al., 1997; Trapp et al., 1998; Lisak, 2007), and is thought to lie at the heart of disease course and progressive disability (Fig. 1-4) (Chandran et al., 2008).

Mechanisms of axonal impairment

Demyelination and inflammation, as occurring in MS, lead to a variety of impacts on the underlying neuron. Displacement and expression level changes of ion channels as well as disorganisation of the nodal domains are amongst the first signs occurring in MS lesions and experimental demyelination (Howell et al., 2006). The loss of nodal compartmentalisation of the axon leads to both loss of saltatory nerve conduction and higher conductive energy demands within the axon. The inflammatory microenvironment, mainly provided by microglia and astrocytes, contributes with a variety of substances, such as nitric oxide, inflammatory cytokines or glutamate, further inhibiting axonal respiration and energy metabolism (Brown & Borutaite, 2002; Smith & Lassmann, 2002; Lassmann, 2003). Both insults in combination are thought to lead to detrimental energy deficiencies of the axon (Trapp & Stys, 2009). Myelin itself might provide an inflammation-protective effect and its loss might render the axon more vulnerable to such insults (Franklin & ffrench-Constant, 2008). Additionally, demyelinated lesions in MS show axon pathology, including, calibre reduction, axonal transport defects and blockage as well as axoskeletal disorganisation that lead to axonal damage and loss (Vickers et al., 2009). Transected axons are frequent in MS lesions, even early in the disease

(Trapp et al., 1998) and cytotoxic T cells within active lesions are capable of inducing axonal transection and loss by collateral bystander lysis (Babbe et al., 2000; Sobottka et al., 2009).

Axonal impairment due to demyelination

However, it remains unclear to what extent inflammatory damage is responsible for axonal impairment and loss and what is attributable to the consequences of demyelination itself. Additionally to acute axonal injury correlating with acute inflammation, axonal damage and loss has been described both in chronic, non-inflammatory lesions and in normal-appearing white matter (Ferguson et al., 1997; Trapp et al., 1998; Bjartmar et al., 2000; Evangelou et al., 2000; Kornek et al., 2000; Lovas et al., 2000). This suggests that chronic axonal loss in MS might be caused by mechanisms independent of inflammation (Chandran et al., 2008). In light of the undiscovered cause of MS, the unknown autoimmune aetiology and contradictory pathologies, it has been controversially speculated about MS being primarily a neurodegenerative disease (Trapp & Nave, 2008) and the axonopathy may be the initial event triggering autoimmunity (Silber & Sharief, 1999; DeLuca et al., 2006).

Axonal impairment and loss might even underlie the biphasic occurrence of MS. Neurological deficits during the early relapsing-remitting phase of the disease, originating in inflammation-mediated functional axonal impairment and damage as well as the functional impact consequent to axonal demyelination, can be entirely overcome. This is likely achieved by resolution of inflammation, compensating neuronal plasticity, and remyelination restoring full functionality of surviving axons, although the latter is not necessarily required (Franklin & ffrench-Constant, 2008). When the CNS can no longer compensate for additional neuronal loss, the disease transits into a progressive course, in combination with likely secondary axonopathy occurring mostly independent of inflammation (Chandran et al., 2008; Trapp & Nave, 2008; Piaton et al., 2010). This secondary axonopathy remains untreatable, in contrast to and unaltered by efficient immunomodulatory therapies addressing the initial relapsing-remitting phase of MS, and is most probably the consequence of sustained axonal stress, mostly due to myelin loss (Coles et al., 1999; Dutta & Trapp, 2007).

Remyelination

Given the detrimental effects of myelin loss and the resulting vulnerability of the axon to additional insults, the final goal to recover and preserve neurological function after demyelinating insults to the nervous system can only be restoration of physiological tissue conditions, including myelin restoration. This process, called remyelination, occurs spontaneously following demyelination and results in regenerative restoring of entire myelin internodes on denuded axons (Fig. 1-5 A) (Franklin

& ffrench-Constant, 2008; Duncan et al., 2009). It was first described in cat spinal cord demyelination (Bunge et al., 1961) and soon thereafter was found to happen in MS lesions (Perier & Gregoire, 1965). Tissue reconstruction by remyelination is complete, although it results in thinner and shorter myelin sheaths (Blakemore, 1974). This effect is probably due to altered signalling of adult, established axons, as myelination of de-novo generated axons in the adult is impeccable (Rivers et al., 2008). Original g-ratio dimensions typical for developmental myelination are never attained in most tissues following repair (Ludwin & Maitland, 1984; Stidworthy et al., 2003). Remyelination is orchestrated by an interplay of signalling events that generally resemble those seen in developmental myelination, but also differ in distinct aspects; and whose regulation is generally poorly understood (see reviews: Chandran et al., 2008; Franklin & ffrench-Constant, 2008). Remyelination normally proceeds to completion following toxin-mediated myelin damage (see below) or traumatic injury, but fails to do so in inflammatory-mediated demyelination such as in MS (Franklin, 2002; Fancy et al., 2010). This failure can be seen as a specific disease feature rather than a generic failure (Franklin & ffrench-Constant, 2008).

Adult OPCs in remyelination

Remyelination requires the *de novo* generation of mature oligodendrocytes: Remyelinated areas contain more oligodendrocytes than normal white matter (Prayoonwiwat & Rodriguez, 1993) and areas depleted of oligodendrocytes are remyelinated nonetheless (Sim et al., 2002). Besides, mature oligodendrocytes remaining in or transplanted into demyelinated areas do not form new myelin and can only form new myelin segments within a very brief time early in differentiation (Targett et al., 1996; Keirstead & Blakemore, 1997; Crang et al., 1998). Remyelination instead is mediated by new oligodendrocytes originating in a population of adult OPCs that are widespread in white and grey matter, and represent 5-8% of all CNS cells and the majority of proliferative cells under physiological conditions. These cells resemble developmental OPCs, although differences occur (ffrench-Constant & Raff, 1986; Horner et al., 2000; Levine et al., 2001; Dawson et al., 2003). Besides being the source of adult oligodendrocytes in repair, OPCs seem to fulfil distinct physiological roles although the full spectrum of these remains poorly understood. OPCs have a highly ramified cell architecture, contact both synapses and nodes of Ranvier with their processes, receive synaptic input, and generate action potentials, at least in subpopulations (Bergles et al., 2000; Huang et al., 2005; Karadottir et al., 2008). OPCs can be identified by a number of markers, such as the frequently used NG2 or PDGFRα, or Nkx2.2, Ascl1 and MyT1, while oligodendroglial lineage markers such as Sox10, O4, Olig1 or Olig2 are also found in more adult oligodendrocytes or throughout the lineage (Bruce et al., 2010). Additionally, OPCs have recently been shown to be less restricted in the production of progeny than previously recognised: they can differentiate into astrocytes, oligodendrocytes, neurons or even

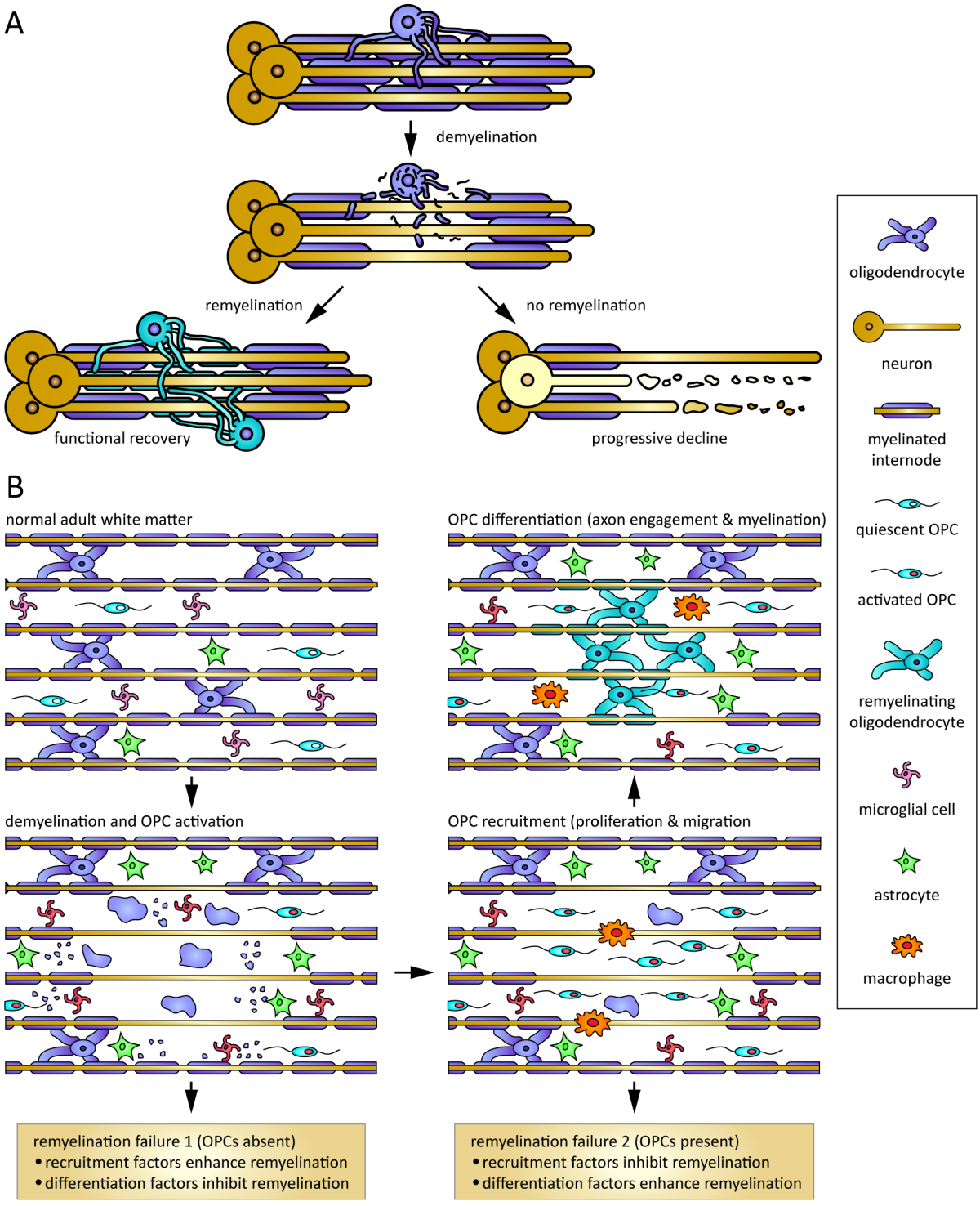

Fig. 1-5: De- and remyelination and its consequences.

(A) After demyelination two fates are possible for the affected axons. The general fate as seen in most animal models is remyelination by newly generated oligodendrocytes. If remyelination fails under certain circumstances such as occurring often in multiple sclerosis, the axon and even the neuron will be vulnerable to degeneration. **(B)** During the phases of remyelination, normal white matter houses quiescent astrocytes, microglia and oligodendrocyte precursor cells (OPCs). Following demyelination, microglia become activated and in turn activate OPCs. Activated OPCs proliferate and migrate, thereby repopulation the demyelinated area in abundance. In the final phase of remyelination, OPCs differentiate into remyelinating oligodendrocytes. (*Adapted from Franklin & ffrench-Constant, 2008)*

Schwann cells, setting them close to adult neural stem cells (Kondo & Raff, 2000; Nunes et al., 2003; Gaughwin et al., 2006; Rivers et al., 2008; Zawadzka et al., 2010).

OPCs can also emerge from stem cells of the adult subventricular zone (SVZ), one of two neurogenic regions in the adult brain (Nait-Oumesmar et al., 1999; Menn et al., 2006). Although cells of this origin have been shown to myelinate corpus callosum fibres, a phenomenon of considerable biological interest, the relevance of this potential for myelin damage repair throughout the neuroaxis is questionable (Bruce et al., 2010).

Steps of remyelination

In response to injury, OPCs transform from rather quiescent cells into a regenerative phenotype. This change involves both a morphological as well as metabolic change including increased proliferative activity, and is thought to be mainly mediated by factors released from astrocytes and microglia in reaction to damage-dependent activation. Besides activation and ongoing proliferation, OPCs also migrate into damaged areas to repopulate them (Fig. 1-5 B).

Following recruitment of OPCs into sites of demyelination, they undergo a differentiation phase, which involves the establishment of contact with the denuded axons, differentiation into a myelin producing oligodendrocyte, and finally reconstitution of myelin internodes by enwrapping and compacting of myelin membrane protrusions (reviewed in: Franklin & ffrench-Constant, 2008; Bruce et al., 2010).

Pitfalls in remyelination

If remyelination is such a well established mechanism and the cells responsible for it are quite abundant within the CNS and quite efficient in replenishment of their pools (Chari & Blakemore, 2002), then why does it fail so frequently especially in MS? Like all regenerative processes, remyelination declines with age, especially in males, but is –although less efficient– still present in aged individuals (Franklin & ffrench-Constant, 2008). Inflammatory response to demyelination has been put in focus as a key player and source of regenerative factors that promote OPC activation, recruitment, and even differentiation (Ludwin, 1980; Raine & Wu, 1993; Morell et al., 1998; Wolswijk, 2002). Phagocytic cells are besides astrocytes key players in remyelination, as they not only sense the insult and signal accordingly, but also play a critical role in the removal of myelin debris. This activity is crucial, as remaining myelin generated during demyelination both sterically separates the axons from the environment, and as well contains proteins that inhibit OPC differentiation (Kotter et al., 2006; Syed et al., 2008). Interestingly, the availability of OPCs generally does not seem to be the limiting factor, as OPCs can even repopulate after repeated episodes of demyelination

(Penderis et al., 2003), although this might be different with sustained insults (Mason et al., 2004). OPCs could of course be a direct target of disease mechanisms, but a failure in recruitment, differentiation or maturation is more likely. Although failed recruitment due to perturbed guidance clues is occurring (Williams et al., 2007), a failure of OPC differentiation and maturation is likely the most common cause for remyelination failure in MS (Wolswijk, 1998; Chang et al., 2000; Kuhlmann et al., 2008). Chronically demyelinated plaques contain a variety of factors inhibitory to OPC differentiation (reviewed in: Franklin, 2002; Franklin & ffrench-Constant, 2008) and naked axons might contribute to the inhibition, maybe due to pathological changes or as a consequence of being chronically demyelinated (Chang et al., 2002; Charles et al., 2002). However, the inflammatory contribution to remyelination and its failure remains unclear and has been obscured in a field dominated by an immune system-centred view on MS and inflammatory animal models thereof (Franklin & ffrench-Constant, 2008).

Magnetic resonance imaging in demyelination

Key to both diagnosis and monitoring, but also to understanding the nervous system and especially demyelinating diseases, are excellent high-resolution non-invasive imaging techniques. Conventional MRI has evolved as the imaging method of choice and provided valuable insight into the disease course. It is widely used in MS diagnosis, as it proved to be reliable in monitoring dissemination of demyelinated plaques in space and time, as well as in excluding symptomatic conditions that are clinically similar to MS (Polman et al., 2005; Charil et al., 2006). MRI readouts such as gadolinium-enhanced MRI to assess BBB opening or transverse relaxation time (T2)-weighted MRI to assess brain tissue oedema, both accompanying inflammatory processes in MS lesions, have proven to be valuable diagnostic tools and are highly sensitive in detecting early pathogenesis prior to what classical neurological assessment methods allow (Leist & Marks, 2010).

Limitations of conventional MRI

Although very sensitive to inflammatory processes, conventional MRI has proven to be only weakly sensitive to tissue pathology within the lesion or even less so to diffuse white matter damage or grey matter involvement, and rather futile in the assessment of the heterogeneity of MS lesions (Bakshi et al., 2008; Filippi & Agosta, 2009). This is reflected by a generally poor association of MRI radiological statement and clinical findings. Lack of histopathological MRI specificity, especially towards axonal impairment, insensitivity and underestimation of subtle white and grey matter damage, and masking effects by cortical adaptation might underlie this ‘clinico-radiological paradox’ (Barkhof, 2002). It is widely believed that advanced, non-conventional MRI approaches –along with evolution of

conventional MRI methods– will help to overcome these limitations and will provide further insights into both lesion evolution and heterogeneity. Additionally, a stronger weighting of neurodegenerative processes rather than readouts directed towards inflammatory processes is needed (Leist & Marks, 2010).

Advanced MRI

A variety of advanced MRI methods for research or clinical use in MS have recently emerged and proven to be promising and valuable. Amongst the most promising are magnetisation transfer imaging (MTI) and diffusion tensor imaging (DTI): MTI images the exchange of water between hydrated hulls associated with macromolecules and free bulk water, and is considered a measure of macromolecular structures and thereby a good indicator of myelination and myelin integrity (Wolff & Balaban, 1994). DTI assesses diffusion of water, which is hindered in its free motion by cellular structures such as membranes and therefore underlying well defined constraints in such a structurally highly organised tissue as the CNS. By applying diffusion-weighting gradients within the magnetic field in many directions, preferred directional diffusitivity can serve as an indicator of both fibre orientation and axon/myelin integrity (Basser et al., 1994; Audoin et al., 2007). Additionally, MRI methods might prove useful in monitoring the regenerative aspect of the disease (Zivadinov, 2007).

In summary, combining different MRI methods and thereby addressing the eclectic aspects of MS pathology in a multiparametric approach will improve diagnostics and prognosis of MS, provide further insight into the disease and likely allow new applications in other neurodegenerative or demyelinating diseases. To achieve this, however, there is a strong need to validate MRI findings and correlate them with distinct underlying pathologies, both clinically and experimentally in animal disease models (Bakshi et al., 2008; Filippi & Agosta, 2009).

Animal models of demyelinating diseases and MS

To understand pathophysiological events especially in such a complex disease as MS, animal models have proven to be useful in discovering the underlying pathological mechanisms, as well as dissecting them, ultimately aiming for successful therapeutic treatments. A variety of vertebrate species has been used to study demyelinating diseases, including cats and monkeys; due to their requirements and generation times, rodents are most suitable –especially mice, given the possibility and availability of various genetic modifications in these animals. Animal models for demyelinating diseases can be classified into three major categories: 1) genetic models, where genes important for CNS myelination, myelin maintenance or glial function have been altered; 2) immune-mediated

models of induced pathogenesis towards myelin; and 3) toxin-mediated models using toxic substances that preferentially affect myelin.

Genetic mouse models of demyelination

Genetic mouse models with perturbed growth factor, myelin or oligodendroglial gene function have provided fundamental insights into the process of myelination and myelin maintenance, as well as the interplay of myelinating cells within the parenchyma (for further details, see: Nave & Trapp, 2008; Miller & Fyffe-Maricich, 2010). Although they have proven to be extremely valuable for our understanding of inherited demyelinating diseases, such as hereditary motor and sensory neuropathies (Suter & Scherer, 2003) or Pelizaeus-Merzbacher disease (Nave & Trapp, 2008; Nave, 2010a), they offered only limited insights into the consequences of and the events following the loss of intact adult oligodendrocytes.

Inflammatory demyelinating models

Immune-mediated models of demyelination on the other hand have proven extremely valuable in mimicking the disease pathology of MS and identifying key inflammatory components and players, but their complexity hampers the understanding of single events. Some of the immune-mediated models involve virally-mediated inflammatory demyelination, using Theiler's, mouse hepatitis or Semliki Forest virus injections into the CNS (Knobler et al., 1982; Bradl & Linington, 1996), direct injections of LPS (Felts et al., 2005), or peroxynitrite scavengers (Touil et al., 2001). An intermediate form between transgenic and inflammatory models uses tumour necrosis factor (TNF) expression in CNS glia (Akassoglou et al., 1998). Nonetheless, the most prominent inflammatory model is experimental autoimmune encephalomyelitis (EAE). EAE is the model of choice in MS research, as it resembles most closely the overall disease pathology. It was established nearly a century ago by immunizing animals with CNS components (Rivers & Schwentker, 1935; Mix et al., 2010). In mice, depending on background of the host strain and antigen stimulation used for immunisation, the disease pattern varies and can result both in relapsing-remitting EAE, mimicking the early phase of MS, or in monophasic chronic EAE simulating late events in MS disease course (Baxter, 2007). Additionally, focal EAE models to affect certain CNS regions have been developed (Merkler et al., 2006). Although EAE has illuminated major pathways and mechanisms in immune-mediated demyelination (Miller & Fyffe-Maricich, 2010), especially in combination with transgenic alterations of host mice (for further insight, refer to: Scheikl et al., 2010), it displays some limitations as an MS animal model. The dissimilarity between EAE model variants and its close but not entire resemblance of MS in humans has led to confusions and partially hampered the understanding of cellular events underlying MS disease correlates. Additionally, the outcome regarding therapeutic approaches was

limited (Sriram & Steiner, 2005; Friese et al., 2006; Croxford et al., 2011). Despite its limitations, EAE remains a valuable and even crucial tool in inflammatory demyelination research, when used appropriately (Gold et al., 2006).

Toxin-mediated demyelination models

Unfortunately, to study the events involved in demyelination and remyelination in a sequential manner, both mutation-mediated and inflammatory models exhibit the disadvantage of diffuse onset and unsynchronised events, and therefore complicate the understanding of the distinct mechanisms. To overcome this drawback, several toxin-mediated demyelination models have been developed and increased our understanding especially of remyelination (Blakemore & Franklin, 2008). Feeding mice with chronic low doses of the copper-chelator cuprizone leads to a specific and local insult to oligodendrocytes, especially within the corpus callosum, finally leading to oligodendroglial apoptosis and demyelination, followed by remyelination after removal of the toxin (Blakemore, 1972; Matsushima & Morell, 2001; Kipp et al., 2009). Application of irradiated chow exhibits similar, but more wide-spread effects (Duncan et al., 2009). In contrast, focal injections of lysolecithin or ethidium bromide result in efficient, locally restricted demyelination and fast subsequent remyelination within white matter tracts, and allow detailed studies of the well orchestrated sequential steps of de- and remyelination (Woodruff & Franklin, 1999; Blakemore & Franklin, 2008). Unfortunately, the specificity of these toxins towards myelinating oligodendrocytes is limited, and the models are confined in their spatial distribution within the CNS. To overcome these handicaps, genetically mediated, cell-type specific expression of toxins has been used. However, in these models, toxin expression has been either limited to development and differentiation states of myelinating glia (Messing et al., 1992; Brockschnieder et al., 2004; Jalabi et al., 2005) or directed towards non-CNS cell types (Lee et al., 1998; Saito et al., 2001; Ivanova et al., 2005).

In-vitro models

In vitro models of myelination/demyelination do not really mimic the complex pathology and factorial interplay in CNS myelin damage and disease, but provide useful tools to dissect certain aspects. Myelinating slice cultures of CNS tissue have provided valuable insight into myelination and the influential role of the immune system on CNS myelin (Birgbauer et al., 2004; Mi et al., 2009; Sobottka et al., 2009). Unfortunately, these models at best simulate early events due to their origin from developing tissues. Co-culturing of myelinating glia with neurons has proven to be a very helpful technique to investigate manipulations of one or the other side of the axoglial interplay, but they fail completely to simulate the complex orchestra of CNS glial networks and interplay (Fex Svenningsen et al., 2003; Wang et al., 2007; Paivalainen et al., 2008; Chen et al., 2010).

Study aim and genetic tools

All these models together have provided extensive knowledge regarding demyelination and MS as well as general aspects of CNS glia and repair, but a more integrated view on the different models as well as additional models are needed to deepen the insight into specific aspects and mechanisms underlying both general CNS function as well as diseases such as MS (Gold et al., 2006; Mix et al., 2010). Of special interest are additional models that focus on examining issues outside of the "autoimmune hypothesis" of MS (Sriram & Steiner, 2005) and address pathologies currently underrepresented, like type III/IV MS lesions, that currently still lack an animal model (Lassmann et al., 2001). Understanding the consequences implicated in the loss of adult, myelinating oligodendrocytes originating in the glial cell, as well as debarring the immune system during triggering of demyelination will shed light on the different contributions to neuronal tissue damage in MS and demyelinating diseases (Kassmann & Nave, 2008). A model of selectively induced demyelination by targeted adult cell death of oligodendrocytes would allow dissection of the neural responses involved in de- and remyelination, as well as provide insight into the interdependency of oligodendrocytes and axons and might hold a key to understand their metabolic relationship (Miller & Fyffe-Maricich, 2010; Nave, 2010b).

Transgenic approach

The following study addresses these aims by the generation of a mouse model for systemic demyelination, using genetically-mediated, intrinsic, spatially and temporally controlled triggering of cell death in myelinating glia. To generate the mouse model, I used two established transgenic mouse lines (Fig. 1-6 A). First, a mouse line expressing the causes recombination protein (Cre) of bacteriophage P1 (Sternberg & Hamilton, 1981) fused to a modified ligand binding domain of the human estrogen receptor (CreERT2) (Feil et al., 1997), resulting in a recombination inactive enzyme in the absence of tamoxifen (TAM) (Leone et al., 2003). Here, CreERT2 is expressed under the control of the mouse *PLP*-promotor and its expression is therefore restricted to myelinating glia. This *PLP:CreERT2* line was combined with a transgene allowing Cre-dependent expression of diphtheria toxin fragment-A (DT-A) in the ubiquitous *ROSA26* locus (Brockschnieder et al., 2004; Brockschnieder et al., 2006). The myelinating glia-specific expression of CreERT2, as well as the TAM-administration-dependent enzyme activity, allows spatial and temporal control of DT-A expression. Intracellular expression of DT-A, subsequent to TAM-mediated transgene recombination, will induce apoptotic cell death by triggering both intrinsic and extrinsic apoptotic pathways (Fig.1-6B). DT-A ribosylates elongation factor 2 (EF-2) (Collier, 1975) resulting in both activation of Fas-associated death domain (FADD) (Thorburn et al., 2003) as well as protein synthesis block (Collier, 2001). Both pathways will

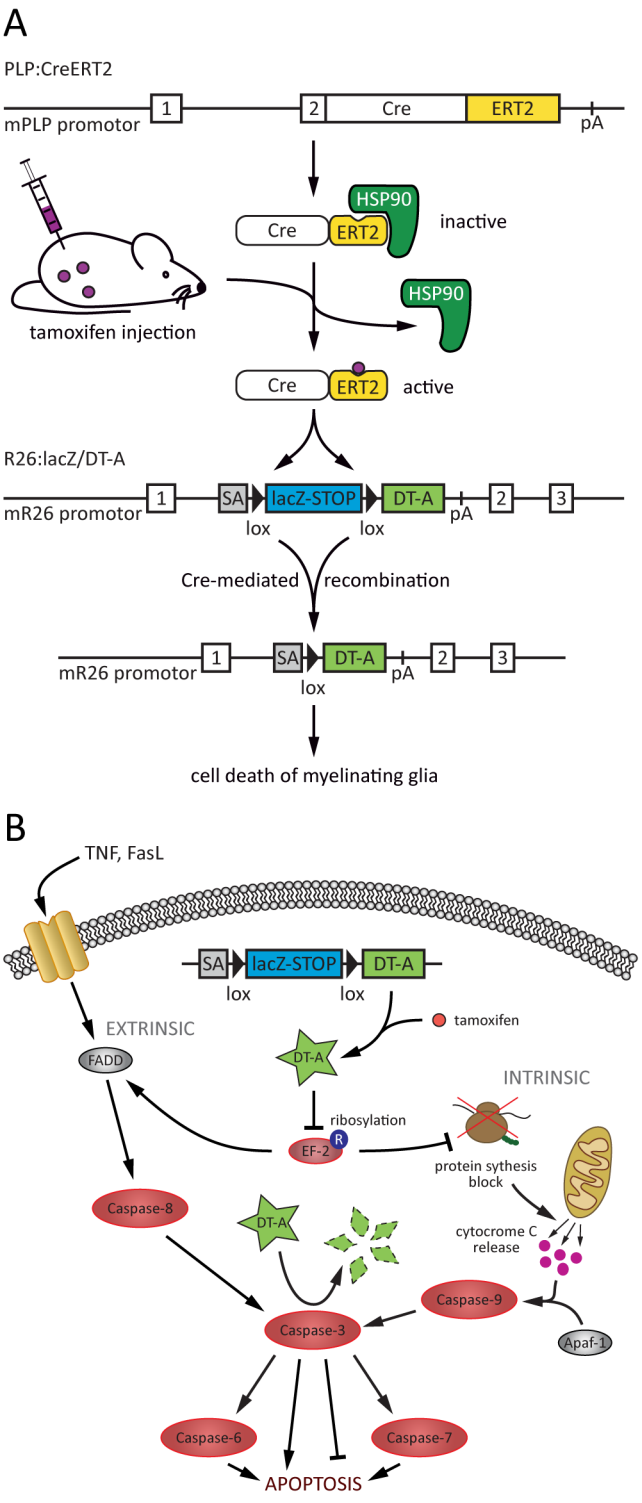

Fig. 1-6: Transgenic approach and DT-A action.

(A) Mice doubly transgenic for *PLP:CreERT2* and *R26:lacZ/DT-A* will express diphtheria toxin fragment A (DT-A) and induce cell death in myelinating glia upon tamoxifen administration. **(B)** DT-A expression triggers both intrinsic and extrinsic apoptotic pathways via ribosylation of elongation factor-2 (EF-2). DT-A is subsequently inactivated by effector caspases.

trigger downstream caspase cascades and finally induce apoptotic cell death, regardless of the proliferation state of the cell (Senchenkov et al., 2001). Using TAM-mediated DT-A expression via an inducible *Cre* line has many advantages: 1) Inducible Cre-mediated recombination and target gene expression is fast, timely defined, and efficient (Brocard et al., 1997; Leone et al., 2003); 2) diphtheria toxin is a highly potent inducer of apoptosis at extremely low intracellular concentrations (Yamaizumi et al., 1978); and 3) bystander effects on non-targeted cells are extremely unlikely, given that diphtheria toxin is cleaved and inactivated by the consequently activated caspases (Epinat & Gilmore, 1999), DT-A lacking the receptor binding-mediating B-domain exhibits very limited toxicity when applied extracellularly (Collier, 2001), mice are very insensitive to extracellular diphtheria toxin (Middlebrook & Dorland, 1977; Pappenheimer et al., 1982), and release of cytosolic components is very unlikely following apoptotic events.

Thus generated double-transgenic animals turned out to have many of the characteristics desired of a novel mouse model of primary oligodendrogliopathy, and are described here.

Material and Methods

Materials

General chemicals and solutions

All solid chemicals were obtained from Sigma-Aldrich, all organic liquids from Merck, if not stated otherwise. All solutions are water-based, if not stated otherwise.

	MilliQ processed water all buffers were prepared in MilliQ processed water
EtOH	Ethanol absolute
PBS	phosphate buffered saline, pH 7.25 140 mM NaCl, 30 mM KCl, 6.5 mM , 1.5 mM
TBS	Tris buffered saline, pH 7.5 200 mM NaCl, 50 mM Tris-HCl
PB	0.1 M phosphate buffer, pH 7.5 193.5 ml 0.4 M , 56.5 ml 0.4 M , 750 ml
Standard BB	standard blocking buffer 10 % foetal calf serum (Brunschwig), 1 % bovine serum albumin, 0.1 % Triton X-100, in PBS
Citrate buffer	18 ml 0.1M citric acid, 82 ml, 0.1 M sodium citrate tribasic trihydrate, 900 ml , pH 6.0
Basic AGR buffer	Basic antigen retrieval buffer, pH 9.0 40 mM Trizma®-base, 1.3 mM EDTA, pH 9.0

Markers

protein standard	precision plus protein standard (BIO-RAD)
DNA standard	1 kb DNA ladder (MBI Fermentas)

Primary antibodies

α-APP	mouse monoclonal (Millipore), 1:400 (IF)
α-B220	rat monoclonal (BD Biosciences), 1:200 (IHC)
α-Caspr	mouse monoclonal (NeuroMab), 1:400 (IF)
α-CD4	rat monoclonal (BD Biosciences), 1:200 (IHC)
α-CD8	rat monoclonal (BD Biosciences), 1:200 (IHC)
α-CNPase	mouse monoclonal (Sigma), 1:500 (WB), 1:100 (IF)
α-degMBP	rabbit monoclonal (Millipore), 1:1’000 (IHC)

α-GAPDH	mouse monoclonal (Hytest), 1:10'00 (WB)
α-GFAP	rabbit polyclonal (Dako), 1:500 (IF/IHC)
α-GFP	rabbit polyclonal (Molecular Probes), 1:200 (IF)
α-Iba-1	rabbit polyclonal (WAKO Chemicals), 1:300 (IF/IHC)
α-IdU	mouse monoclonal (BD Biosciences), 1:50 (IF)
α-Kv1.2	mouse monoclonal (NeuroMab), 1:200 (IF)
α-MBP	rat polyclonal (AbD Serotec), 1:300 (IF/IHC), 1:1'000 (WB)
α-MOG	mouse serum (in house), 1:50 (WB)
α-NF-M	rabbit polyclonal (Millipore), 1:300 (IF/IHC)
α-NG2	rabbit polyclonal (Millipore), 1:500 (IF)
α-non-phospho-NF (SMI32)	mouse monoclonal (Abcam), 1:1'000 (IF/IHC)
α-Olig2	rabbit polyclonal (Millipore), 1:500 (IF)
α-Sox10	goat serum (SantaCruz), 1:50 (IF)

Secondary antibodies

α-goat Cy3	donkey monoclonal (Jackson Lab), 1:500 (IF)
α-mouse AP	goat monoclonal (Promega), 1:5'000 (WB)
α-mouse Cy2	goat monoclonal (Jackson Lab), 1:500 (IF)
α-mouse Cy3	goat monoclonal (Jackson Lab), 1:500 (IF)
α-mouse biotin	donkey monoclonal (Jackson Lab), 1:500 (IHC)
α-mouse HRP	goat monoclonal (Promega), 1:5'000 (WB)
α-rabbit biotin	donkey monoclonal (Jackson Lab), 1:500 (IHC)
α-rabbit FITC	goat monoclonal (Jackson Lab), 1:500 (IF)
α-rabbit Cy3	goat monoclonal (Jackson Lab), 1:500 (IF)
α-rat AP	goat monoclonal (Promega), 1:8'000 (WB)
α-rat biotin	donkey monoclonal (Jackson Lab), 1:500 (IHC)
α-rat Cy2	goat monoclonal (Jackson Lab), 1:500 (IF)
α-rat Cy3	goat monoclonal (Jackson Lab), 1:500 (IF)

Primer

Oligonucleotide primer were obtained lyophilised from Microsynth. The following primer combinations were used for genotyping PCR in the annotated concentrations, yielding amplified fragments in the annotated sizes:

To detect *PLP:CreERT2*:

Cre for	5' ACC AGG TTC GTT CAC TCA TGG 3'	(1 µM)

Cre rev	5’ AGG CTA AGT GCC TTC TCT ACA C 3’	(1 µM)

Fragment sizes: 217 bp for *Cre*$^{+}$, none for *Cre*$^{-}$

To detect *R26:lacZ/DT-A*:

DT322up	5’ TCA CTG AAC CGT TGA TGG AGC AAG TC 3’	(1 µM)
DT529lo	5’ TAC ATC GCA TCT TGG CCA CGT TTT C 3’	(1 µM)

Fragment sizes: 208 bp for *DT-A*$^{+}$, none for *DT-A*$^{-}$

To detect *R26:lxSTOP/eYFP* and *R26:lxSTOP/lacZ*:

R26R SoA	5’ AAA GTC GCT CTG AGT TGT TAT 3’	(1 µM)
R26R SoB	5’ GCG AAG AGT TTG TCC TCA ACC 3’	(1 µM)

Fragment sizes: 260 bp for *YFP/lacZ*$^{+}$, none for *YFP/lacZ*$^{-}$

To detect *Rosa26 wt*:

R26R SoA	5’ AAA GTC GCT CTG AGT TGT TAT 3’	(1 µM)
R26R SoC	5’ GGA GCG GGA GAA ATG GAT ATG 3’	(1 µM)

Fragment sizes: 280 bp for *R26:wt*$^{+}$, none for *R26:wt*$^{-}$

To detect *RAG-1*:

oIMR 0189	5’ TGG ATG TGG AAT GTG TGC GAG 3’	(1 µM)
oIMR 1764	5’ GAG GTT CCG CTA CGA CTC TG 3’	(1 µM)
oIMR 3104	5’ CCG GAC AAG TTT TTC ATC GT 3’	(0.5 µM)

Fragment sizes: 474 bp for *RAG-*, 530 bp for *RAG-1*^{null}

Instruments

Behavioural test	Rotarod (TSE Systems)
Cryostat	HM560 (Microm)
Densitometer	GS-800 (BIO-RAD)
Electron microscope	Morgani 268 (FEI)
Fine microtome	Ultracut E (Leica)
Gel electrophoresis equipment	(BIO-RAD)
Isoflurane disperser	Combi-Vet anaesthetic system (Rothacher)
Light & fluorescence microscope	Zeiss AxioImager A1 or Axioplan2 with AxioCam MRc5 (Zeiss) confocal microscope TCS-SP1 (Leica) binocular Stemi 2000-C with light source KL1500 (Zeiss)
Magnet tomograph	Pharmascan 47/16 (Bruker BioSpin MRI) with birdcage transmit-receive coil (qT2 and MTR) and cryogenic transmit-receive radiofrequency (RF) surface coil (Ratering et al., 2008) (DTI)
Medical film processor	FPM-100A (FUJIFILM)
Microwave	Histoprocessor T/T MEGA (Milestone)
Paraffin tissue processor	TPC15 Duo and embedding station TES99 (Medite)
PCR Thermocycler	Biometra® T3000 (BIOLABO)
Rotary microtome	HM355S (Microm)
Software	Axiovision 4.5 (Zeiss)

	Photoshop CS4 (Adobe) ImageJ (NIH) Quantity One (BIO-RAD) Excel 2007 (Microsoft)

Mouse lines

C57Bl/6j	wild type (Elevage Janvier)
PLP:CreERT2	expression of tamoxifen-inducible Cre under control of the mouse proteolipid-protein gene regulatory region (Leone et al., 2003)
P0Cx32:CreERT2	expression of tamoxifen-inducible Cre under control of the rat myelin protein zero promoter fused to untranslated regions of the human connexin32 gene (Leone et al., 2003)
R26:lacZ/DT-A	expression cassette under the control of the mouse *Rosa26* promoter, expressing β-galactosidase normally, but diphtheria toxin fragment A upon Cre-mediated recombination (Brockschnieder et al., 2006)
R26:lxSTOP/eYFP	expression cassette under the control of the mouse *Rosa26* promoter, expressing enhanced yellow fluorescent protein upon Cre-mediated recombination (Srinivas et al., 2001)
R26:lxSTOP/lacZ	expression cassette under the control of the mouse *Rosa26* promoter, expressing β-galactosidase upon Cre-mediated recombination (Soriano, 1999)
RAG-	deleted gene locus for recombination activation gene 1, necessary for differentiation of functional lymphocytes (Mombaerts et al., 1992)

Methods

Generation, maintenance, treatment and scoring of mice

Generation and maintenance

The previously characterized mouse lines *PLP:CreERT2* (Leone et al., 2003) and *R26:lacZ/DT-A* (Brockschnieder et al., 2006) were crossed to obtain double transgenic *PLP:CreER/DT-A* model mice allowing spatially and temporally controlled induction of cell death of myelinating glia. The mouse lines *PLP:CreERT2* (Leone et al., 2003) and Cre-dependent *R26:lxSTOP/eYFP* (Srinivas et al., 2001) or *R26:lxSTOP/lacZ* (Soriano, 1999) were crossed to analyse recombination efficiency. *PLP:CreER/DT-A* double transgenic mice were crossed with *RAG-* mice (Mombaerts et al., 1992) until *RAG-1*-deficient mice double-positive for *PLP:CreER/DT-A* were obtained. *P0Cx32:CreERT2* mice (Leone et al., 2003) were used in combination with *R26:lacZ/DT-A* transgenes to monitor long term effects of DT-A expression in the PNS. None of these transgene combinations showed any alterations in the absence

of recombination induction. Mice were housed under a normal light/dark circle (12/12h) with standard rodent chow and tap water ad libitum at defined pathogen exposure. All experiments were carried out in strict adherence to the Swiss Law for Animal Protection, and were approved by the veterinary office of the Canton Zurich, Switzerland.

Genotyping

Genotypes were determined by PCR on genomic DNA derived from ear punch biopsies according to published protocols (Leone et al., 2003; Brockschnieder et al., 2006). In short, biopsy material was incubated for 30 min in 100 µl lysis buffer (25 mM NaOH, 0.2 mM disodium EDTA, pH 12) at 95°C to obtain genomic DNA and the reaction was stopped with 100 µl neutralising buffer (40 mM Tris-HCl, pH ~5) and stored at 4°C (Truett et al., 2000). Polymerase chain reaction (PCR) was used to amplify DNA fragments of interest. PCR reaction to detect a single transgene in one mouse was mixed as follows:

	for *PLP:CreER, DT-A* and *YFP*	for *RAG-1*
H2O	21.25 µl	19.45 µl
10x PCR buffer (Invitrogen)	3 µl	3 µl
50mM	0.9 µl	1.2 µl
Primer (each, see above)	1.5 µl	1.5 µl
dNTPs (10 mM each, Invitrogen)	0.6 µl	0.6 µl
Template solution from digest	1 µl	1 µl

PCR reaction was carried out using the following programs:

	for *PLP:CreER, DT-A* and *YFP*		for *RAG-1*		
initial denaturation	95°C	2 min	95°C	2 min	
denaturation	94°C	30 s	94°C	30 s	} 35 cycles
primer annealing	54°C	45 s	58°C	45 s	
fragment elongation	72°C	45 s	72°C	45 s	
final elongation	72°C	5 min	72°C	5 min	
cooling	4°C	hold	4°C	hold	

Fragments amplified via PCR were visualised using agarose gel electrophoresis. After PCR, 15 µl of the reagent solution were mixed with 5 µl 4x orange loading dye (20% Ficoll®, 50 mM EDTA, pH 8, OrangeG), loaded onto a 1.2 % (2.5 % for *RAG-1* detection) agarose gel in 1x TAE buffer (40 mM Trizma®-base, 20 mM glacial acetic acid, 1 mM EDTA, pH 8), and fragments were separated in an electrical field by applying 10 V/cm. Ethidium bromide (1 µg/ml) mixed into the gel before casting was used to visualise DNA under UV light.

Treatment and clinical assessment

Mice at the age of 8-12 weeks were used. Induction of DT-A, YFP or β-galactosidase expression in experimental mice was achieved by intraperitoneal (i.p.) injections of 2 mg TAM, dissolved in a

sunflower oil/ethanol mixture (10:1), for 5 consecutive days (first injection = day 1). Double-transgenic *PLP:CreER/DT-A* littermates injected with vehicle solution lacking TAM were used as controls (w/o TAM). Mice were monitored regularly and their impairment assessed with a specially developed clinical scoring procedure, broadly modelled after scorings used in EAE (see table 2-1) (Matthaei et al., 1989). Investigated time points were defined as follows. Onset: day 20 referring to first observable impairments (score ≤0.5); intermediate: day 34 referring to moderate impairments (score ~1.5); end stage: day 39-42 when mice reached the strongest impairment (score 3).

Table 2-1: Clinical scoring of mice following ablation of myelinating glia.

score	clinical observance	action
0.00	no clinical signs	
0.50	animal looks slightly unsteady, seems to toddle sometimes, looks slightly shaky especially when lifted at the tail	
1.00	animal looks unsteady, walks with broadened hind legs. Animal is shaking and twisting strongly when lifted by the tail. Grip force of hind legs on the cage grid is slightly reduced when lifted by the tail	
1.50	hind leg grip is clearly weakened; one leg falls occasionally through the cage grid while walking on it the animal does not lift the anus properly while walking on the table	provide food in the cage and put water bottle upright so that its reachable for the animal without sitting up
2.00	hind legs are really weak and can't suspend the animals weight properly on the plain table but are still able to be used in movement of the animal	Check mice daily from now on
2.50	struggling and shaking of the animal when lifted by the tail has stopped completely, the animal hangs still and is bend forward in mid-air; when it's put down onto the table it will touch down with the back of its head first	
3.00	animal falls frequently –at least with the hip- onto the side, especially on the plain table the animal is not instantly able to lift itself back on its feet but needs a few tries	sacrifice no later than this stage

Standard operating procedure SOP 83/2005 to determine the clinical demyelination score in PLP:CreER/DT-A-mice after initiation of glial cell death by TAM-injections. Mice were monitored at least every second day, a clinical demyelination score (left column) was given accorting to clinical appearance (middle column), and appropriate measures (right column) were taken.

EAE was induced in *C57Bl6/j* mice by immunization against MOG35-55 peptide according to standard protocols (Mendel et al., 1995). Proliferating cells were labelled by injections of iodo-deoxyuridine (IdU) (80 µg/g body weight) three times daily for five consecutive days followed by a five day wash-out period prior to sacrifice.

To obtain a more quantitative measure of behavioural abnormalities, mice were placed on a Rotarod apparatus (TSE Systems, Bad Homburg, Germany) and the time spent on the rotating rod, which was accelerating from 4 to 40 rpm was measured. Three trials per day at 4h intervals were performed every 3-4 days throughout the disease time course.

Magnetic Resonance Imaging

Group design

For MRI acquisition, 2 experimental groups composed as follows, were used. Group 1 = acquisition of qT2 maps (4 control mice (-TAM) and 8 experimental mice injected with TAM (+TAM)). Subsequent to the acquisition of qT2 maps, group 1 was split, with half of the animals used for MTI and the other half used for the acquisition of T2 post intravenous (i.v.) injections of ultra small particles of iron oxide (USPIO; 340 µmol Fe/kg, 2 ml/kg; Sinerem®, Guerbet). USPIO were injected immediately after first acquisition of qT2 maps (preUSPIO) and were followed up 24 h later (postUSPIO). Only animals spared from USPIO injections were used for time course analysis of qT2. Group 2 = acquisition of DTI maps (2 mice –TAM and 4 mice +TAM). Native qT2 acquisition was carried out at day 2, 9, 16, 23, 30, 37 and 41. T2 postUSPIO acquisition was carried out at day 3, 10, 17, 24, 31 and 38. The elimination half-life of the USPIO used is approximately 5 h (Dousset et al., 1999b) and detection of USPIO-labelled macrophages is possible for approximately 2-3 days post injection (Rausch et al., 2001). Therefore measurement intervals of 7 days should be sufficient to exclude interference of previous USPIO injections with native qT2 acquisition. MTI was performed at day 2, 9, 37 and 41 and DTI was performed at day 3, 8, 11, 35 and 39.

Animal preparation for MRI acquisition

Mice were anesthetized using 1.8 % isoflurane (Abbott) in an oxygen/air (20/80 %) mixture applied via a face-mask with integrated tooth-bar and placed on water-heated cradle. Body temperature was monitored using a rectal probe coupled to a fluoroptic module (QUASYS AG) and kept constant at 37±0.5°C. Ear bars secured reproducible positioning and reduced motion artifacts during DTI acquisition. After completion of MRI studies all animals were immediately sacrificed by transcardial perfusion fixation and the brain was removed for histological analysis.

MRI parameters

Quantitative T2 values were obtained using a multi spin echo (SE) sequence with the parameters: field-of-view (FOV) = 19 x 19 mm; matrix dimension (MD) = 132 x 132; in plane resolution of 144 x 144 µm; repetition time (TR) = 2000 ms; echo spacing (TE) = 10 ms; number of echoes = 14; number

of averages (NA) = 6 and slice thickness (SLTH) = 0.8 mm. For DTI a multi-slice spin echo-echo planar imaging (EPI) sequence was used with: number of slices (NSL) = 15; SLTH = 0.5 mm; interslice gap = 0.25 mm; FOV = 20 x 15 mm; MD = 133 x 100; TE/TR = 28.3/3000 ms; b-values: 1000 s/ with 30 diffusion encoding directions. High resolution anatomical images were acquired using a standard SE-RARE sequence (Hennig et al., 1986) with FOV = 20 x 18.4 mm; MD = 256 x 256; in plane resolution of 78 x 72 µm; TE/TR = 12/3500 ms; effective echo time ( ) = 36 ms; RARE factor = 8; NA = 7; SLTH = 0.8 mm; NSL = 9. MTI was performed using a 3D-gradient echo (GE) sequence with FOV = 15 x 15 x 12 mm; MD = 60 x 60 x 48; isotropic voxel dimension of 250 ; TE/TR = 2.0/30.0 ms; flip angle: 30°. A Gaussian pulse with pulse length of 1 ms, a B1 amplitude of 80 µT and an offset frequency of 5 kHz was used for saturation of the bound water fraction. The reference sequence was obtained using the same parameters without application of the saturation pulse.

Image analysis

To calculate T2-maps, images from the same animal were manually co-registered, and T2 values were plotted as a function of time for the defined regions of interest. MTR maps were calculated using Biomap (M. Rausch) with MTR calculated as MTR (%) = (/)×100, where and are the signal magnitude in the absence of a saturation pulse (control experiment) and the steady-state signal magnitude during MT saturation, respectively. Calculations of the invariant DTI-based parametric maps, performed on a voxel-by-voxel basis, were done using in-house developed software routines written in IDL (RSI). Diffusion-weighted images were processed to generate the six independent elements of the diffusion tensor D. A real eigenvalue decomposition of the symmetric tensor D defines the matrix of orthonormal eigenvectors and the diagonal matrix comprising the eigenvalues (, and). Quantitative invariant indices, such as axial diffusivity ($\lambda_{\parallel}$ =), radial diffusivity ($\lambda_{\perp}$ = (+)/2), and fractional anisotropy (FA) according to Le Bihan et al. (Le Bihan et al., 2001), were calculated. FA, as a measure of the directionality of the water diffusion within a given voxel, by definition ranges between 0 (isotropic) and 1 (maximally anisotropic). Eigenvector colour-coded DTI maps were generated using ParaVision® Jive (Bruker BioSpin MRI).

Statistical analysis of MRI data

All calculated parasagittal T2 maps from the same animal were co-registered manually and T2 values plotted for baseline (average of values of day 2 and 9) and end stage (average of values of day 37 and 41) for the defined regions of interest (ROIs). ΔT2 changes after USPIO administration in –TAM and +TAM mice were calculated as difference T2 (24 h post)-T2(pre) injection. FA, $\lambda_{\parallel}$ and $\lambda_{\perp}$ were derived by performing anatomy-based ROI analysis. Obtained values were plotted for baseline (average of values of day 3, 8 and 11) and end stage (average of values of day 35 and 39) for the defined ROIs.

Computed MTR maps were re-sliced and co-registered to high-resolution anatomical images. ROIs for quantitative analysis were defined on correlating anatomical images and the values so obtained were plotted for baseline (average of values of day 2 and 9) and end stage (average of values of day 37 and 41). All data are given as mean ± SEM or plotted as box plots (main quartiles, sample minimum and maximum). Data were statistically analysed using ANOVA and Fisher's PLSD posthoc test.

Histology

Tissue preparation and sectioning

Mice were deeply anesthetised using 150 mg/kg pentobarbital (Esconarkon®, Streuli Pharma AG) and transcardially perfused with heparin (250 mg/l) in PBS followed by fixation with 4 % paraformaldehyde (PFA)/PBS for light microscopy, or with 3 % glutaraldehyde and 4 % PFA/PB for electron microscopy. Brain and spinal cord tissues were dissected, and postfixed over-night at 4 °C. For paraffin sectioning, tissues were dehydrated (see table 2-2), embedded in paraffin (Medite), sectioned into 5 µm coronal or sagittal sections, taken up on polylysine-coated glass slides (Menzel), dried overnight at 37°C and stored at room temperature (RT). For cryo-sectioning tissues were cryo-protected with 30 % sucrose/PBS at 4 °C over-night, embedded in OCT (Medite), sectioned into 10 µm sections, taken up on Superfrost Plus® glass slides (Menzel), dried at RT for 1h, and stored at -20°C. For semi- and ultrathin resin sectioning, tissues were postfixed and contrasted with 2 % osmium tetroxide (ElectronMicroscopyService EMS), dehydrated with acetone, embedded in corrected Spurr's resin (EMS) (see table 2-3) (Ellis, 2006), sectioned into 0.5 µm or 80 nm sections, and taken up on standard glass slides (Menzel), or copper EM grids (EMS), respectively. Semithin sections for light microscopy were contrasted with 1 % toluidine blue (in 1 % borax/sodium borate) by letting the dye solution dry onto the resin sections on a heating plate and differentiating out with and EtOH. Ultrathin sections for electron microscopy were contrasted with 3 % uranyl acetate and 1 % lead citrate, each for 5 min and with three washes with in between.

Table 2-2: Paraffin-embedding procedure.

step	solution	time	temp
1	EtOH 70%	45 min	37°C
2	EtOH 80%	45 min	37°C
3	EtOH 90%	30 min	37°C
4	EtOH 96%	45 min	37°C
5	EtOH 100%	30 min	37°C
6	EtOH 100%	60 min	37°C
7	EtOH 100%	60 min	37°C
8	xylene	30 min	37°C
9	xylene	45 min	37°C
10	xylene	60 min	37°C
11	paraffin	45 min	62°C
12	paraffin	60 min	62°C
13	paraffin	60 min	62°C

Tissue dehydration and paraffin-penetration programm used for embedding of nervous system tissue in an automated tissue processor.

Table 2-3: Resin-embedding procedure.

step	solution	time	temp
1	PB	rinse	RT
2	PB	20 min	RT
3	PB	40 min	RT
4	PB	80 min	RT
5	2% OsO_4	ON	4°C
6	PB	rinse	RT
7	PB	20 min	RT
8	PB	40 min	RT
9	PB	80 min	RT
10	acetone 30 %	20 min	RT
11	acetone 50 %	20 min	RT
12	acetone 70 %	20 min	RT
13	acetone 90 %	20 min	RT
14	acetone 96 %	20 min	RT
15	acetone 100 %	20 min	RT
16	acetone 100 %	60 min	RT
17	spurr:acetone 1:2	90 min	RT
18	spurr:acetone 1:2	90 min	RT
19	spurr:acetone 1:2	90 min	RT
20	spurr pure	ON	RT
21	fresh spurr	8 h	RT

Tissue contrasting, dehydration and resin-penetration programm used for embedding of nervous system tissue. Tissues were afterwards embedded in small embedding forms and resin polymerised ON at 65°C. ON = over-night; RT = room temperature; PB = 0.1 M phosphate buffer pH 7.4.

Histological stainings with chemical stains

Luxol-Fast-Blue (LFB) and Luxol-Nissl (L-N) stainings were performed according to standard procedures. In short, sections were deparaffinised, rehydrated to 95 % alcohol, heated in 0.1 % LFB in a microwave, and staining differentiated with 0.05 % lithium carbonate followed by alcohol. For L-N, counterstaining with cresyl violet acetate was used. For Oil Red O staining, cryosections were postfixed, incubated in 60 % isopropanol, stained in Oil Red O staining solution (0.3 % Oil Red O in 60 % isopropanol) for 20 min, and washed in 60 % isopropanol and . For co-stainings, Oil Red O staining was carried out after incubation with ABC reagent mix (see below). Fluoro-Jade C staining was performed according to published protocols (Schmued et al., 2005).

Immunohistochemistry on paraffin sections

For immunohistochemistry on paraffin sections, samples were deparaffinised, rehydrated and exposed to heat-mediated antigen retrieval in citrate or basic AGR buffer using a tissue microwave oven (Medite). Endogenous peroxidase was blocked with 3 % /methanol, followed by blocking and permeabilisation with standard BB, and incubation with primary antibodies (see section antibodies above) over-night at 4 °C in blocking buffer. Sections were washed, incubated with corresponding biotinylated secondary antibodies (see section antibodies above) followed by incubation with Vectastain® ABC reagent mix (Reactolab), and developed with DAB metal enhancer solution (Thermo Scientific). Sections were counterstained with cresyl violet acetate, dehydrated, and mounted under coverslips (Menzel) in Entellan® (Merck).

Immunofluorescence on cryosections

For immunofluorescence on cryosections, samples were thawed and dried at RT, postfixed for 10 min with 4 % PFA, and washed, followed by 1 h blocking and permeabilisation with standard BB. Sections were then washed and incubated with primary antibodies (see section antibodies above) over-night at 4 °C in blocking buffer. For IdU/Olig2 stainings, prior to antibody incubation sections were exposed to antigen retrieval according to IdU supplier's recommendations. Sections were washed, incubated for 2 h at RT with corresponding fluorescence-coupled secondary antibodies (see section antibodies above), washed, counterstained with DAPI (1 µg/ml in PBS) and mounted under coverslips (Menzel) in Immu-Mount® (Thermo-Scientific).

TUNEL reaction

Slides containing cryosectioned tissue were thawed and dried at RT, postfixed for 5 min in 4% PFA, washed, and exposed to antigen retrieval in citrate buffer for 15 min at 95°C in a tissue microwave oven (Medite). After cooling down on ice and washing, slides were incubated for 1 h in TUNEL blocking buffer (foetal calf serum (Brunschwig), 1 % bovine serum albumin and 1 % Triton X-100 in PBS), washed, and any desired immunostaining was performed. Afterwards, sections were equilibrated in TdT buffer (30 mM Tris-HCl, 140 mM sodium cacodylate trihydrate, 1 mM cobalt chloride) for 10 min, and incubated in TUNEL reaction mix (8 µl TdT (TUNEL) enzyme, 6 µl biotinylated dUTP, 5 µl 1 mM dATP in 1 ml TdT buffer (all Roche)). Reactions were stopped by incubation for 10 min in 2x SSC (0.3 M NaCl, 30 mM sodium citrate dehydrate), slides were washed, and biotinylated-deoxyuridine incorporated at the ends of DNA strands was visualised with Cy3-coupled streptavidin (1:500, Jackson Laboratories, in 50% standard BB), before counterstaining with DAPI (1 µg/ml in PBS) and mounting under coverslips (Menzel) in Immu-Mount® (Thermo-Scientific).

X-gal staining assay

For X-gal staining on cryosections, samples were thawed and dried at RT, postfixed for 10 min at RT with prefix solution (2 % formaldehyde, 0.2 % glutaraldehyde in PBS), washed, and incubated over-night at 37°C with pre-warmed, freshly prepared and filtered X-gal staining solution (5 mM $(CN)_6$, 5 mM $(CN)_6$, 2 mM , 0.1 % Na-deoxycholate, 0.02 % NP40) freshly supplemented with X-gal (1 mg/ml, AxonLab). Afterwards, samples were washed, fixed for 10 min at RT with postfix solution (0.5 % glutaraldehyde in PBS), and mounted under coverslips (Menzel) in Immu-Mount® (Thermo-Scientific).

Western Blotting

Harvest of protein lysates

Mice were killed with in a dual chamber glass container using small amounts of dry ice in water in a chamber separated from the mice. Afterwards, tissue material was directly dissected, transferred into pre-weighed reaction tubes, immediately quick-frozen in liquid nitrogen, weighed to determine amount of tissue harvested, and stored at -80°C.

Tissues were homogenised using a dry-ice pre-chilled small tissue grinder (Kimble/Kontes), taken up with small volumes of pre-chilled WB lysis buffer (150 mM NaCl, 10 mM Trizma®-base, 5 mM EDTA, 1 % Triton X-100, pH 7.4, freshly added: 1 % PI (SigmaFAST proteinase inhibitor mix), 200 mM PMSF (phenylmethylsulfonylfluorid)), transferred into pre-chilled reaction tubes on ice and filled up with WB lysis buffer to tissue weight-dependent volumes (24 µl WB lysis buffer / 1 mg of nervous tissue). This weight-dependent dilution of protein lysates turned out to be far more accurate in achieving equal loading, as standard protein quantification assays are often inaccurate given the high fat content of nervous tissue. Afterwards, samples were sonicated, cleared of debris by centrifugation, and supernatants were mixed with 5x Laemmli buffer (100 mM Tris-HCl, 14.5 % glycerol, 8 % β-mercaptoethanol, 5 % sodium dodecyl sulphate (SDS), bromphenol blue, pH 6.4), heated for 10 min at 95°C, and stored at -20°C.

SDS-PAGE

SDS-polyacrylamide gel electrophoresis (PAGE) was performed according to standard procedures (Laemmli, 1970). In short, tissue lysates were denatured under reducing conditions using Laemmli sample buffer in a heat block (95°C, 10 min). The following acrylamide gels (thickness: 1 mm, 10 pockets comb: 50µl sample volume/lane) were prepared for the separation of proteins:

Stacking gel (3ml)	
ddH2O (ml)	2.1
Acrylamide (30%) (ml)	0.5
1.0M Tris-HCl pH 6.8 (ml)	0.38
10% SDS (ml)	0.03
10% APS (ml)	0.03
TEMED (ml)	0.003

Separating gel (10ml)	8%	10%	12%	15%
ddH2O (ml)	4.6	4	3.3	2.3
Acrylamide (30%) (ml)	2.7	3.3	4	5
1.5M Tris-HCl pH 8.8 (ml)	2.5	2.5	2.5	2.5
10% SDS (ml)	0.1	0.1	0.1	0.1
10% APS (ml)	0.1	0.1	0.1	0.1
TEMED (ml)	0.006	0.004	0.004	0.004

Samples and 10 µl protein standard were loaded onto the gel. Electrophoresis was performed in 1x SDS-PAGE running buffer (stacking gel at 60 V (~15 mA per gel) and separating gel at 120 V (~25 mA per gel)) until the blue dye front ran out of the gel.

Western Blotting

Proteins separated by SDS-PAGE were semi-dry blotted to a polyvinylidene fluoride (PVDF) membrane (MILLIPORE) for subsequent immuno-detection according to standard procedures. In short, membranes were primed with methanol, together with the SDS-PAGE gel assembled into a transfer stack, and blotting transfer of proteins was performed over-night (30V, 4°C) in transfer buffer (192 mM glycine, 25 mM Trizma®-base, 20 % methanol). The membrane was afterwards washed, blocked for 1 h at RT or over-night at 4°C using WB blocking buffer (10% milk powder (Migros)/TBS), incubated for 2 h at RT or over-night at 4°C with primary antibodies (see section antibodies above) in WB blocking buffer, and washed. Subsequent, the membrane was incubated for 1 h at RT with secondary antibodies (see section antibodies above), and washed. For detection of AP-conjugated secondary antibodies, the membrane was washed in AP buffer (100 mM NaCl, 100 mM Tris-HCl, pH 9.5), and incubated with CDP-Star substrate (1:100 in AP buffer, Roche). For detection of HRP-conjugated secondary antibodies, the membrane was directly incubated with ECL Plus substrate (AMERSHAM). Afterwards, membranes were exposed to photo-films (FUJIFILM,) and the films were developed. Films were scanned using a densitometer and acquired data used for quantification. To use for further detection, the membrane was washed, blocked, and eventually stripped using stripping buffer (100 mM DTT, 62.5 mM Tris-HCl, 2 % SDS, pH 6.8) for 30 min at 50°C, before incubating again with blocking buffer and antibodies. Membranes were stored in TBS at 4°C.

Evans Blue Permeability Assay

Influx of Evans blue-labelled serum albumin into brain tissue was assessed according to published procedures (Hawkins & Egleton, 2006; Ogunshola et al., 2006). In short, a 1 % solution of Evans blue dye (2 µg/g) was injected i.v. 1 h prior to sacrifice. Mice were anesthetised and transcardially perfused with PBS and brain tissue dissected. Dye retained in the tissue was extracted with formamide and absorbance measured at 620 nm.

Quantification

Vacuole counting: Tissue vacuoles were blind-counted manually on MBP-stained paraffin sections on images acquired at 40x magnifications using ImageJ counting software (open software; http://rsbweb.nih.gov/ij/), counting 8 random fields of views (FOV) on 4 different sectioning levels

per tissue of interest. Data are given as mean ± SEM and statistically analysed using Student's t-test; n (animals) = 3.

Counting of Sox10$^+$ cells and recombination efficiency: Sox10$^+$ cells were blind-counted manually on Sox10/DAPI-, SOX10/YFP/DAPI- or NG2/YFP/DAPI-stained sections on images acquired at 10x magnifications using ImageJ, counting 4 random FOV on 2 different sectioning levels per tissue of interest. Data are given as mean ± SEM and statistically analysed using Student's t-test; n=3.

Counting of proliferating OPCs [performed by Cristina Porcheri]: Proliferative OPCs were blind-counted manually on Olig2/IdU/DAPI-stained sections on images acquired at 40x magnifications using ImageJ, counting 10 random FOV on at least 3 different sectioning levels per tissue of interest. Data are given as mean ± SEM and statistically analysed using Student's t-test; n=3.

Analysis of g-ratios: Corpus callosum g-ratios were determined from more than 100 healthy appearing myelinated axons per animal on electron micrographs by manually measuring the areas of axon and myelin using Photoshop (Adobe), calculating diameters assuming circular appearance, and calculating g-ratio=(axon diameter/fibre diameter). Data were dot-plotted or given as mean ± SEM and statistically analysed using Student's t-test; n=3.

Analysis of SMI32 immunofluorescence: SMI32 immunofluorescence intensity was measured on images acquired at fixed settings of SMI32-stained cryo sections of cerebellar core area at 20x magnification using 4 FOV on 2 different sectioning levels per animal. Images were analysed using ImageJ. Mean intensity was calculated by dividing mean grey values by the area above a manually defined, fixed threshold value. Image intensity threshold was set once to exclude background signal and kept constant for all images. Mean of controls was set to 1, data are given as mean ± SEM of relative staining intensity, and were statistically analysed using Student's t-test; n=3.

Counting of nodes of Ranvier: Caspr or Kv1.2-stained spinal cord sections were imaged at 63x magnification at two different focal planes per FOV, using 5 random FOV per animal. The two focal planes were overlaid using Photoshop and the specific pattern of Caspr+ paranodes or Kv1.2+ juxtaparanodes identified and counted manually in a blinded manner. Data are given as mean ± SEM and statistically analysed using Student's t-test; n=3.

Quantification of microglia: Iba-1$^+$ cells were blind-counted manually on Iba-1-stained paraffin sections on images acquired at 40x magnifications using ImageJ, counting 6 FOV on 2 different sectioning levels. Data are given as mean ± SEM and statistically analysed using Student's t-test; n=3.

Quantification of myelin proteins: Quantification of myelin proteins was performed with low exposed photo films to avoid saturation of the photo films. Films were scanned with a densitometer and the signal intensity of the protein bands was determined using a software tool (Quantity ONE®, BIO-RAD). For statistical evaluations, relative signal intensities were calculated by the ratio of intensity of GAPDH to protein of interest. Data are given as mean ± SEM and statistically analysed using Student's t-test; n=3.

Results

Generation of a mouse line allowing ablation of mature oligodendrocytes

To create a mouse line that would allow conditional, spatially and temporally controlled ablation of mature oligodendrocytes, I crossed mice containing the *PLP:CreERT2* (Leone et al., 2003) allele with those containing the *R26:lacZ/DT-A* allele (Brockschnieder et al., 2006) (Fig.1-6). Double transgenic mice (*PLP:CreER/DT-A*) were vital and healthy, and mice homozygous for *R26:lacZ/DT-A* could be used for line maintenance and breeding of experimental animals. To assess recombination efficiency, *PLP:CreERT2*-positive mice were crossed with *R26:lxSTOP/eYFP* mice (Srinivas et al., 2001), which express the yellow fluorescent protein (YFP) upon TAM injections and subsequent Cre-mediated recombination.

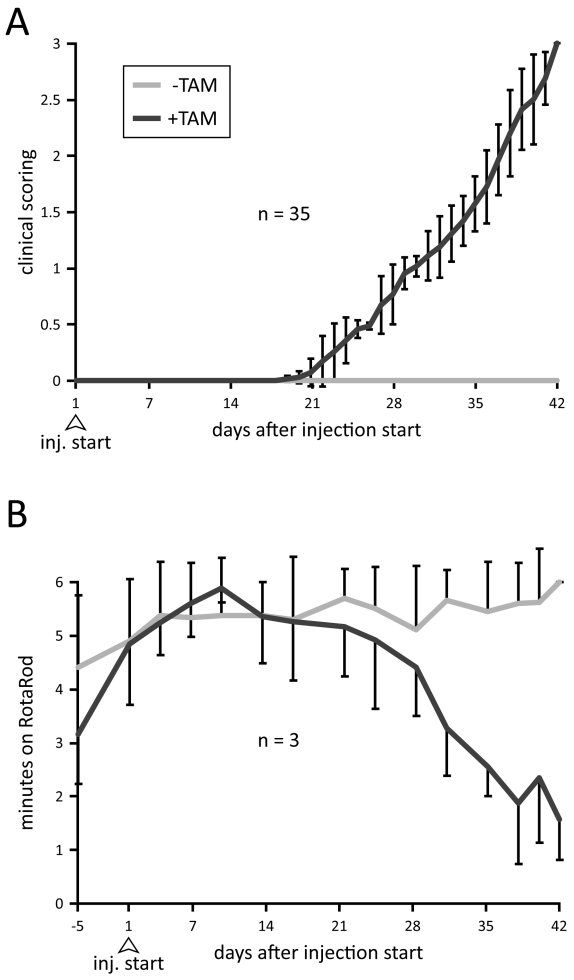

Figure 3-1: Clinical development after genetically-mediated induction of adult oligodendrocyte cell death.

(A) Time course of clinical appearance after TAM-mediated induction in 2-3 month old *PLP:Cre/DT-A* double transgenic mice (+TAM) compared to vehicle-injected control mice (-TAM), as judged by clinical scoring. After an initial lag period lasting 3 weeks, mice develop a steadily increasing clinical impairment. **(B)** Correlative performance in the Rotarod test of motor-coordinatiion. *Data are given as mean ± SD.*

Triggering of cell death in adult oligodendrocytes results in severe impairment after a latency time with a constant progressive disease course

Young adult *PLP:CreER/DT-A* mice at the age of 2-3 month were treated with 2 mg TAM/day for 5 consecutive days. These animals developed a highly consistent disease course with very little variation in onset of clinical impairment or its progression (Fig. 3-1 A). This disease course was evaluated using a specifically developed scoring assay (see Materials and Methods) to allow comparison with existing mouse models such as EAE (Matthaei et al., 1989). However, the models are quite distinct due to the nature of the initiation. Clinical progression in TAM-treated double-transgenic animals (henceforth referred to as 'experimental mice') was characterised by an initial lag period of three

weeks without evident disease signs. Around 21 days after injection start, the experimental mice showed increasing tremor and ataxia, motor deficits accompanied by muscle atrophy, and weight loss. The severity of disability increased steadily over the next three weeks and the animals could not be kept longer on welfare grounds. Such clinical changes were never observed in control animals (vehicle-injected double-transgenic animals or TAM-treated single transgenic animals of either mouse line; data not shown). Additionally, no obvious differences were found between male and female mice, but 8 month old mice showed a slightly slower clinical development. To obtain a quantitative measure of the increasing deficits, I analysed experimental and control mice using the Rotarod test (Fig. 3-1 B). The results mirrored the clinical scoring, thus confirming the strikingly uniform and steady time course of disease progression. Thus, I could show that induced cell death of adult oligodendrocytes generates a defined and clinically highly reproducible mouse phenotype.

Longitudinal quantitative T2 MRI provides a suitable method to follow pathological consequences of adult oligodendrocyte loss

Being able to trace pathological tissue changes over time within the same individual has many advantages. In particular, it is a suitable method for correlating clinical development with pathology, and enables one to detect irregularities in tissue alterations that remain unreflected by clinical impairment. Additionally, comparing observed changes in standard MRI methods with the underlying pathology in comparison with existing models might help to fine-tune statement, diagnosis and our understanding of correlation between pathologies and radiologic diagnosis in disease.

I therefore carried out serial MRI assessing quantitative T2 values throughout the disease course. Parasagittal T2 maps obtained from experimental mice showed consistent regional alterations by increasingly hyperintense areas. First changes were observable around clinical onset (day 23), especially pronounced in cerebellar core white matter, brain stem regions of pons and medulla, midbrain and cervical cord (Fig. 3-2 A). Quantification of T2 relaxation times in defined regions of interest (ROIs) (Fig. 3-2 B) revealed no changes in control mice throughout the analysis, with T2 relaxation times fluctuating only slightly around tissue-specific, physiological T2 values. Experimental mice showed a change towards increasing T2 values over time, especially in cerebellar white matter and brain stem parenchyma. This pronounced increase becomes apparent towards late time points and matched with symptomatic progression. Changes were most pronounced in white and mixed matter tissues such as cerebellar core, anterior commissure, striatum and brain stem; but not in grey matter tissues like frontal cortex (Fig. 3-2 C). A ventricular dilatation could not be verified, although minor effects cannot be excluded. Thus, longitudinal MRI using quantitative T2 is suitable for

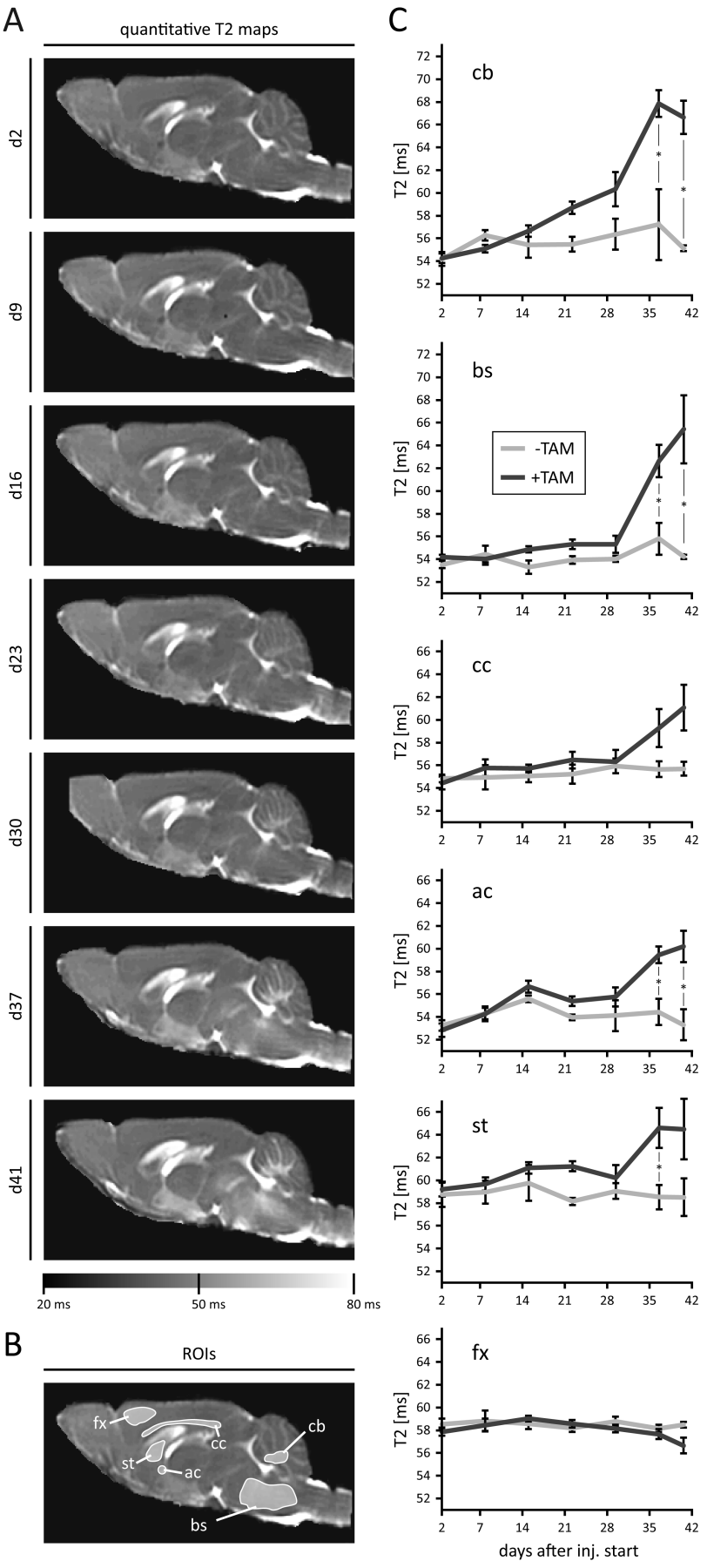

Figure 3-2: Longitudinal assessment of disease development using quantitative T2 MRI.

(A) Parasagittal quantitative T2 MRI maps of a representative experimental animal throughout the disease course after TAM injections. Hyperintensities in cerebellar core (cb), brain stem (bs), midbrain and cervical cord appear with symptomatic onset (day 23) and become pronounced with increasing clinical impairment. **(B)** Representative T2 map with superimposed ROIs used for quantifications. **(C)** Quantitative T2 values derived from ROIs in cb, bs, corpus callosum (cc), anterior commissure (ac), striatum (st) and frontal cortex (fx) throughout the disease course. In experimental animals (+TAM), significance in the increase of T2 relaxation times compared to controls (-TAM)was reached at day 37 in most white and mixed matter structures with the exception of the cc. The fx grey matter showed a slight decrease towards the end. *Data are given as mean ± SEM. n= 2 -TAM / 4 +TAM; *=p<0.05, repetitive ANOVA.*

following pathological changes due to induced cell death of adult oligodendrocytes. Both tissue alterations observed by T2 relaxation values match clinical findings and tissue disruptions cannot be detected before clinical impairment occurs. Additionally, T2 changes in accordance with clinical progression follow a similar increasing course.

To evaluate the observed changes in T2 relaxation time in more detail, an expanded comparative analysis of pooled baseline and end stage time points was performed, including preUSPIO qT2 assessments of mice later used in order to assess phagocyte infiltration (Fig. 3-3 A). To investigate differences between affected white and mixed matter towards grey matter, a special focus was put on cerebellar white matter, brainstem and frontal cortex ROIs in comparison to the olfactory bulb as

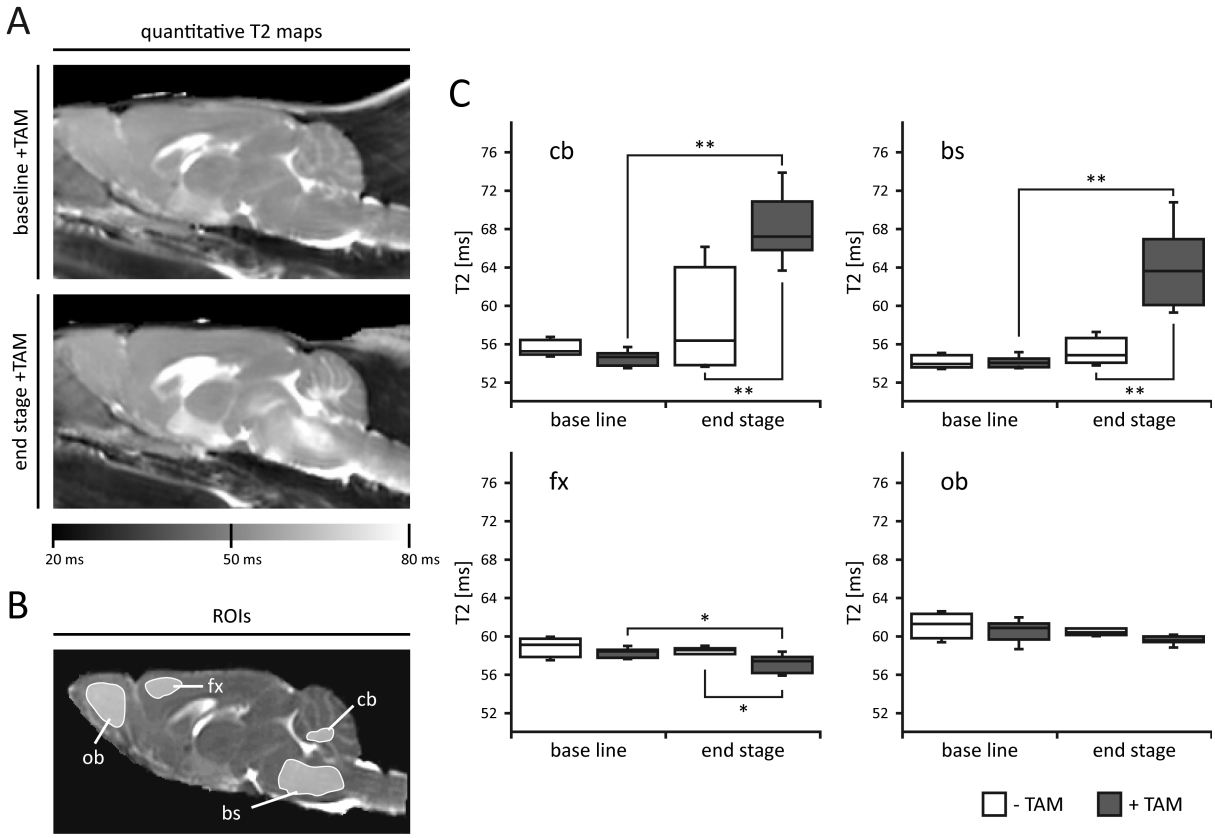

Figure 3-3: Quantitative T2 MRI in baseline and end stage experimental animals.

(A) Parasagittal quantitative T2 MRI maps of a representative animal at baseline (day 3) and end stage (day 41) after TAM-mediated ablation of oligodendrocytes. Hyperintense areas are obvious in brain stem and cerebellar core at end stage. **(B)** Representative T2 map with superimposed ROIs used for quantifications. **(C)** Box plots of T2 relaxation times derived from ROIs cerebellar core (cb), brain stem (bs), frontal cortex (fx) and olfactory bulb (ob) at baseline (pooled day 2 and 9) and end stage (pooled day 37 and 41) control (-TAM) and experimental (+TAM) animals. Both white and mixed matter of cb and bs show significant increase in T2 relaxation times, while fx grey matter shows a light but significant decrease compared to baseline +TAM or control. No changes were found in ob tissue used as an internal control. *Data are given as median, 1st and 3rd quartiles, sample minimum, sample maximum. n= 4 -TAM / 8 +TAM; *=p<0.05, **=p<0.01, ANOVA and Fisher's PLSD posthoc test.*

an internal control (Fig. 3-3 B). Quantitative T2 values revealed comparable values for both control and experimental animals at baseline in pre-symptomatic animals, indicating no detectable pathological changes during acute oligodendrocyte cell death (Fig. 3-3 C). Experimental animals at end stage showed strongly increased T2 values in the cerebellar white matter or the mixed matter brainstem compared to control animals at end stage, or compared to both control and experimental animals at baseline. Interestingly, a slight decrease of T2 relaxation times was found in the grey matter of the frontal cortex of experimental mice at end stage compared to base line or control animals, while no changes could be observed in the olfactory bulb between the groups. These data suggest both high sensitivity as well as reliability of detected T2 value changes in response to tissue disruption following ablation of adult oligodendrocytes. Taken together, T2-based MRI is well suited to monitor pathological changes following oligodendrocyte death non-invasively and can be used to monitor effects of disease modulating experimental strategies.

Efficient and immediate loss of oligodendrocytes follows genetically-mediated cell death induction

To determine both efficacy and dynamics of the loss of oligodendrocytes following genetically triggered cell death, I used the pan-oligodendroglial marker Sox10 (Wegner, 2001; Rivers et al., 2008) at representative time points of phenotypic development: Before TAM-mediated induction; early during acute cell death at days 3, 6 and 11; at onset of clinical signs (day 20); intermediate stage (day 34); and end stage (day 39-42). Oligodendrocyte densities varied distinctly between different CNS tissues under physiological conditions (Table 3-1). Densities of $Sox10^+$ cells are strongly decreased in experimental animals at disease end stage with reductions ranging between 60% and 80% in white and mixed matter tissues (Fig. 3-4 A). Interestingly, the frontal cortex grey matter showed only an unincisive reduction in oligodendrocytes. Further analysis of different sequential time points throughout the disease course was performed on exemplary white, grey and mixed matter tissues (Fig. 3-4 B). The loss of $Sox10^+$ cells is immediate upon TAM-injection, beginning as early as day 3 of TAM treatment and reaches maximal ablation 11 days after treatment start. The reduction reached for most tissues is approximately 80%, except for the frontal cortex showing 60% reduction. Although oligodendroglial cell loss is immediate and pronounced, with more than 500 cells/ disappearing within a few days in cerebellum or brain stem (Table 3-1), only a minor increase of $TUNEL^+$ cells (Fig. 3-4 C) to approximately 2 cells/ could be detected. Only a minute proportion of apoptotic cells could be identified as oligodendroglial cells. Additionally, no oligodendroglia positive for cleaved caspase-3 and no overall increase in cleaved-caspase-3 could be observed (data not shown). Neither could DT-protein be detected after TAM-mediated expression induction (data not shown).

Table 3-1: Densities of oligodendrocytes in end stage and control tissues.

	Sox10+ cells / mm^2				
	control	day 11	p-value	end stage	p-value
cb	651.42 ±37.6	76.15 ±10.0	0.00002	143.27 ±59.5	0.0002
bs	659.46 ±80.8	78.48 ±6.6	0.0002	297.28 ±76.6	0.0049
ac	1524.60 ±257.1	n.a.	n.a.	597.19 ±174.2	0.0066
cc	1119.41 ±261.9	161.61 ±22.1	0.0033	396.15 ±53.4	0.0094
spc wm	599.73 ±149.4	n.a.	n.a.	113.84 ±47.5	0.0058
spc gm	490.60 ±62.7	n.a.	n.a.	160.60 ±31.2	0.0012
fx	123.27 ±61.8	52.96 ±5.5	0.0488	89.43 ±31.3	0.46

Listed are the ascertained densities of Sox10+ oligodendrocyte cells in cerebellar white matter (cb), brain stem (bs), anterior commissure (ac), corpus callosum (cc), spinal cord white (spc wm) and grey (spc gm) matter, and frontal cortex (fx) in diseased mice at end stage and in day 11 mice compared to control animals. *Data are given as mean ± SEM. n=3; n.a.=not assessed; p-values obtained with Student's t-test.*

The observed reductions in oligodendroglial cells found are in line with recombination efficiencies found in these tissues using the Cre-dependent *R26:lxSTOP/eYFP* reporter mouse line combined with the *PLP:CreERT2* line and identical TAM regimens (Fig. 3-4 D). In the same experimental setting, a fraction of OPCs was also found to be recombined (Fig. 3-4 E). These recombined cells likely represent more mature OPCs, given that *plp-gene* activity is associated with differentiation (Levine et al., 2001; Mallon et al., 2002). The lower efficiency in recombination or ablation of cells throughout the whole oligodendroglial population in the grey matter of the frontal cortex is not surprising, given that at least 30% of this population are $NG2^+$ OPCs (Rivers et al., 2008), and oligodendroglial cells are relatively sparse. Following ablation, most tissues show a slow and tardily upturn in $Sox10^+$ cell numbers. However, this recovery varied between the different CNS regions in experimental mice. While the white matter of the cerebellum showed no increase in oligodendrocyte lineage cell density, brain stem $Sox10^+$ cells increased again at end stage indicating a late recovery. In contrast, the corpus callosum showed an earlier increase between disease onset and intermediate stage (Fig. 3-4 B). The grey matter of the frontal cortex showed the most pronounced recovery. Therefore, differences in severity between the tissues are not due to differences in oligodendrocyte ablation, but might be due to differences in the activity of OPCs replenishing the oligodendroglial pools.

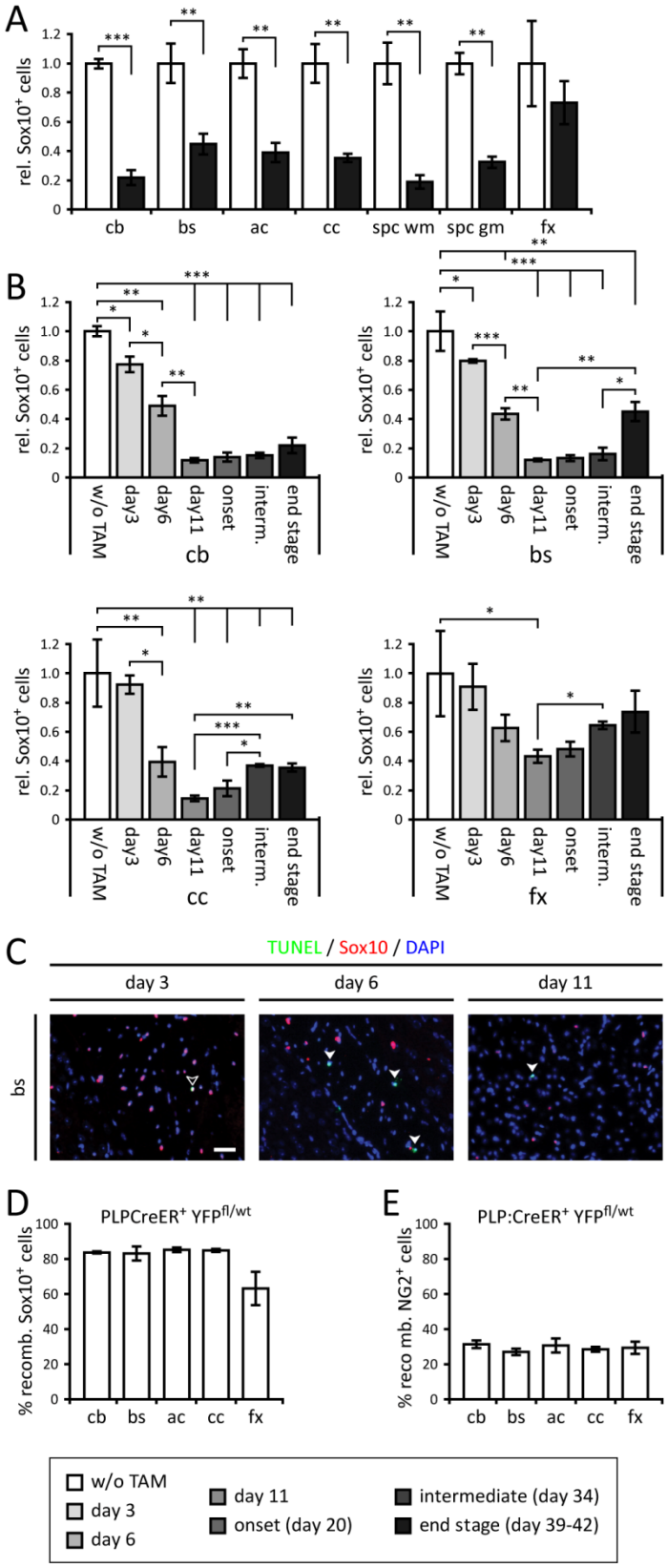

Figure 3-4: Loss of oligodendroglial cells following induction of cell death.

(A) Loss of Sox10$^+$ oligodendroglial cells following TAM-mediated recombination and subsequent cell-intrinsic expression of DT-A in various CNS areas: cerebellar white matter (cb), brain stem (bs), anterior commissure (ac), corpus callosum (cc), spinal cord white (spc wm) and grey matter (spc gm), and frontal cortex (fx) at end stage of clinical development compared with control mice. Sox10$^+$ cell numbers are strongly diminished with the exception of the fx. **(B)** Reduction of oligodendroglial cells starts immediately after TAM-induced recombination and reaches maximal decrease at day 11. Cell numbers remain low in most tissues, although generally a trend for recovery at late time points is observed. Ablation of oligodedroglial cells in the fx is less pronounced and recovery seems more efficient. **(C)** Only a minor increase in TUNEL$^+$ cells (arrowheads) could be detected early after induction of oligodendrocyte cell death, and only sparse TUNEL$^+$/Sox10$^+$ double positive cells (empty arrowhead) could be detected. **(D)** Recombination efficiencies are generally comparable between CNS tissues when analysed with the *R26:lxSTOP/YFP* (YFP) reporter line in combination with the *PLP:CreERT2* line and standard TAM injection paradigm. Recombination rate reflects well the maximally achieved oligodendroglial ablation at day 11. **(E)** In the same experimental setup, recombination is observed in a constant fraction of OPCs throughout the different CNS regions. *Data are given as mean ± SEM. n=3; *=p<0.05, **=p<0.01, ***=p<0.001, Student's* t*-test.*

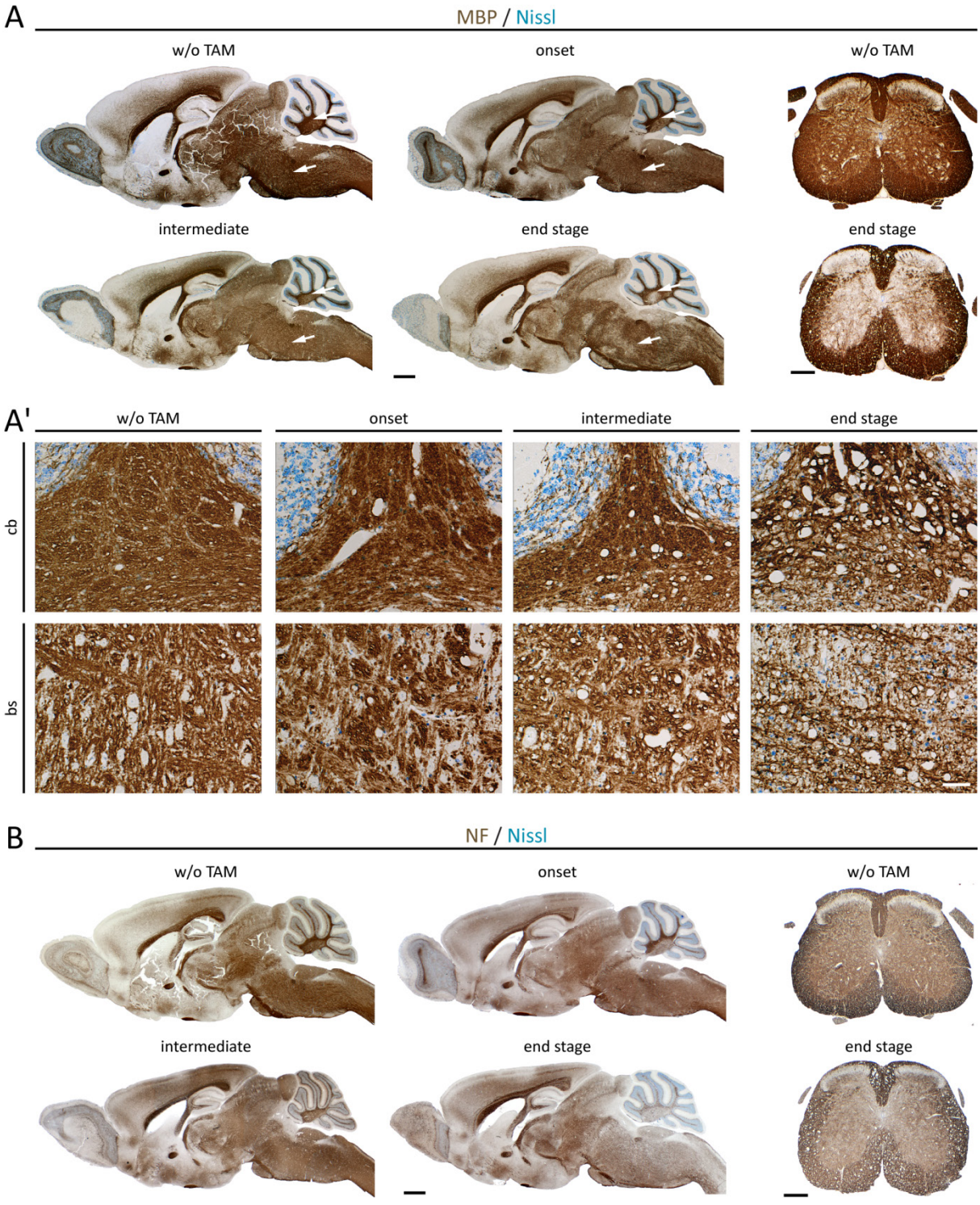

Figure 3-5: Histological assessment of brain and spinal cord tissue after induction of adult oligodendrocyte loss.

(A) MBP staining on brain sagittal sections (left) and spinal cord cross sections (right) at different time points of disease progression. Note the reduced MBP staining over time, most pronounced in cerebellar white matter (cb) and brain stem (bs) (arrows). **(A')** Magnifications of cb and bs regions show reductions of myelin staining over time and remarkably increasing tissue vacuolation. **(B)** Neurofilament (NF) staining on brain sagittal sections (left) and spinal cord cross sections (right) at different time points of disease progression. Note the reduced NF staining intensity in impaired regions, especially at end stage. *Scale bars: 1mm for brain overview (A,B), 200 µm for spinal cord sections (A,B), 20 µm for magnifications (A').*

Acute loss of adult oligodendrocytes leads to status spongiosus

To assess changes in tissue morphology in experimental mice and to correlate these to the behavioural and imaging data, I performed immunostainings at representative time points of phenotypic development (Fig. 3-5). First, I examined myelin by immunolabelling for MBP. Myelin staining was progressively reduced over time in the cerebellar white matter, brain stem, midbrain, and spinal cord white and grey matter (Fig. 3-5 A). In addition to the reduction in myelin, a pronounced tissue vacuolation reassembling classical *status spongiosus* (Adornato & Lampert, 1971) in several white matter regions was observed. Vacuoles were at first observable with the onset of clinical signs and increased in size and number over time, reflecting the observed incremental impairment (Fig. 3-5 A', 3-6 A,B,C). Staining for neurons with neurofilament (NF) revealed a progressive loss of staining intensity. These findings are consistent with secondary axonal damage due to primary loss of adult oligodendrocytes and the subsequent myelin alterations (Fig. 3-5 B).

The severity of vacuolation differed throughout the neuroaxis. Most severely affected were the cerebellar white matter, brain stem and spinal cord white matter, while the spinal cord grey matter showed no prominent vacuole load, as reflected by a quantitative assessment (Fig. 3-6 A). Analysis of vacuoles in the severely affected regions of cerebellar white matter and brain stem at the different disease stages showed a steady increase over time, in parallel to the progression of clinical signs (Fig. 3-6 B). Interestingly, myelinated regions of the forebrain were variably affected, with degeneration being especially severe in the anterior commissure, while the corpus callosum was only mildly altered at end stage (Fig. 3-6 A).

To determine the cellular origins of the *status spongiosus*, I performed a morphological analysis on toluidine blue-contrasted resin sections. As shown in the representative region of the spinal trigeminal tract of experimental mice (Fig. 3-6 C), the observed tissue abnormalities were similar in distribution to those revealed by myelin staining (Fig. 3-5 A). Vacuoles were restricted to single myelin lamellae at initial stages, but over time the expanding vacuoles caused widespread tissue disruption. Ultrastructural analysis confirmed that vacuolation was due to alteration of myelin membranes (Fig. 3-6 D). Vacuoles arose due to splitting at various places within the myelin sheath, between the axolemma and the myelin sheath, or by a combination of both. Membrane splitting and vacuolation occurred locally along the internode, with the rest of the myelin sheath remaining compact. In accordance with the histological analysis, resin sections showed varying vacuole load between different CNS tissues (Fig. 3-7). Anterior commissure, corpus callosum and optic nerve showed only small, distributed vacuoles, although tissue damage throughout the anterior commissure was very heterogeneous and could locally be severe. In contrast, tissue disruption and

vacuolation in the white matter of brainstem, spinal cord and cerebellum were pronounced and pervasive. Characteristic findings were vacuoles, myelin splitting, axonal abnormalities and appearance of phagocytic cells (Fig. 3-8 to 3-13). Summarising, experimental mice show major progressive myelin vacuolation in parallel with the development of clinical signs.

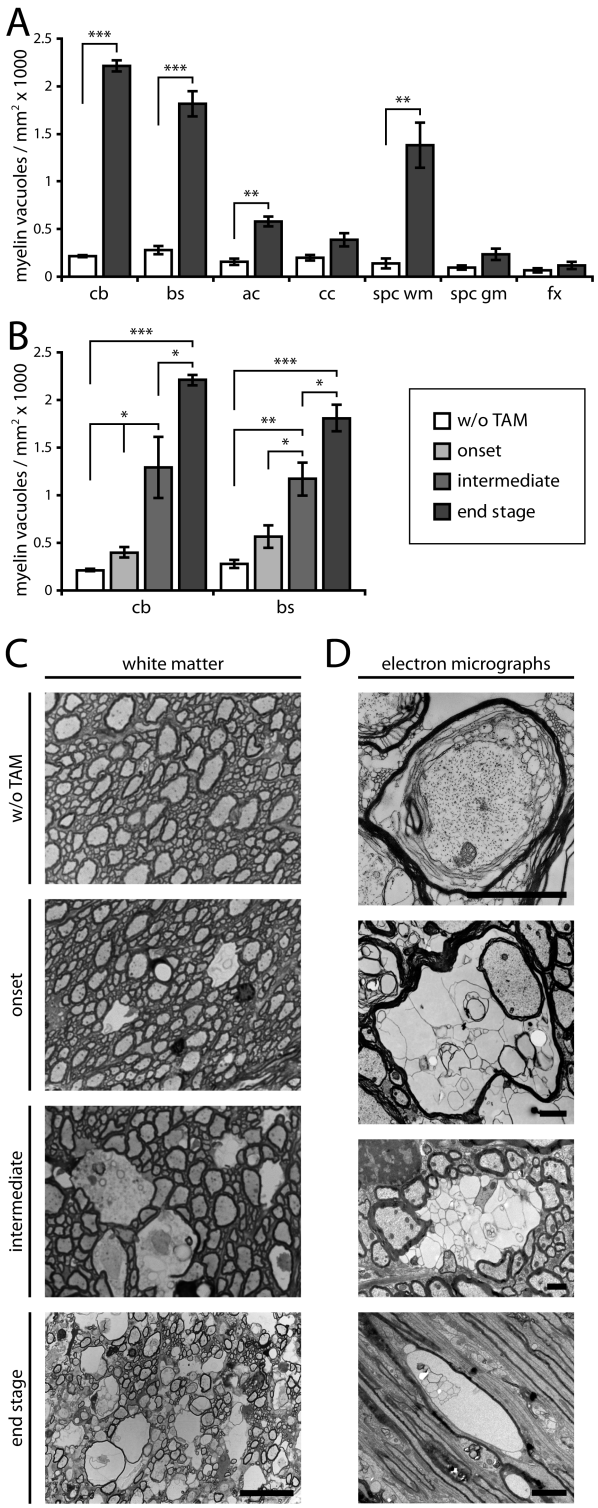

Figure 3-6. Tissue vacuolation after induction of adult oligodendrocyte death.

(A) Tissue vacuolation at end stage of mice affected by genetically induced oligodendrocyte cell death: cerebellar white matter (cb), brain stem (bs), anterior commissure (ac), corpus callosum (cc), spinal cord white (spc wm), and gray (spc gm) matter, and frontal cortex (fx). **(B)** Accumulation of vacuoles is most prominent in severely affected white matter tissues; vacuoles appear at clinical onset, and increase in numbers during disease development as quantified by manual counting on histological sections. **(C)** Morphology of representative spinal trigeminal tract regions of the bs on toluidine blue-stained resin sections. Vacuoles appear in parallel to clinical signs and increase in both size and numbers while impairment of the mice progresses. Widespread tissue vacuolation is observed at end stage. Note the abundance of disrupted, degenerated, but not yet cleared myelin. **(D)** Electron micrographs of vacuolated tissue reveal pronounced status spongiosus of myelin sheaths appearing adaxonal, within myelin layers, or even affecting the entire myelin sheath. Vacuolation can also be a local event along an internode. *Data are given as mean ± SEM. n=3; *=p<0.05, **=p<0.01, ***=p<0.001, Student's* t-*test. Scale bars: 20 µm (C), 2 µm (D).*

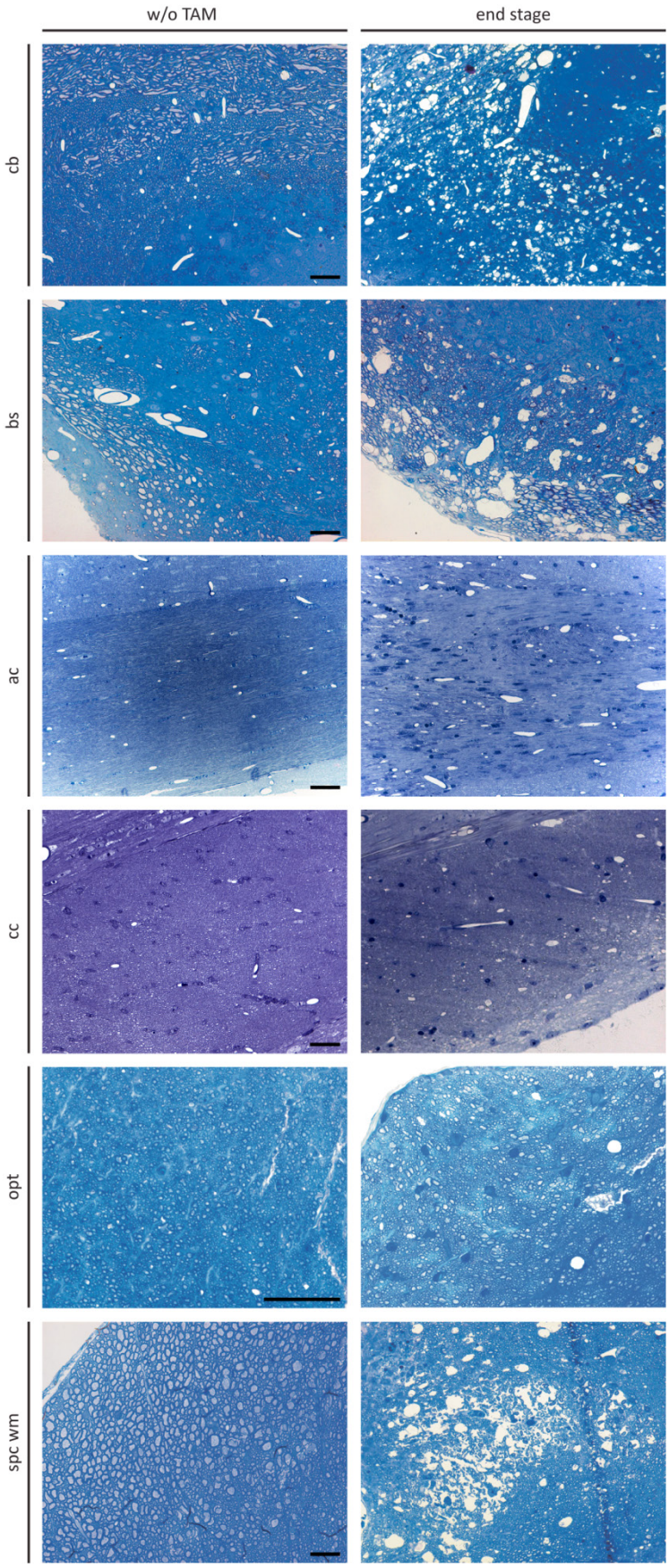

Figure 3-7: Morphological comparison of different CNS tissues.

Toluidine blue-stained resin sections show pathological processes subsequent to genetically-mediated ablation of adult oligodendrocytes throughout myelinated CNS tissues in experimental animals compared to controls. While cerebellum (cb), brain stem (bs) and spinal cord white matter (spc wm) are severely affected and show varying degrees of widespread damage, damage in white matter tissues containing smaller axons, such as corpus callosum (cc) and optic nerve (opt), was more disperse and less pronounced. Damage in the anterior commissure (ac) was heterogeneous throughout its spatial extension. *Scale bars: 20 µm.*

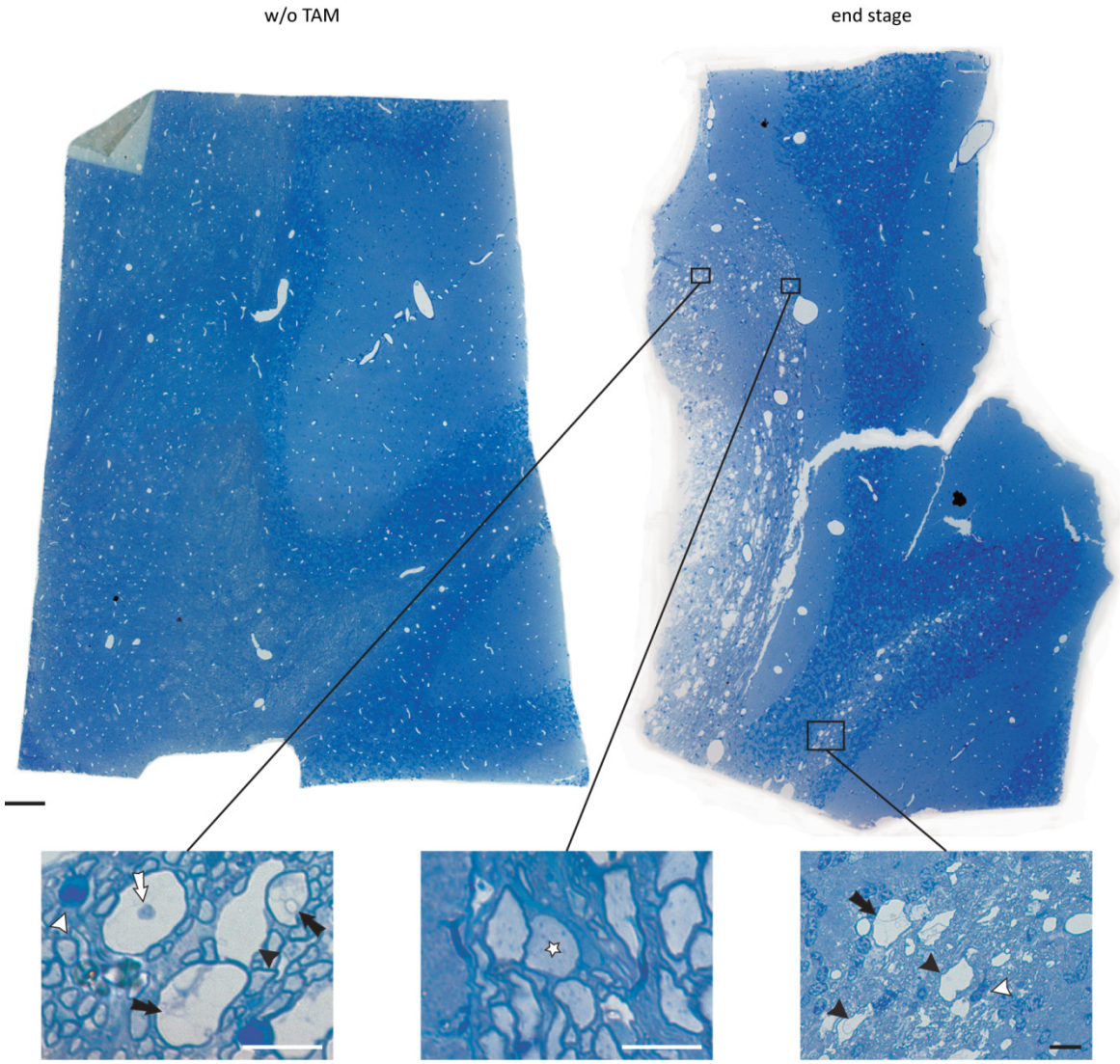

Figure 3-8: Morphology of the cerebellar white matter after genetically induced oligodendrocyte ablation.

Toluidine-blue stained transverse resin sections show pathological processes subsequent to genetically-mediated ablation of adult oligodendrocytes in cerebellar white matter of experimental animals at end stage compared to controls. Wide-spread status spongiosus was observed in white but not grey matter. Frequent observations included: Vacuoles (black arrowhead), myelin membrane splitting (black arrow), phagocytic cells filled with myelin debris (white arrowhead), condensed axons (white arrow), but also thinly myelinated axons (white asterisk) could be occasionally observed. *Scale bars: 50 µm for overview, 10 µm for magnifications.*

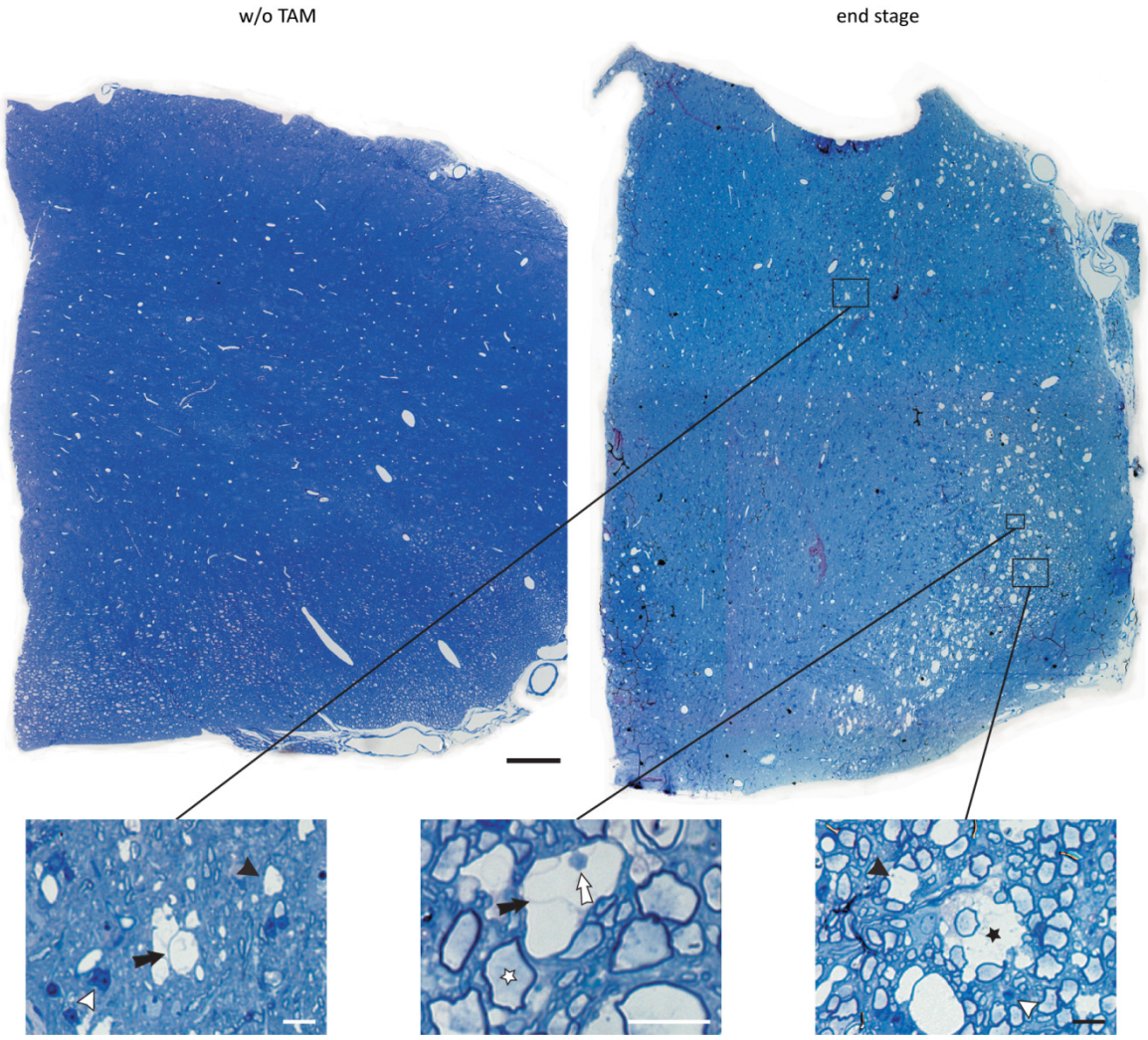

Figure 3-9: Morphology of the brain stem after genetically induced oligodendrocyte ablation.

Toluidine-blue stained coronal resin sections show pathological processes subsequent to genetically-mediated ablation of adult oligodendrocytes in brain stem tissue of experimental animals at end stage compared to controls. Wide-spread status spongiosus was observed in white but not grey matter, although small vacuoles were present throughout the parenchyma. Frequent observations included: Vacuoles (black arrowhead), widespread tissue vacuolation (black asterisk), myelin membrane splitting (black arrow), phagocytic cells filled with myelin debris (white arrowhead), condensed axons (white arrow), but also thinly myelinated axons (white asterisk) could be occasionally observed. *Scale bars: 100 µm for overview, 10 µm for magnifications.*

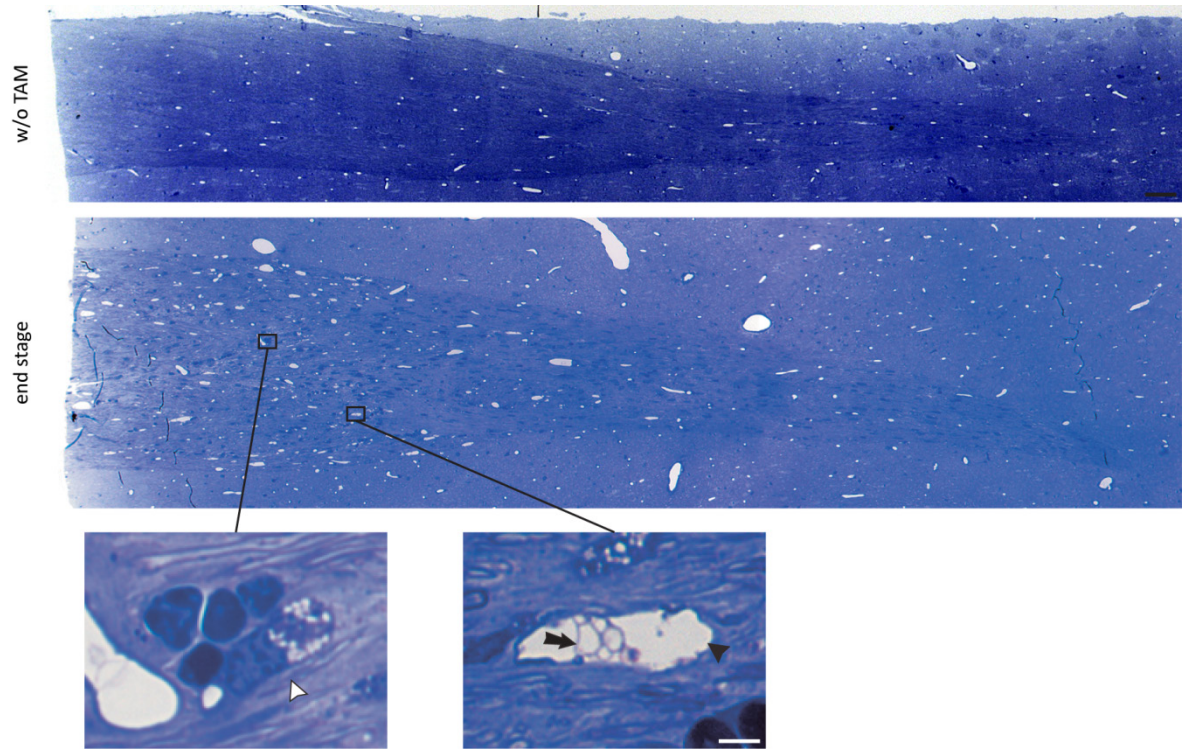

Figure 3-10: Morphology of the anterior commissure after genetically induced oligodendrocyte ablation.

Toluidine-blue stained coronal resin sections show pathological processes subsequent to genetically-mediated ablation of adult oligodendrocytes in the anterior commissure of experimental animals at end stage compared to controls. Tissue vacuolation was observed throughout the parenchyma but vacuole load varied along the fibre tract, with more pronounced damage in central parts compared to distal areas. Frequent observations throughout were: Vacuoles (black arrowhead), myelin membrane splitting (black arrow), and phagocytic cells filled with myelin debris (white arrowhead). Scale bars: 50 µm for overview, 10 µm for magnifications.

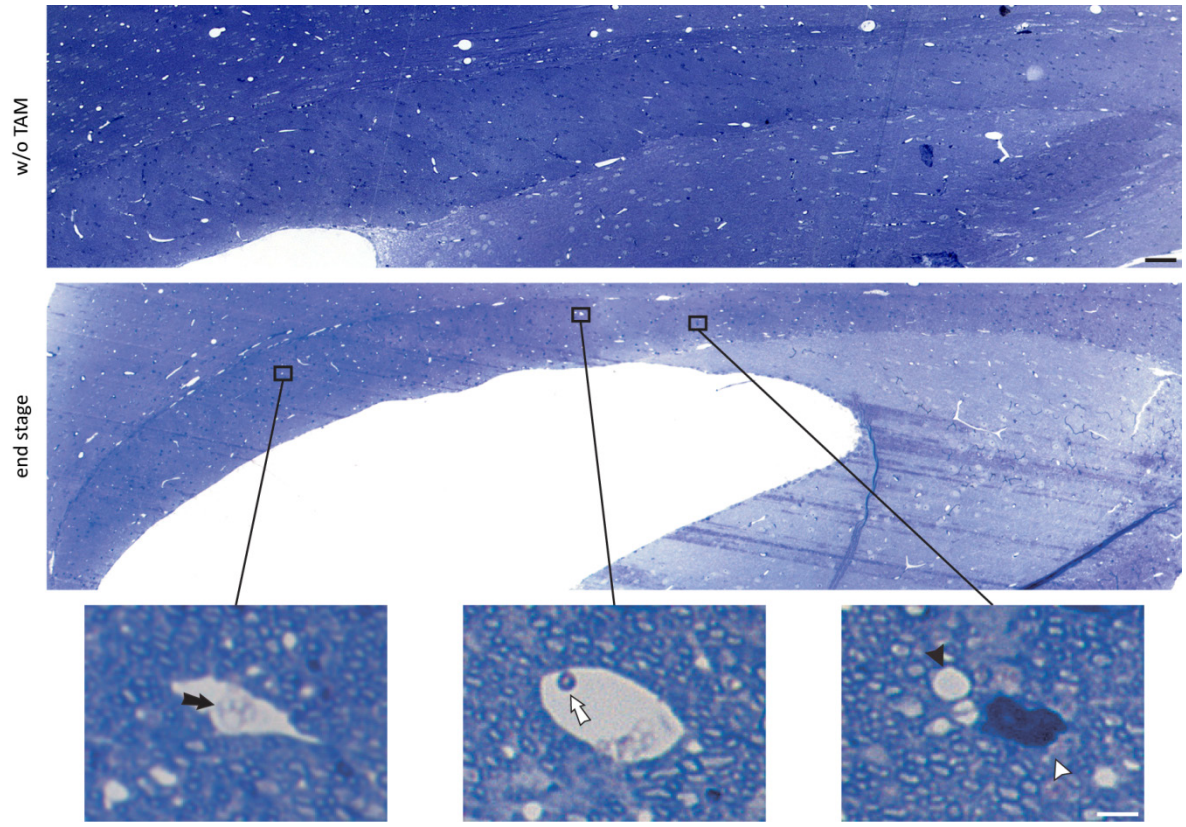

Figure 3-11: Morphology of the corpus callosum after genetically induced oligodendrocyte ablation.

Toluidine-blue stained sagittal resin sections show pathological processes subsequent to genetically-mediated ablation of adult oligodendrocytes in the corpus callosum of experimental animals at end stage compared to controls. Vacuolation was observed throughout the parenchyma, although less pronounced compared to other white matter tissues. Frequent observations throughout were: Vacuoles (black arrowhead), myelin membrane splitting (black arrow), condensed axons (white arrow), and phagocytic cells filled with myelin debris (white arrowhead). *Scale bars: 50 µm for overview, 10 µm for magnifications.*

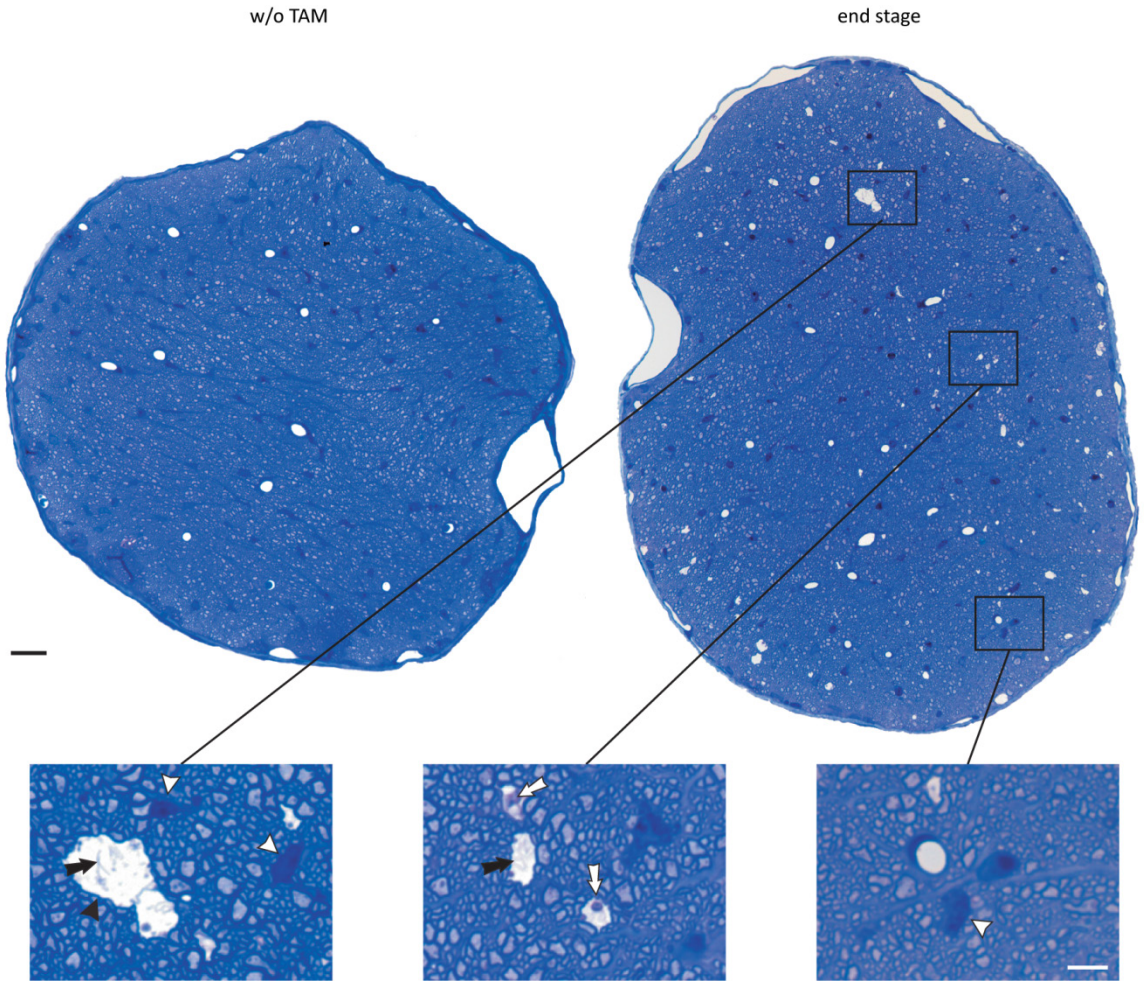

Figure 3-12: Morphology of the optic nerve after genetically induced oligodendrocyte ablation.

Toluidine-blue stained transverse resin sections show pathological processes subsequent to genetically-mediated ablation of adult oligodendrocytes in the optic nerve of experimental animals at end stage compared to controls. Vacuolation was observed throughout the parenchyma, although less pronounced compared to other white matter tissues. Frequent observations throughout were: Vacuoles (black arrowhead), myelin membrane splitting (black arrow), condensed axons (white arrow), and phagocytic cells filled with myelin debris (white arrowhead). *Scale bars: 20 µm for overview, 5 µm for magnifications.*

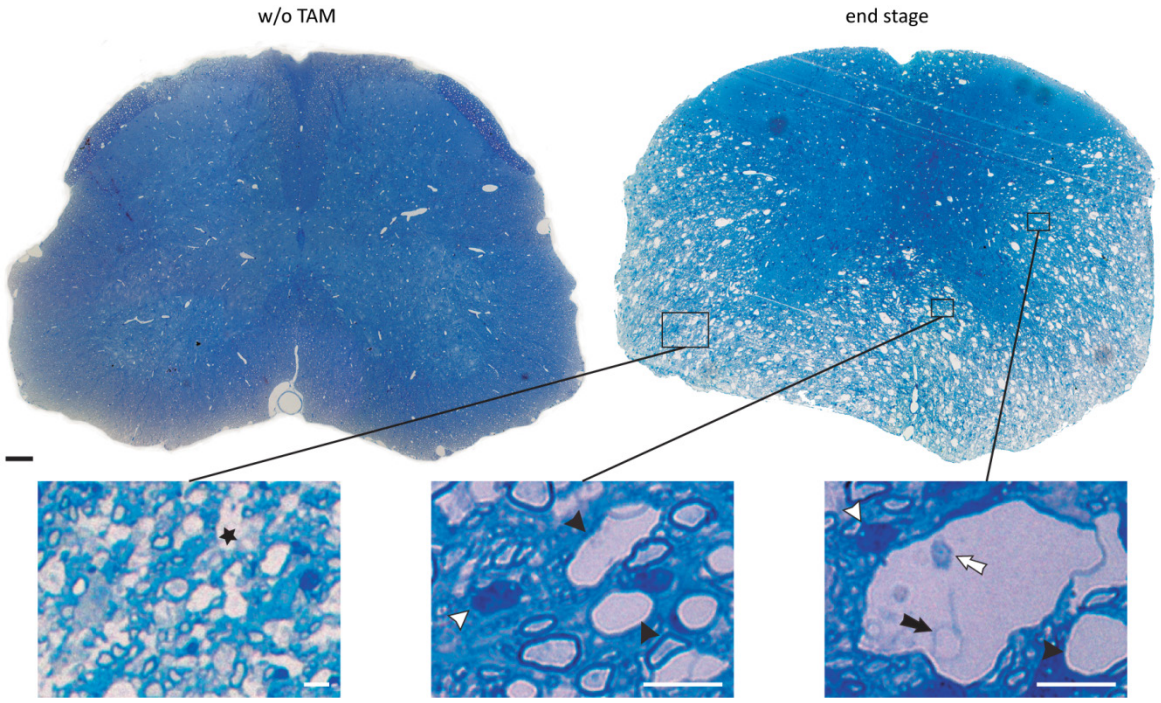

Figure 3-13: Morphology of the spinal cord after genetically induced oligodendrocyte ablation.

Toluidine-blue stained transverse resin sections show pathological processes subsequent to genetically-mediated ablation of adult oligodendrocytes in spinal cord tissue of experimental animals at end stage compared to controls. Wide spread, severe status spongiosus was observed in white but not grey matter, although small vacuoles were present throughout the parenchyma. Frequent observations included: Vacuoles (black arrowhead), widespread tissue vacuolation (black asterisk), myelin membrane splitting (black arrow), phagocytic cells filled with myelin debris (white arrowhead), and condensed axons (white arrow). Scale bars: 50 µm for overview, 10 µm for magnifications.

Myelin persists despite efficient ablation of adult oligodendrocytes

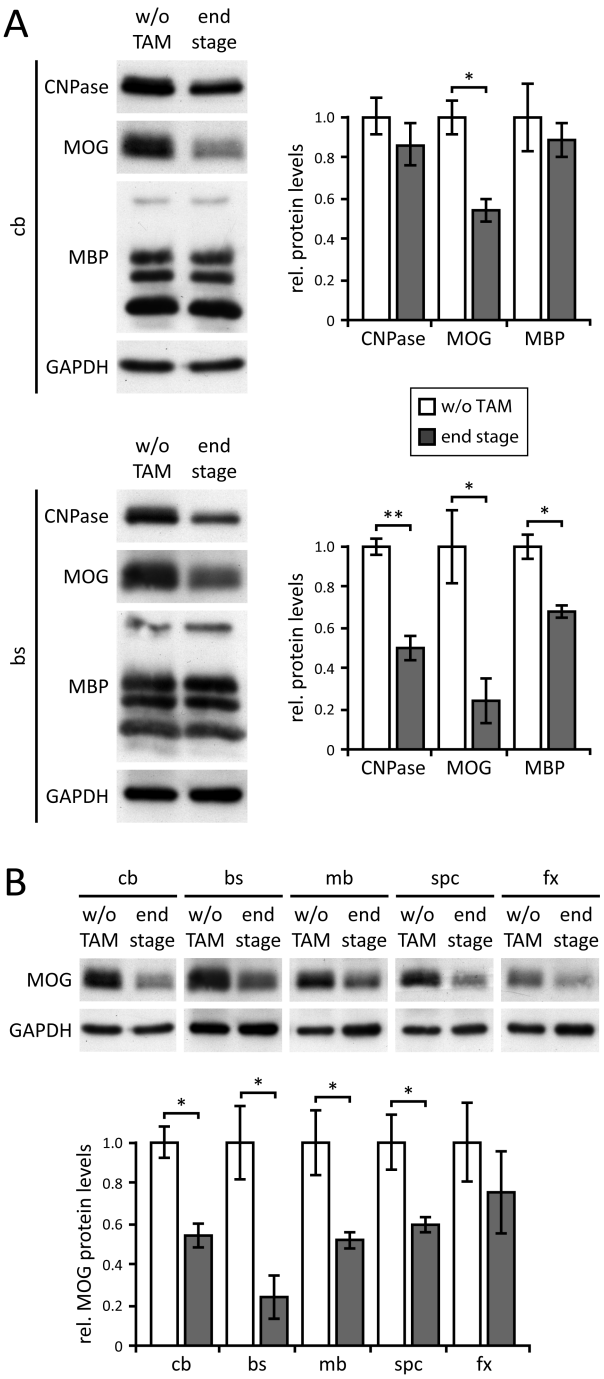

Although adult oligodendrocytes are efficiently and rapidly ablated in experimental mice, aberrant myelin structures remain throughout damaged CNS tissues. To assess residual myelin, western blot analysis of myelin proteins was performed (Fig. 3-14 A). Quite substantial amounts of residual myelin proteins could be found. Interestingly, MOG levels turned out to be most sensitive towards oligodendrocyte loss and are strongly reduced, reflecting ablation efficiencies of oligodendroglial cells. Loss of CNPase was less pronounced and reduction of MBP was minor. These differences were not surprising, given that CNPase is localised in non-compact myelin and MOG is associated with the myelin lamellae but not involved in membrane compaction, in contrast to MBP. Additionally, myelin proteins and especially MBP have long half-lifes, with approx. 100 days for MBP clearly exceeding the time frame analysed here (Fischer & Morell, 1974; Singh & Jungalwala, 1979). Due to its sensitivity, MOG was used for a trans-tissue comparison (Fig. 3-14 B). Interestingly, residual myelin proteins indicative of remaining myelin vary

Figure 3-14: Western blot analysis of residual myelin proteins.

(A) Protein composition of residual myelin in brain stem (bs) and whole cerebellum (cb). While bs tissue is clearly reduced in its content of MOG, CNPase and MBP, the reduction is less obvious in cb tissue. Overall, MOG is depleted strongly after genetically-mediated oligodendroglial ablation, while reduction of CNPase is less pronounced and MBP remains present in almost normal amounts within residual myelin. **(B)** Comparison of myelin protein content of the CNS tissues cb, bs, midbrain (mb), spinal cord (spc) and frontal cortex (fx). Residual MOG protein content varied between the different tissues, although variations do not entirely reflect damage inhomogeneities between the regions. *Data are given as mean ± SEM. n=3; *=p<0.05, **=p<0.01, Student's* t*-test.*

between the different CNS regions analysed in a way that is not entirely reflected by the occurrence of damage. This might indicate tissue-specific variations in myelin decay. Subsuming, in combination with the morphological analysis, these data strongly suggest that oligodendrocytes –when genetically triggered to undergo cell death– disappear with the associated myelin internodes remaining behind, and the latter becomes subject to uncontrolled decay.

Magnetisation transfer ratio changes with myelin defects

MTI has more and more come into focus as a promising method to visualise changes at the macromolecular level, and is thought to represent in nervous tissue predominantly a measure of myelin integrity. MTI therefore was used in this mouse model to test its suitability to monitor the developing myelin damage and evaluate its sensitivity towards such damage. Coronal maps colour-coded for magnetisation transfer ratio (MTR) from control and experimental mice indicated a decrease of MTR values in affected areas of brainstem and cerebellum at end stage only in diseased mice (Fig. 3-15 A). Quantitative MTR values were obtained from different ROIs of representative white, mixed and grey matter as well as from the olfactory bulb as an internal control (Fig. 3-15 B). MTR was found to be approximately 50-55% within brain tissue and was slightly decreased in experimental mice at end stage (Fig. 3-15 C). However, a significant decrease was found only in the brainstem. In cerebellar ROIs a high variance but no significant decrease could be observed, while the grey matter frontal cortex showed only minor alterations and MTRs in the olfactory bulb remained unchanged. In summary, the sensitivity of MTI towards the underlying tissue pathology is limited in this mouse model. Additionally, the possible resolution with the given setup is limiting for a detailed analysis of the small structures within the mouse brain.

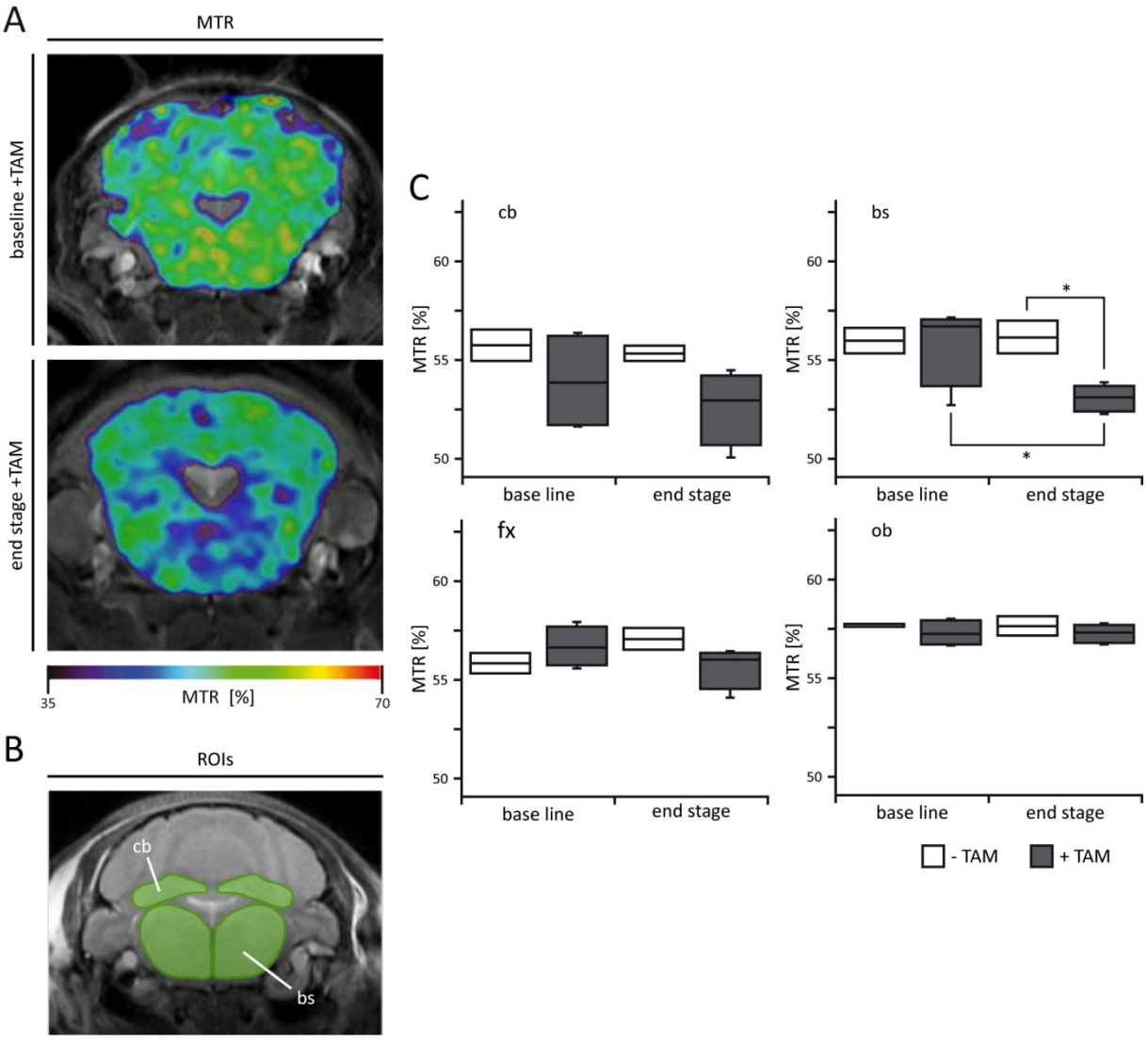

Figure 3-15: Magnetisation transfer ratio MRI to image tissue integrity.

(A) Transverse T2-weighted MRI sections with superimposed, percentage colour-coded MTR maps of a representative animal at baseline (day 2) and end stage (day 41) after TAM-mediated ablation of oligodendrocytes. Reductions of MTRs are visible in brain stem (bs) and ventral cerebellum (cb) areas. **(B)** Representative T2-weighted MRI section with superimposed ROIs used for quantification. **(C)** Box plots of percent MTR derived from ROIs cb, bs, frontal cortex (fx) and olfactory bulb (ob) at baseline (average of day 2 and 9) and end stage (average of day 37 and 41) control (-TAM) and experimental (+TAM) animals. Both white and mixed matter of cb and bs show decreased transfer ratios, being significant only in the bs compared to baseline +TAM or control at end stage. Grey matter fx and ob tissues show little to no variation. *Data are given as median, and quartiles, sample minimum, sample maximum. n= 2 -TAM / 4 +TAM; *=p<0.05, ANOVA and Fisher's PLSD posthoc test.*

Phagocytic cells react late consequently to cell death of adult oligodendrocytes

To investigate cellular responses of the innate immune system, I first used Iba-1 histology to assess activation of phagocytic cells. Widespread increase and activation –as judged by increase in Iba-1-positivity, morphologically ramified appearance, proliferative, and phagocytic activity (see below)– of cells of the monocyte/macrophage lineage, therefore including activated microglia, was detected within damaged tissues (Fig. 3-16 A). Pronounced increase at disease end stage was found especially in regions with severe damage and high vacuole load such as brain stem, cerebellar core or anterior commissure, indicative of myelin decay and the presence of debris. Iba-1$^+$ cells were also found to be proliferative (Fig. 3-24). Activated monocytic cells were found in all tissues, but were relatively sparse in the mildly affected corpus callosum or grey matter tissues. While activated cells were sparse at disease onset and only obvious in the severely affected cerebellar white matter and brain stem, they accumulated with disease progression, comparable to the appearance of tissue damage (Fig. 3-16 B). Interestingly, no activation was observed early during the disease course as an immediate reaction to oligodendroglial cell death (data not shown). This indicates that monocytic cells react to myelin decay and debris appearance rather than to insults to oligodendroglia *per se*.

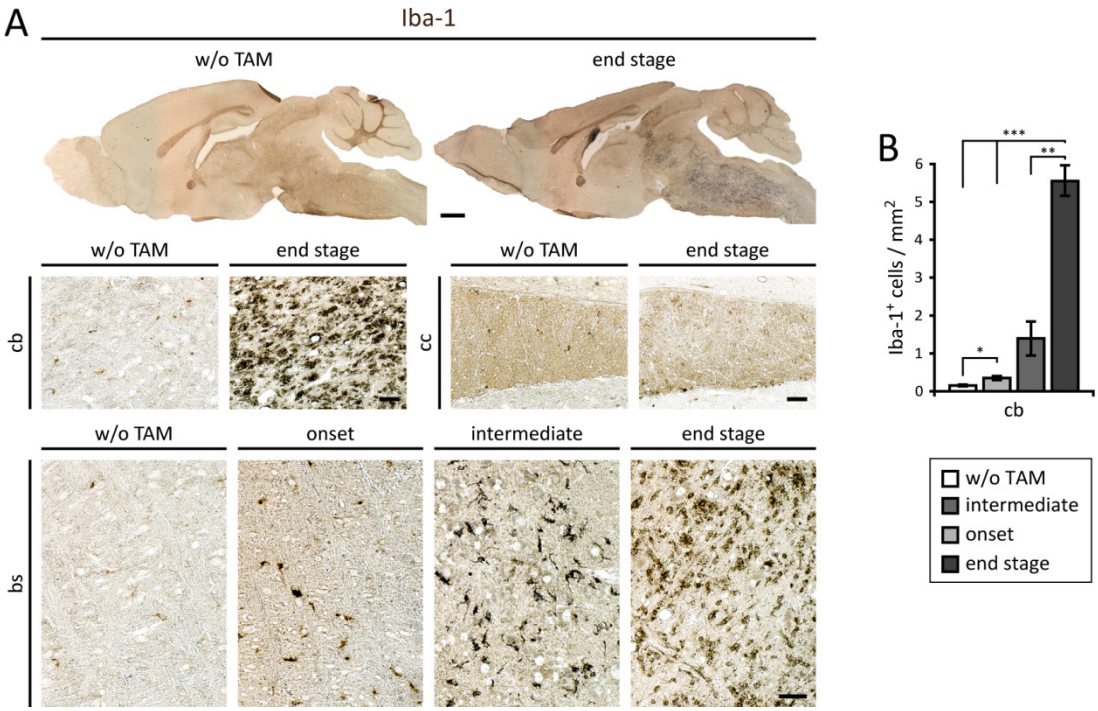

Figure 3-16: Monocytic phagocytes react to myelin damage.

(A) Iba-1 staining for activated phagocytes at different time points of disease progression. Pronounced accumulation of activated monocytes in damaged tissues including cerebellum (cb) and brain stem (bs), but less so in the less-affected corpus callosum (cc) of experimental mice at end stage was observed. Monocytic cells accumulate with disease development and tissue disruption (shown for bs). **(B)** Quantifications of Iba-1$^+$ cells during disease development shows increasing accumulation of reacting monocytes in the severely affected cb. Accumulation of phagocytic cells becomes pronounced at late disease stages. *Data are given as mean ± SEM. n=3; *=p<0.05, **=p<0.01, ***=p<0.001, Student's* t*-test. Scale bars: 1 mm for brain overview, 50 µm for magnifications.*

Moderate astrocytosis appears consequent to oligodendroglial ablation

In parallel to phagocytic cells, I investigated the astrocytic reaction resulting from tissue damage after induced oligodendrocyte cell death. A pronounced increase of $GFAP^+$ astrocytes was observed in strongly affected tissues, similar to monocytic activation (Fig. 3-17). Interestingly, a disappearing of Bergmann glia from the cerebellum could be observed. Astrogliosis also appeared with disease progression and seemed even more delayed than monocytic activation, with barely any observable at clinical onset. Additionally, mildly affected tissues such as the corpus callosum and grey matter tissues did not show obvious astroglial activation. Therefore, astrocytes –being the brain's intrinsic reactive cells– react only late with increasing myelin decay and tissue damage, but not consequent to

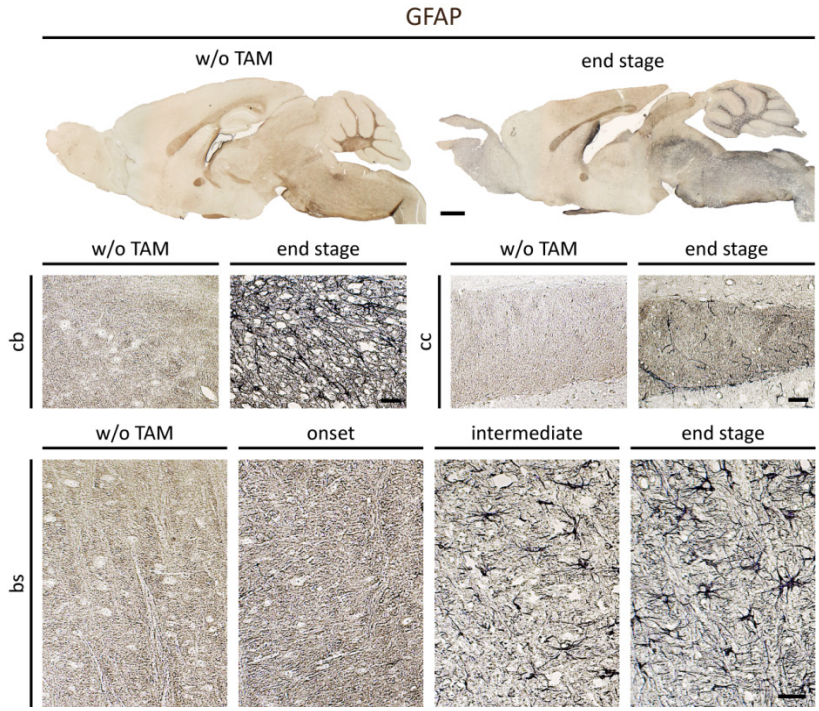

Figure 3-17: Astroglia are activated upon myelin damage.

Histological staining for astrocytes, with glial fibrillary acidic protein (GFAP) as marker, shows astroglial activation in damaged tissues after genetically mediated oligodendrocyte ablation. Activation is noticeable in severely damaged tissues such as brain stem (bs) and cerebellar white matter (cb) and appears late during the disease course. Mildly damaged tissues such as the corpus callosum (cc) show only little astroglial activation. Scale bars: 1 mm for brain overview, 50 µm for magnifications.

cell death induction in adult oligodendrocytes.

No blood-brain barrier leakage appears consequent to oligodendrocyte ablation and subsequent myelin disruption

As both astrocytic reorganisation and putative inflammatory events triggered by oligodendroglial loss and subsequent myelin damage can potentially lead to a disruption of the BBB, I analysed its integrity using an Evans Blue penetration assay. Evans Blue is a fluorescent dye that binds to serum albumin, allowing tracing of blood serum leakage into brain parenchyma when injected intravenously. In experimental mice, no penetration of Evans Blue into CNS tissue could be observed (Fig. 3-18 A,B) and spectrometric analysis of dye extracted from lysed brain tissue revealed dye levels comparable

to those found in control animals (Fig. 3-18 C). In contrast, dye penetration in the inflammatory demyelinating model EAE was pronounced. This indicates that in the model I present here, the BBB is not compromised and remains tight towards macromolecules.

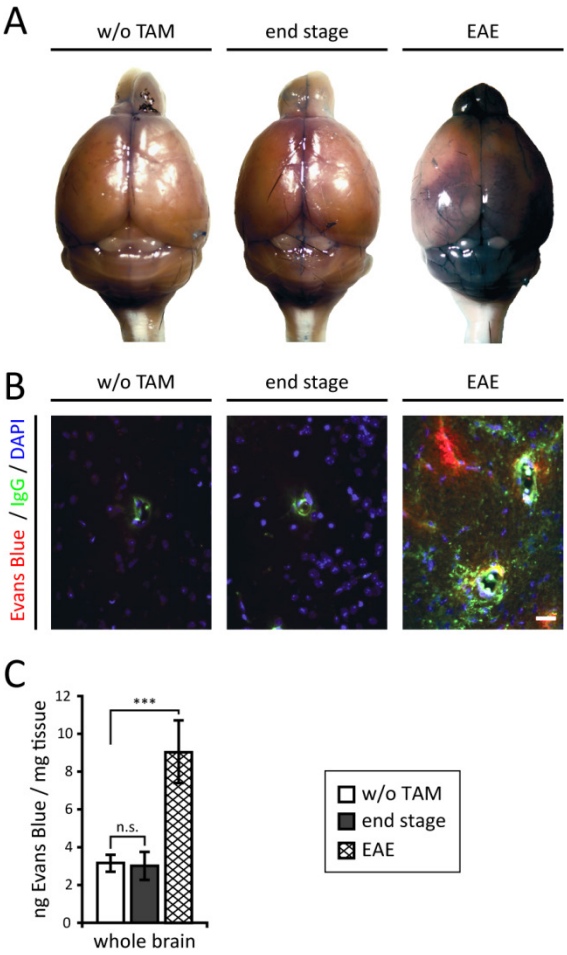

Figure 3-18: Blood-brain barrier is not compromised following white matter damage mediated by oligodendroglial cell death.

(A) Evans blue penetration assay reveals no leakage of serum albumin into the CNS parenchyma. Blue staining of brain tissue can only be observed in positive control brains compromised by the inflammatory demyelination model EAE. **(B)** No auto-fluorescence of Evans blue or leakage of IgG immunoglobulins out of vessels into the parenchyma was found in control or experimental mice. In contrast, extravascular fluorescence is abundant in EAE with both markers. **(C)** Spectrometric quantification of Evans blue dye extracted from whole brain lysates revealed no difference between experimental and control areas, but a pronounced increase in EAE. *Data are given as mean ± SEM. n=3; ***=p<0.001, Student's* t*-test. Scale bar: 20 µm.*

USPIO-mediated tracing of macrophages via T2 MRI reveals no immigration of blood-borne phagocytes

Although the BBB remains intact, the origin of activated phagocytes in areas of pronounced myelin damage remains unclear, given that macrophages could extravasate across an intact BBB (McMahon et al., 2002). To trace blood-originating phagocytic cells possibly extravasating into the brain parenchyma, a tracing of macrophages using ultra small particles of iron oxide (USPIO) was performed. When USPIO are injected intravenously, they are phagocytosed by monocytic cells circulating within the vascular system. When these cells extravasate into the brain, their iron content will lead to a pronounced reduction in T2 relaxation times. However, no clear alterations of T2 relaxation times between pre- and 24h post-injection (ΔT2) MRI acquisition could be observed for any investigated tissue throughout the disease course (Fig. 3-19 A). Histological stainings for ferric iron using Prussian blue at clinical end stage revealed only very sparse and negligible numbers

(1-3 per sagittal brain section) of positive cells, which were mostly associated with blood vessels (Fig. 3-19 B). In contrast, Prussian blue positive cells were abundant in the liver of USPIO injected control animals but absent in vehicle-injected animals. These findings strongly suggest that the main source of activated phagocytic cells found in damaged tissue is CNS parenchyma-derived microglia.

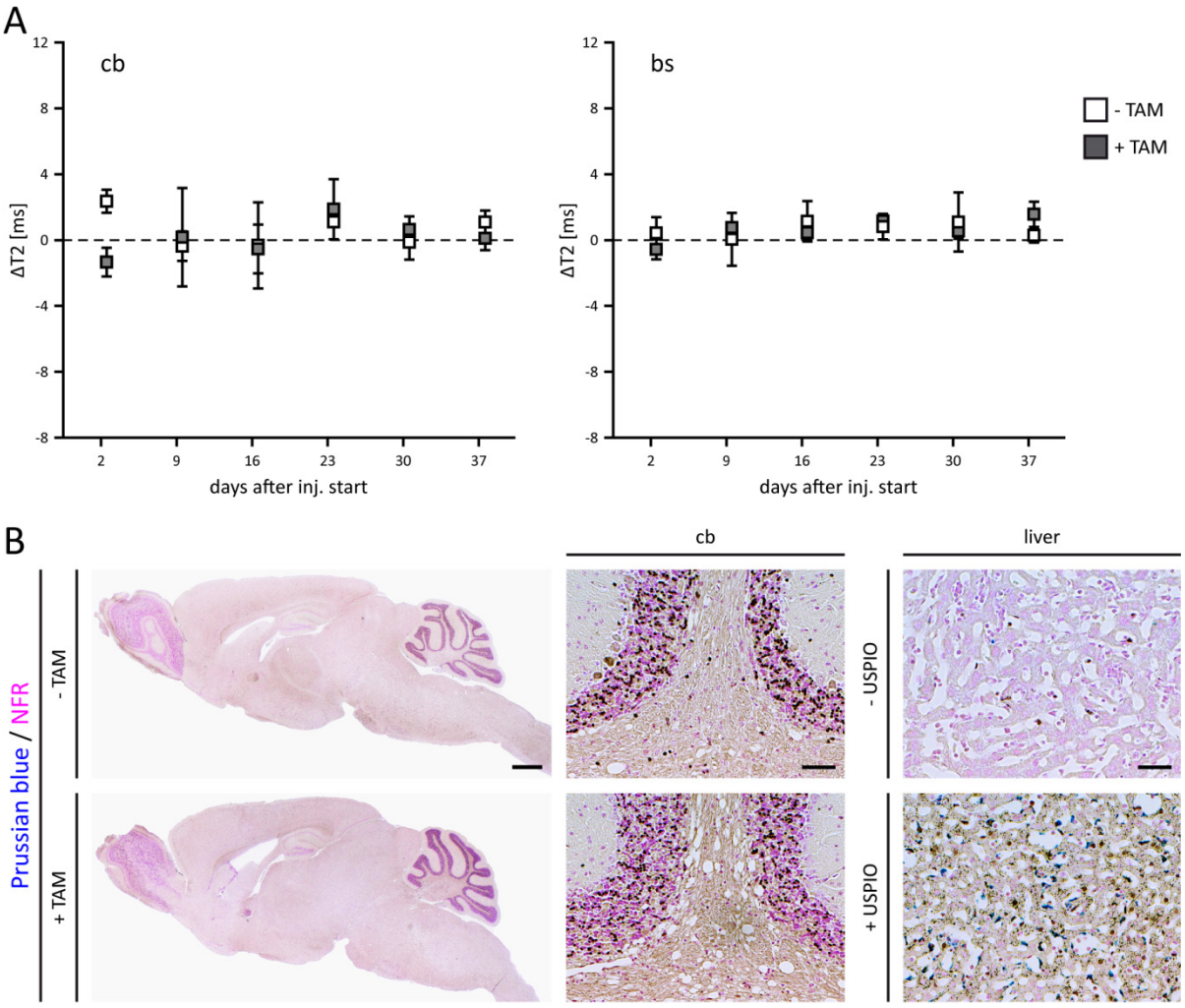

Figure 3-19: No infiltration of macrophages can be observed with USPIO-mediated tracing MRI.

(A) ΔT2 values of MRI assessment at pre-USPIO versus 24h post-USPIO acquisition of quantitative T2 values throughout disease progression revealed no changes in experimental mice (+TAM) with clinical course or compared to control animals (-TAM) in the strongly affected cerebellar core (cb) and brain stem (bs). **(B)** Corresponding histological sections of a representative animal sacrificed immediately after end stage 24h post-USPIO MRI acquisition. Staining with Prussian blue for iron and nuclear fast red (NFR) revealed no USPIO-loaded cells within the brain parenchyma. Staining of liver of untreated control animals (-USPIO) versus 24h post-USPIO (+USPIO) injection shows abundant iron loaded cells in USPIO-injected animals only. *Data are given as mean ± SEM. n= 2 -TAM / 4 +TAM; *=p<0.05, repetitive ANOVA. Scale bars: 1 mm for brain overview, 20 µm for magnifications.*

No infiltration of leukocytes is detectable and the adaptive immune system is not involved in the pathology following genetically-triggered oligodendrocyte cell death

As it has been suggested that oligodendrogliopathy, general CNS damage or axonal impairment might precede or even cause inflammation or autoimmunity, it was crucial to investigate the adaptive immune response to genetically triggered oligodendrocyte cell death. However, I could not detect any accumulation of B ($B220^+$), T helper ($CD4^+$), or cytotoxic T cells ($CD8^+$) within the brain parenchyma (Fig. 3-20). This shows that besides an intact BBB, no infiltration of leukocytes is initiated by oligodendrocyte cell death or subsequent demyelination, and a contribution by adaptive immune components is unlikely.

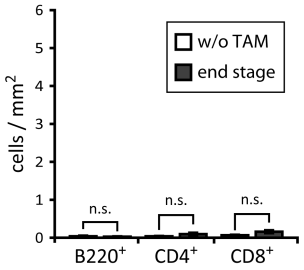

Figure 3-20: No infiltration of adaptive immune cells after adult oligodendrocyte cell death.

Quantification of stainings for B220, CD4, and CD8 at end stage showed no significant extravasation of T- and B-cells into the brain parenchyma as a reaction to myelin damage resulting from oligodendrocyte ablation. This suggests no major adaptive immune response caused by the damage. *Data are given as mean ± SEM. n=6; n.s.=p>0.1, Student's* t-*test.*

To investigate whether adaptive immune cells, although only present in very low numbers, might be involved in the modulation of the observed pathology, I crossed the experimental mice onto a *RAG-1*-deficient background (Mombaerts et al., 1992), which is depleted of functional lymphocytes. When ablation of oligodendrocytes was induced in these mice, the clinical development and pathology was indistinguishable from that seen in mice with a fully functional immune system (Fig. 3-21 A,B). There were also no significant differences in tissue vacuolisation, activation of phagocytic cells, or axonal damage (Fig. 3-21 C-E). These data show that the adaptive immune system is not involved in the pathology following genetic triggering of oligodendroglial depletion and does not react or become activated upon damage.

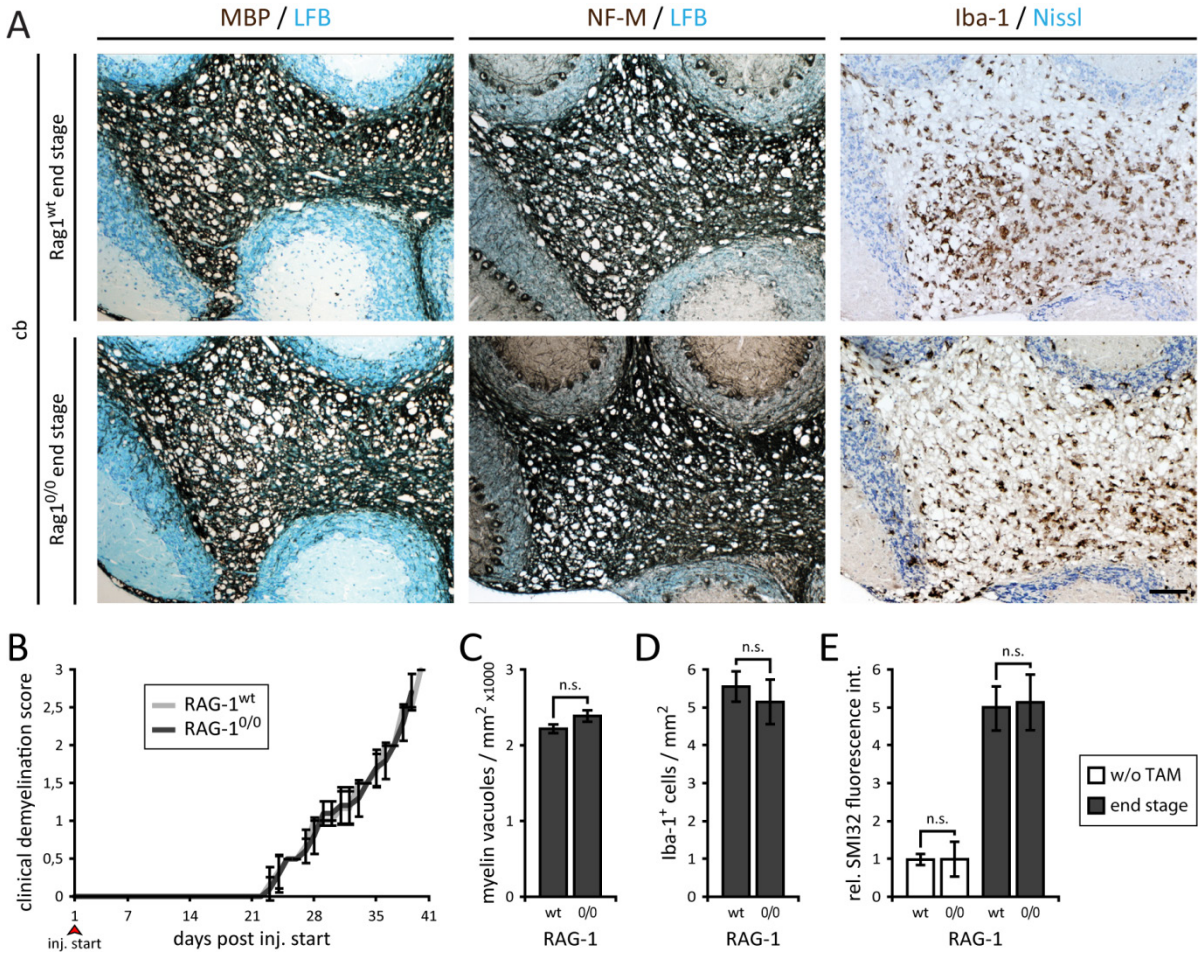

Figure 3-21: No modulation of the disease by adaptive immune system components.

(A) Histological stainings for MBP, neurofilament (NF-M) and activated microglia (Iba-1) reveals no differences in experimental mice depleted of functional lymphocytes by breeding on a *RAG-1*-null background compared to *RAG-1* wild-type mice at end stage, as shown for the cerebellum (cb) as an examply. **(B)** Clinical development was similar between *RAG-1*-null and *RAG-1* wild-type experimental mice. **(C-E)** There were also no observable differences regarding tissue vacuole load, accumulation of activated microglia, or axonal impairment judged by relative fluorescence intensity using SMI32-mediated immunofluorescence. *Data are given as mean ± SEM. n=3; n.s.=p>0.1, Student's* t*-test. Scale bar: 100 µm.*

Genetically induced cell death leads to oligodendrocyte precursor proliferation

Oligodendroglial cell numbers recover after initial depletion to some extent in many tissues during the disease course (Fig. 3-4, Table 3-1). Additionally, both astroglial and microglial activation is observed following genetically-mediated ablation of oligodendrocytes. Both cell types are known to promote OPC activation and proliferation upon their own activation. It was therefore plausible, that proliferative OPCs might be the source underlying the re-increase of $Sox10^+$ cells. To investigate this issue further, dividing cells were labelled with injections of the thymidine analogue IdU, and proliferative OPCs were identified using double labelling of IdU with the oligodendroglial marker

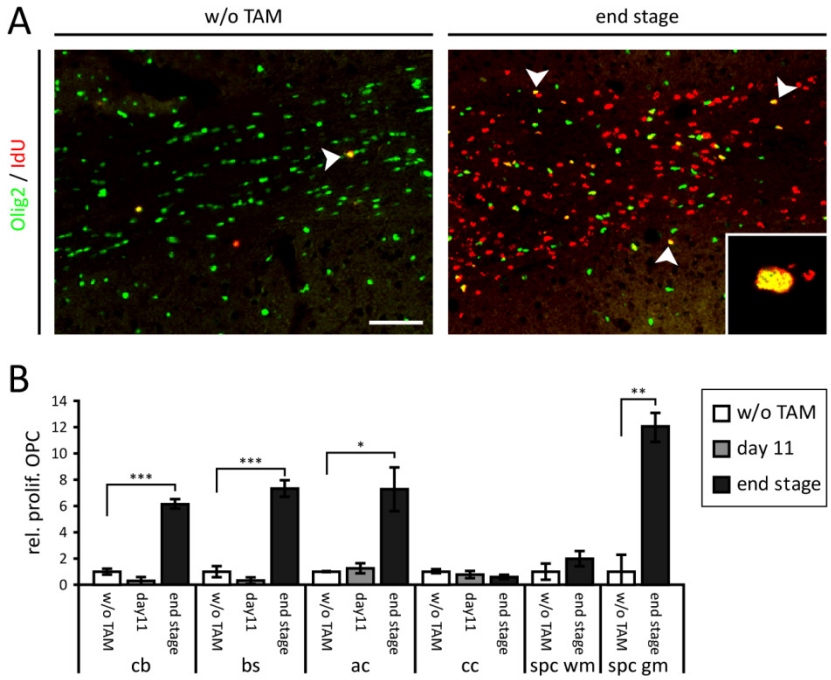

Figure 3-22: Oligodendrocyte precursor cells proliferate subsequent to oligodendrocyte ablation.

(A) Proliferating Olig2$^+$ OPCs in the anterior commissure after labelling for 5 consecutive days with the thymidine analogue IdU, starting 10 days prior to sacrifice at end stage. Proliferating OPCs were frequent in most damaged CNS regions, in particular within the forebrain as seen here in the anterior commissure as a representative example. Examples of proliferating OPCs are marked with arrowheads; Inset shows single optical confocal microscopy section of a double-positive cell. **(B)** Quantification of OPCs in the CNS tissues cerebellar core (cb), brain stem (bs), anterior commissure (ac), corpus callosum (cc), spinal cord white (spc wm) and grey (spc gm) matter. An increase was observed at end stage in all areas analysed, except the cc and spc wm but not earlier after oligodendroglial ablation at day 11. *Data are given as mean ± SEM. n=3; *=p<0.05, **=p<0.01, ***=p<0.001, Student's* t*-test. Scale bar: 50 µm. (Data obtained by Cristina Porcheri)*

Table 3-2: Densities and proliferative activity of OPCs in end stage and control tissues.

	prolif. Olig2+ cells / mm^2			NG2+ cells / mm^2
	control	end stage	p-value	control
cb	5.19 ±1.5	32.04 ±3.5	0.0002	62.78 ±10.7
bs	7.87 ±5.7	58.39 ±7.5	0.0007	40.56 ±18.4
ac	15.30 ±0.5	112.18 ±45.0	0.02	44.44 ±20.1
cc	20.40 ±4.5	11.90 ±4.4	0.084	59.44 ±9.2
spc wm	1.39 ±1.4	2.76 ±1.4	0.29	n.a.
spc gm	1.90 ±3.3	22.90 ±3.9	0.0021	n.a.
fx	n.a.	n.a.	n.a.	60.00 ±6.0

Listed are the densities of IdU$^+$/Olig2$^+$ proliferative, and overall NG2$^+$ oligodendrocyte precursor cells in cerebellar white matter (cb), brain stem (bs), anterior commissure (ac), corpus callosum (cc), spinal cord white (spc wm) and grey (spc gm) matter, and frontal cortex (fx) in diseased mice at end stage compared to control animals. *Data are given as mean ± SEM. n=3; n.a.=not assessed; p-values obtained with Student's* t*-test.*

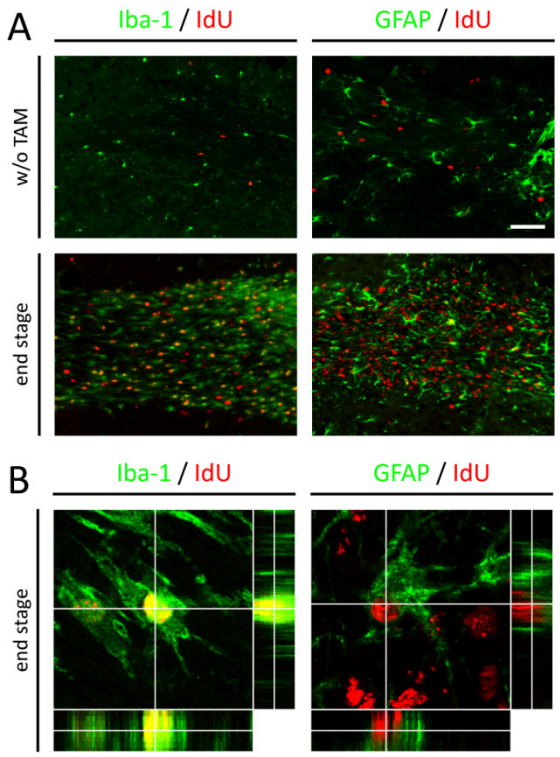

Figure 3-23: Ectopic proliferation is mostly due to microglial activation and astrocytes.

(A) Proliferating Iba-1$^+$ microglia and GFAP$^+$ astrocytes in the anterior commissure after labelling for 5 consecutive days with the thymidine analogue IdU, starting 10 days prior to sacrifice at end stage. Co-labelling revealed that most proliferating cells are microglia, although also astrocytes contribute along with OPCs (see Fig. 3-22). **(B)** Single-cell magnification of confocal images of exemplary proliferative cells. *Scale bar: 50 µm. (Data obtained by Cristina Porcheri)*

Olig2. Proliferative cells were abundant and often double-labelled with Olig2 although a majority of proliferative cells were not oligodendroglia (Fig. 3-22 A). Densities of proliferative OPCs varied between the tissues analysed (Table 3-2). The vast majority of proliferative cells were microglia, although astrocytes also proliferated at the sites of myelin damage (Fig 3-23). Nonetheless, proliferative OPCs were highly increased in most affected areas (cerebellar white matter, brain stem, anterior commissure) but not in the mildly affected corpus callosum (Fig. 3-22 B). Interestingly, proliferative OPCs in the spinal cord were predominantly found within the grey matter and only very few in the white matter. Thus, besides synchronous and consistent oligodendroglial cell ablation throughout CNS tissues, the subsequent induction of OPC proliferation varies to some degrees, much so as the resulting tissue damage and pathology.

Late appearance of myelin debris and phagocytic clearance

Myelin clearance, activation of OPCs, and their subsequent differentiation leading to remyelination usually follow demyelination. Therefore, I investigated experimental animals for characteristic signs of events relevant to successful myelin clearance and remyelination. Although microglial activation was widespread (Fig. 3-16), and phagocytic cells filled with myelin-debris containing vacuoles were numerous in all damaged tissues (Fig. 3-25 A), even at end stage large amounts of partially disrupted myelin and myelin debris remained present. Myelin debris subjected to phagocytic clearance was visualised using Oil Red O staining. Oil red O$^+$ fatty droplets appeared late during the disease course and were abundant in affected tissues at end stage (Fig. 3-24 A). These lipid droplets are linked with ongoing clearance of myelin debris, shown by their association with Iba-1$^+$ activated microglia (Fig. 3-24 B). These findings were in line with an antibody-mediated staining that specifically detects an MBP

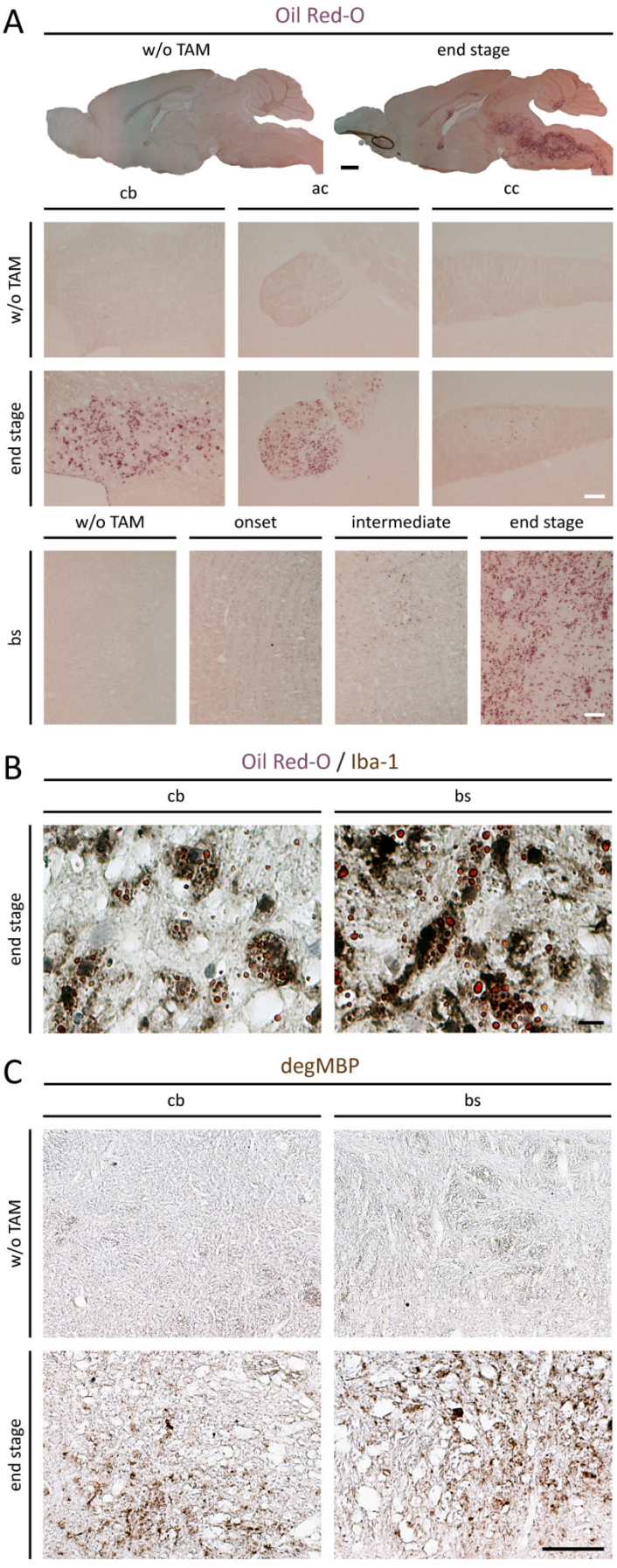

Figure 3-24: Late appearance of myelin debris and phagocytic clearance.

(A) Oil Red O staining to visualise myelin debris subjected to phagocytic clearance. Oil Red O stained fatty droplets appear late during disease development and are abundant in damaged tissues such as cerebellum (cb), brain stem (bs) and anterior commissure (ac) at end stage. Areas of strong stainings overlap with areas positive for activated microglia (compare Fig. 3-16 A). The mildly damaged corpus callosum (cc) shows only mild myelin debris load. **(B)** Co-staining of Oil Red O with Iba-1 shows association of lipid droplets with microglial cells. **(C)** Staining for degenerated MBP (degMBP) shows widespread presence of degenerated myelin, although not necessary overlapping with distribution of tissue vacuoles but similar to that of Oil Red O and Iba-1. *Scale bar: 1mm for overview (A), 50 µm (A+C) or 10 µm (B) for magnifications.*

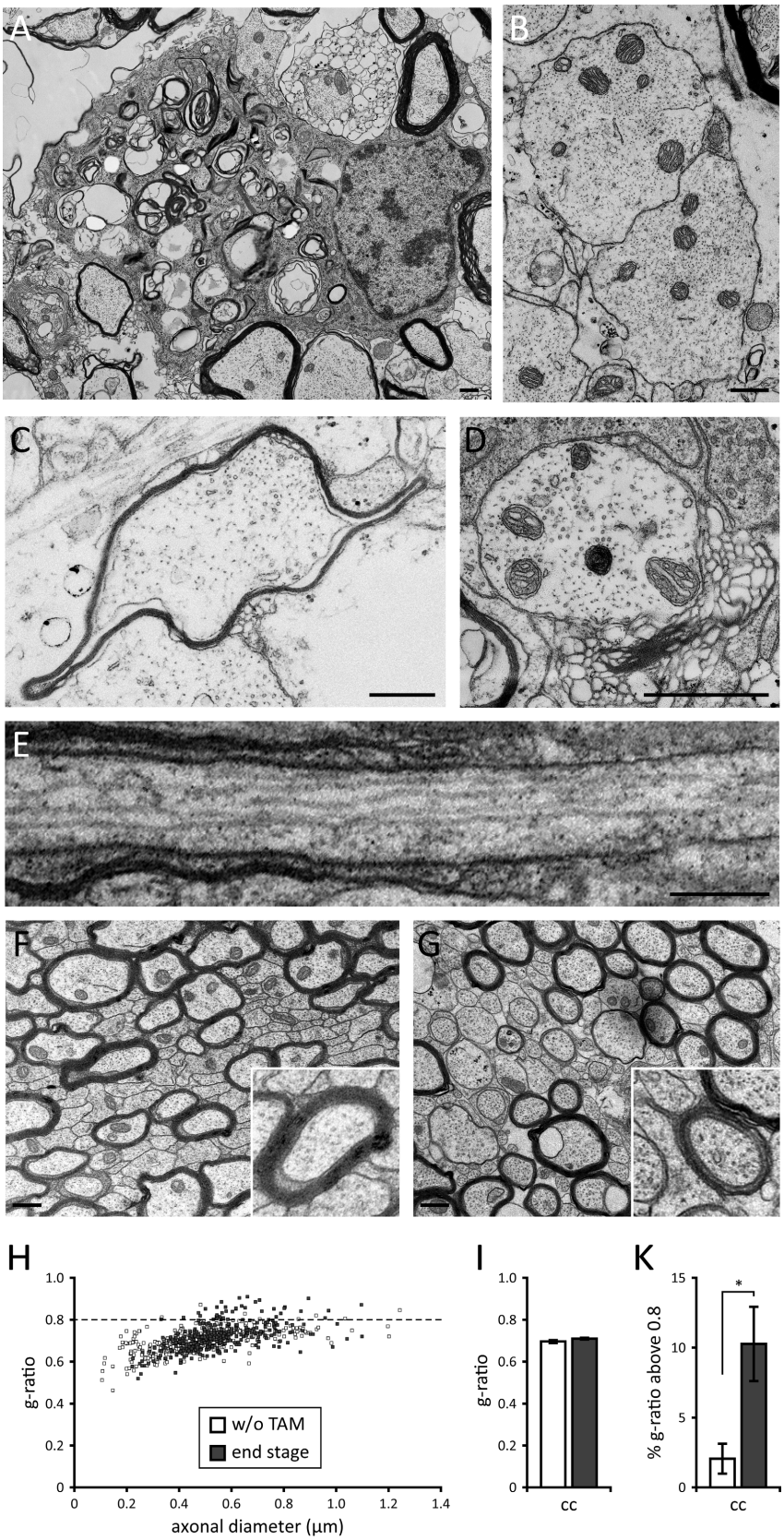

Figure 3-25: Myelin debris clearance and remyelination.

(A) Phagocytic cell engaged in clearance of myelin debris, as demonstrated by myelin debris-filled cytoplasmic vacuoles, were frequently found within damaged tissue at end stage. **(B)** Completely denuded axons can be found in strongly affected tissues. **(C)** Occasionally, thin myelin sheaths indicative of remyelination were present. **(D)** Presence of myelin debris in the vicinity of naked axons, likely to inhibit remyelination. **(E)** Demyelination affecting only a selected internode leading to heminode formation. **(F,G)** Comparison of the weakly myelinated corpus callosum (cc) between control **(F)** and experimental **(G)** mice at end stage showing some thinner myelin sheaths in the latter, indicative of remyelination. Inserts show magnifications of myelinated axons of comparable size. **(H)** Scattergram of g-ratios in relation to axonal diameters reveals a population of thinly myelinated axons with g-ratios >0.8 specifically in experimental animals. **(I)** Mean g-ratios do not show a significant difference but **(K)** the percentage of fibres with g-ratios >0.8 is significantly increased in experimental mice, indicating a population of remyelinated axons. *Data are given as mean ± SEM. n=3; *=p<0.05, Student's* t*-test. Scale bars: 1 µm.*

epitope during myelin degradation (Takahashi et al., 2007) (Fig. 3-24 C). This staining seems to be often linked with ongoing myelin debris clearance and active myelin disassembly (Zhao & Franklin, personal communication) as MBP degradation without active processes might be rarely detectable due to its stability (Fischer & Morell, 1974; Singh & Jungalwala, 1979).

Myelin clearance finally resulted in denuded axons (Fig. 3-25 B), although the majority of axons were still associated with disrupted myelin (Fig. 3-6 D), myelin debris remnants (Fig. 3-25 C), or rarely with normal appearing myelin. Occasionally, abnormally thin but normal appearing myelin sheaths indicative of remyelination were observed (Fig. 3-25 D). However, such remyelinated fibres were sparse and dispersed. Loss of myelin sometimes affected only individual internodes along a given axon as indicated by the presence of heminodes (Fig. 3-25 E). In line with observed variations in tissue disruption and reactive cells compared to other tissues, thin but intact myelin sheaths were frequent in the corpus callosum (Fig. 3-25 F,G). Analysis of g-ratios revealed no significant differences between experimental and control mice, but g-ratios above 0.8 indicative of ongoing remyelination were found associated with 10% of the axons in experimental mice (Fig. 3-25 H-K). Axonal diameters of myelinated axons did not differ between the two groups. These data indicate that remyelination occurred in the corpus callosum after acute oligodendrocyte cell death, although its extent was difficult to assess given that g-ratios of myelinated and remyelinated axons are indistinctive due to the small diameters of the majority of axons in this tract (Stidworthy et al., 2003). Overall myelin clearance and subsequent remyelination in this model was not sufficient to cause functional recovery in the experimental mice before the experiment had to be terminated.

Genetically targeted cell death of adult oligodendrocytes causes axonal damage

As briefly indicated before and shown in Fig. 3-5, adult oligodendrocyte loss and subsequent persisting myelin damage affects axonal integrity. To investigate axonal impairment, I first performed immunohistochemistry using SMI32 antibodies that specifically recognise a non-phosphorylated neurofilament epitope, in combination with an antibody that recognises neurofilament M. A striking increase in immunoreactivity in the cerebellar white matter of experimental mice was detected at end stage, indicative of a structural impairment of the axonal cytoskeleton (Fig. 3-26 A). Consistent with these findings, also increased neuronal staining of amyloid precursor protein (APP), an indicator of impaired axonal transport, and Fluoro-Jade C, a marker of general axonal/neuronal impairment (Schmued et al., 2005), showed increased signal intensity (Fig. 3-26 B). Morphological observations of axonal accumulation of cell organelles (Fig. 3-26 E) and axon atrophy (Fig. 3-6 C,D) corroborated these findings. Quantitative analysis of SMI32 immunoreactivity over time revealed a tendency of axonal damage to increase starting with onset of clinical signs, with the impairment being significant at end stage (Fig. 3-26 C). To investigate structural changes at nodes of Ranvier, Caspr (localised in the paranodal axolemma) and Kv1.2 (juxtaparanodal axolemma) were analysed by immunohistochemistry on spinal cord longitudinal sections in experimental mice at end stage. Both marker proteins were lost at approximately half of nodes of Ranvier in experimental mice (Fig. 3-26 D), indicating loss of nodal compartmentalisation and therefore saltatory impulse propagation. However, terminal axonal ovoids, a typical structure appearing in dye-back axonopathy subsequent to axonal transection (Trapp et al., 1999) could rarely be detected. Neither was obvious axonal loss observed. Additionally, apoptotic neurons were not detected anywhere in the CNS (data not shown). In summary, these data indicate that axons are vulnerable to the death of adult oligodendrocytes resulting in structural and likely functional impairment, despite the lack of involvement of an adaptive immune system reaction.

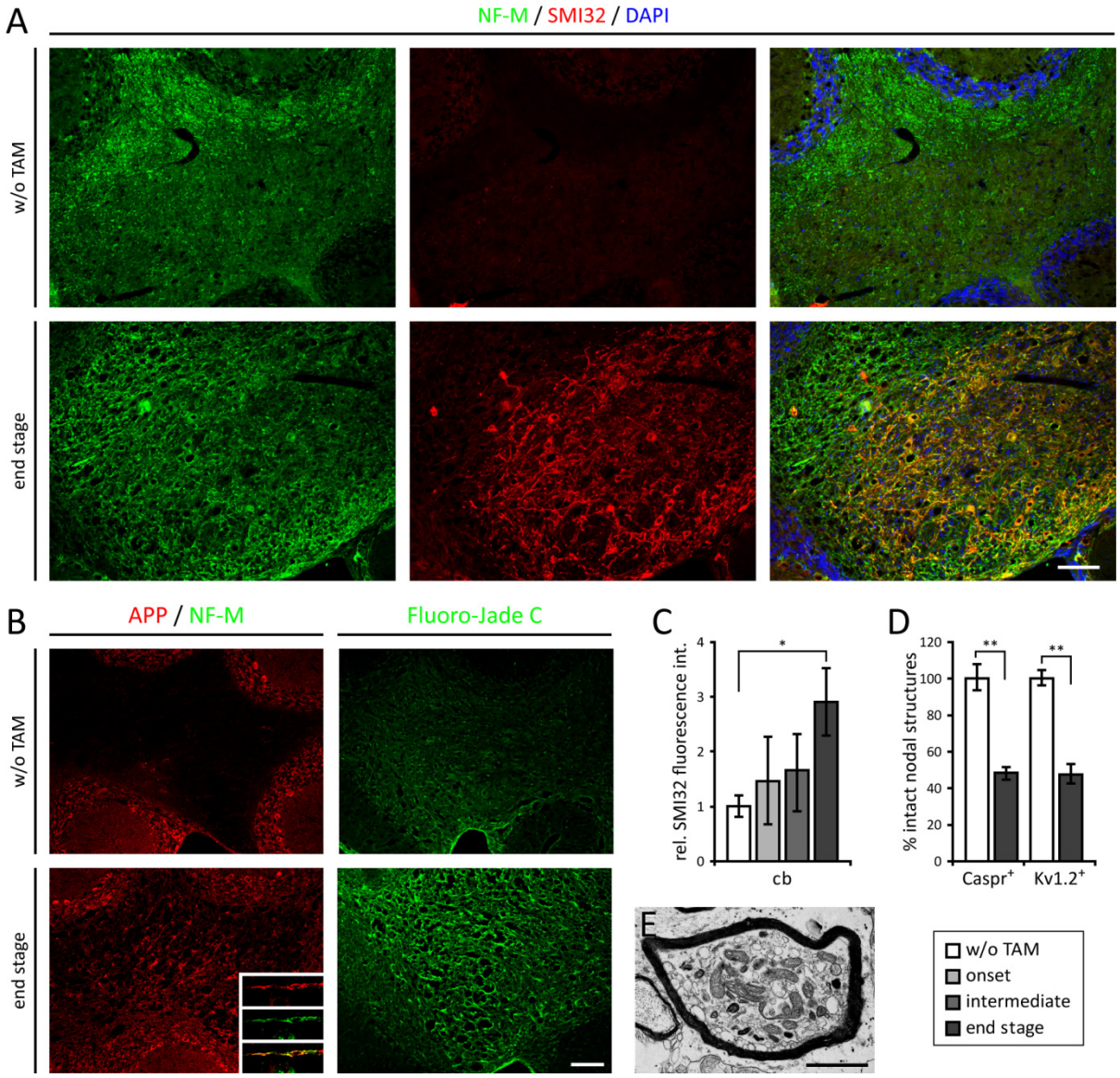

Figure 3-26: Axonal impairment resulting from loss of adult oligodendrocytes.

(A) Animals at end stage show increased immunefluorescence staining for nonphosphorylated neurofilament (SMI32), **(B)** amyloid precursor protein (APP) and Fluoro-Jade C, indicative of secondary axonal damage in damaged areas such as the cb. Inlet shows single confocal plane optical section of an exemplary neuron double-positive for APP and NF-M. **(C)** Quantification of SMI32 staining over the time course of disease development in cb shows increased neurofilament derangement indicative of axonal impairment, reaching significance in increase at end stage. **(D)** Quantification of intact nodal structures with the axonal markers Kv1.2 (juxtaparanodal) and Caspr (paranodal) reveals a strong reduction in the spinal cord at end stage. **(E)** Example of aberrant accumulation of organelles in an axon indicative of defective axonal transport. *Data are given as mean ± SEM. n=3; *=p<0.05, **=p<0.01, Student's* t-*test. Scale bars: 100 µm (A,B), 2 µm (D).*

DTI is sensitive to axonal damage following loss of adult oligodendrocytes

Axonal impairment is the underlying disease correlate in most demyelinating diseases. It is therefore desirable to possess a non-invasive imaging method allowing monitoring of axonal alterations. Therefore DTI was performed on experimental and control animals at base line and end stage phases using fractional diffusion anisotropy (FA), axial ($\lambda_{\parallel}$), and radial diffusitivity ($\lambda_{\perp}$) as readouts. Transverse colour-coded eigenvector DTI maps revealed a pronounced loss of directed diffusitivity in experimental animals that spatially matched with the areas of pronounced damage following genetically-mediated oligodendrocyte ablation (Fig. 3-27 A). Loss of intense colours indicating strong directional limitation of diffusion was apparent in cerebellar fibre tracts and brain stem white matter. Quantitative analysis of FA, $\lambda_{\parallel}$ and $\lambda_{\perp}$ was performed on cerebellar and brain stem ROIs (Fig. 3-27 B). Both FA and $\lambda_{\parallel}$ values were decreased in cerebellum and brain stem at end stage in experimental mice, but not $\lambda_{\perp}$, although there was a tendency for radial diffusitivity to be increased (Fig. 3-27 C). These data suggest that structural organisation of the tissue as well as axonal integrity is lost, despite rather unchanged radial diffusion barriers. These findings are well in line with the morphological observations of vacuolation, axonal impairment and defective myelin occupying most axons, and indicate that DTI is a sensitive and suitable method to monitor myelin and axon defects after demyelinating insults.

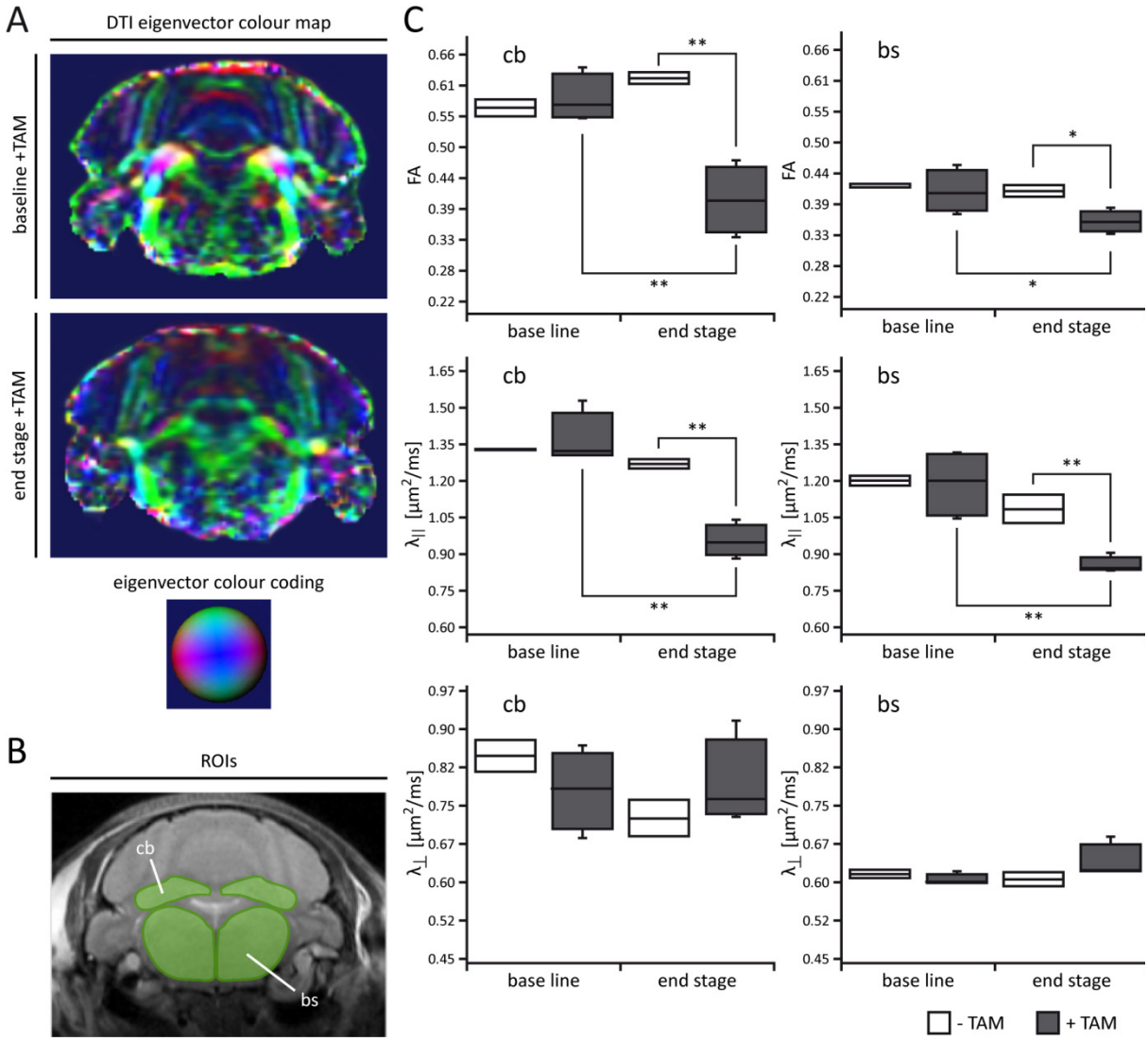

Figure 3-27: Diffusion tensor imaging to monitor axonal and myelin impairment.

(A) Transverse diffusion direction-dependent eigenvector colour-coded DTI maps of a representative animal at baseline (day 3) and end stage (day 39) after TAM-mediated ablation of oligodendrocytes. Red, blue and green colours indicate structures aligning along the lateral, anterior-posterior, and superior-inferior orientation axes, respectively. **(B)** Representative T2-weighted MRI section with superimposed ROIs used for quantification. **(C)** Box plots of quantitative DTI parameters fractional anisotropy (FA), axial ($\lambda_{\parallel}$), and radial diffusitivity ($\lambda_{\perp}$) derived from ROIs in cerebellum (cb), brain stem (bs), frontal cortex (fx) and olfactory bulb (ob) at baseline (average of day 3, 8 and 11) and end stage (average of day 35 and 39) control (-TAM) and experimental (+TAM) animals. Both white and mixed matter of cb and bs show decreased FA and $\lambda_{\parallel}$, but no clear increase in $\lambda_{\perp}$. This indicates general loss of tissue order, loss of fibre tract integrity –(likely axonal based), but no severe loss of lateral diffusion barriers such as constituted by myelin. *Data are given as median, 1st and 3rd quartiles, sample minimum, sample maximum. n= 2 -TAM / 4 +TAM; *=p<0.05, **=p<0.01, ANOVA and Fisher's PLSD posthoc test.*

Grey matter tissue is affected by oligodendroglial ablation despite only minor signs of tissue disruption

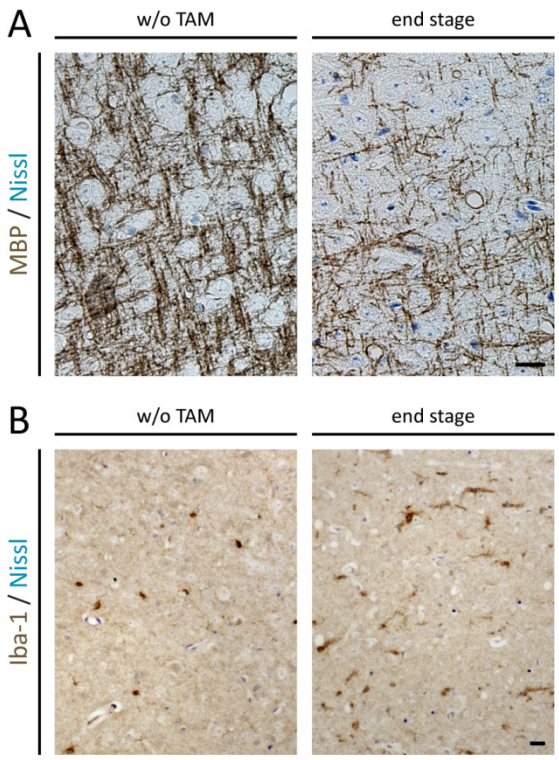

Figure 3-28: Cortical grey matter damage following genetically-mediated ablation of myelinating glia.

(A) MBP histological stainings of frontal cortex grey matter. Note reduction of staining but only sparse vacuolation. **(B)** Iba-1 histological staining of frontal cortex grey matter showing only mild microgliosis at end stage. *Scale bars: 20 µm.*

Grey matter tissue alterations are frequently found in demyelinating diseases such as MS, although they have not received the same interest as white matter damage, partially due to their inconspicuousness on radiological examination. It was therefore of general interest to investigate the mouse model introduced here for grey matter pathologies and its potential suitability as a model for grey matter demyelination. Grey matter of the frontal cortex (Fig. 3-28 A) or spinal cord (Fig. 3-5 A) displayed noticeable demyelination, as visualised by MBP stainings. Morphological analysis revealed also minor tissue vacuolation (Fig. 3-6 A). Additionally, phagocytic cells with ramified appearance were present at end stage (Fig. 3-28 B). These changes might underlie the observed decrease in T2 values (Figs. 3-2; 3-3), which are generally thought to indicate hypercellularity as well as myelin loss without increase of free water. The mouse model presented here might therefore provide a convenient model to study grey matter demyelination events.

The PNS remains unaltered despite recombination

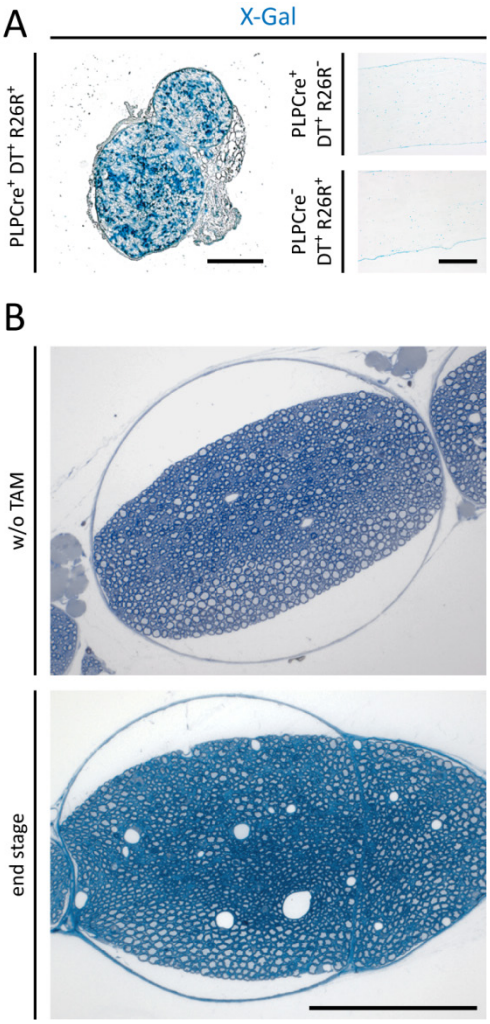

Figure 3-29: *PLP:CreER*-mediated recombination does not lead to PNS impairment in experimental mice.

(A) X-Gal staining of sciatic nerves of triple-transgenic experimental mice harbouring additionally the *R26R26:lxSTOP/lacZ* reporter transgene revealed recombination and subsequent β-gal expression only when Cre and reporter transgene were present. **(B)** Although recombination likely occurs, the sciatic nerve of experimental animals remains morphologically unaltered at end stage, as shown on toluidine blue stained resin sections. *Scale bars: 200 µm.*

Adult demyelination of the PNS is a field of considerable interest. I therefore investigated PNS tissue after induction of glial cell death. Recombination occurs in the sciatic nerve of experimental mice, and is absent in control mice or in mice treated with TAM but lacking the *Cre* transgene, as monitored with the *R26:lxSTOP/lacZ* mouse line (Soriano, 1999) (Fig. 3-29 A). But interestingly, the nerve tissue remains morphologically unaltered as much as 40 days after recombination induction, even though recombination has occurred (Fig. 3-29 B). Recombination in the *ROSA26*-promotor driven reporter line but not the *R26:DT-A* line, harbouring a very similar construct within the same locus, is very unlikely. Additionally, no increase in cell density, apoptotic cells or DT-A expression could be observed. Furthermore, *R26:DT-A* mice additionally carrying an inducible Cre under control of the *P0*-promotor, remained unaffected, and the nerve was structurally unaltered for very long periods (data not shown). Why the genetic system does not work in PNS Schwann cells remains to be clarified.

Discussion

In the last decades, the view on the role of myelin and myelinating glia has changed remarkably. While myelin was formerly thought to solely be the nerve's insulation that allows saltatory nerve conduction, it is nowadays well accepted that its role is more complex: myelin and myelinating cells serve multiple purposes in the maintenance of proper nervous system function, and therefore demyelination results in more than just loss of insulation.

To provide a powerful tool to study these complex interactions, I established a novel genetic mouse model based on inducible ablation of oligodendrocytes. This model aims to complement existing models and is described in this work. Cell-intrinsic ablation of adult myelinating oligodendrocytes in the intact, fully developed nervous system provides a highly reproducible and well controllable model to examine the biology of axo-glial interactions, consequences of myelin loss, and myelin repair.

Currently available models to study the interplay of axons with the myelinating cell and the consequences of a disruption of this relationship are based on gene-specific mutations (Nave & Trapp, 2008), induced autoimmunity against CNS components (Baxter, 2007), or the use of various toxins (Blakemore & Franklin, 2008). Each of these established models is provides valuable insight into specific aspects underlying mechanisms of myelin pathology, and a significant gain of understanding of myelin function in health and disease will continue to emerge from their use (Lassmann, 2008). However, none allows well defined and specific ablation of adult myelinating glia without confounding primary effects on other CNS cell types. In the model described here, oligodendrocytes are directly depleted instead of being only compromised, and importantly, neither associated axons nor immune system components are primarily involved.

Cellular events following genetically-triggered cell death of adult oligodendrocytes

After induction of genetic recombination and subsequent triggering of cell death in myelinating glia, an unexpected slow disease progression with an initial lag period and a late onset was observed. Yet, the clinical course following ablation of oligodendrocytes was strikingly constant and highly reproducible, suggesting a well defined and orchestrated sequence of underlying events.

Upon TAM injection, oligodendroglia were depleted relatively rapidly, efficiently, and synchronously in all CNS regions analysed. This is in line with findings documenting the very fast clearance of dying oligodendrocytes (Barres et al., 1992; Barnett & Prineas, 2004). Interestingly, although the time span of Sox10+ cell loss was short and well defined, very few apoptotic cells and only sporadic apoptotic

oligodendroglia could be detected using apoptosis markers. This suggests that adult oligodendrocytes undergo apoptotic cell death without displaying classical apoptotic markers. Concordantly, dying adult oligodendrocytes have been found to only rarely display DNA fragmentation and very little or no positivity for cleaved caspase 3 in MS or gene mutation-mediated myelin defects (Skoff et al., 1994; Williams & Gard, 1997; Knapp et al., 1999; Cerghet et al., 2001; Barnett & Prineas, 2004; Stadelmann et al., 2005). Nonetheless, myelin did not immediately disappear upon oligodendrocyte loss, and pathological changes of tissue and myelin morphology were not observable early in the disease course. These data indicate that when oligodendrocytes undergo apoptotic cell death, internodal myelin segments are shed from the cell bodies instead of being actively degraded, similarly as suggested in Wallerian degeneration (Vargas & Barres, 2007). While the oligodendroglial cell bodies were cleared, their associated myelin remained behind (Fig. 4-1 B).

The first clinical signs coincided with the appearance of myelin pathologies, including progressive vacuolation, likely occurring due to the decay of structurally important myelin components (Baumann & Pham-Dinh, 2001). Given, that clinical signs are caused by impairment of normal axonal function, these findings indicate that on the one hand, short-term loss of metabolically active oligodendrocytes has no distinct impact on axonal function and integrity, and on the other hand, that remaining internodes shed from their cell body are capable of maintaining axonal compartmentalisation and efficient conduction. Myelin vacuoles increased both in size and number with clinical progression, and structural integrity of myelinated internodes was gradually lost. This structural decay likely leads to disruption of axo-glial interactions, especially at the axo-glial junction, and finally resulted in the loss of nodal structures, consequent impairment of saltatory conduction, and neurologic impairment (Arroyo et al., 2004; Howell et al., 2006) (Fig. 4-1 C).

With increasing myelin decay and structurally impaired myelin lamella resulting in myelin decrease, microglia and less so astrocytes, became successively activated, proliferated and augmented within damaged tissues. Activated microglia were also found to be involved in phagocytic myelin debris clearance, although with rather late onset and overall being slow and inefficient. Additionally, the BBB remained intact and within the CNS parenchyma neither blood-derived macrophages nor adaptive immune cells were found that could facilitate or stimulate debris clearance (Fig. 4-1 D). Consequently, resident microglia appear to be inefficient in debris clearance in the present setting, a process believed to be vital for tissue regeneration and dependent on at least a limited amount of inflammatory processes such as recruitment of phagocytes and BBB penetrability (Vargas & Barres, 2007; Neumann et al., 2009).

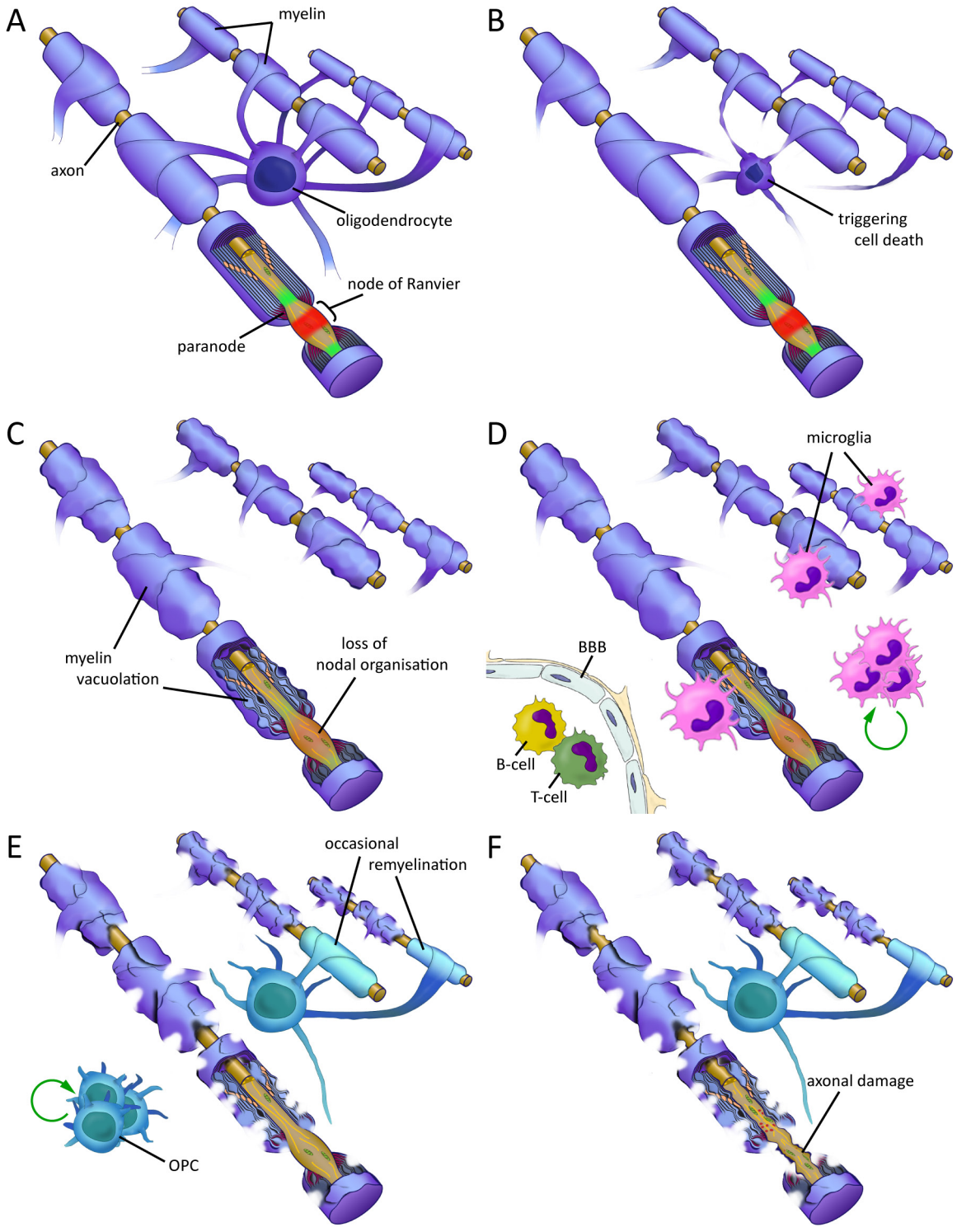

Fig. 4-1: Model of events following genetically-mediated induction of oligodendrocyte cell death.

(A) In adult oligodendrocytes forming intact myelin internodes, cell death is triggered genetically. **(B)** Triggering of cell death leads to loss of oligodendroglial cell bodies, but myelin internodes remain behind. **(C)** Myelin vacuolation and detachment occurs, likely due to structural decay of myelin components. Myelin decay leads to disruption of the axoglial junction, loss of axonal compartmentalization, and saltatory conduction is lost. **(D)** Microglia react in response to myelin damage, proliferate and phagocytose myelin. The blood brain-barrier (BBB) remains intact; lymphocytes do neither extravasate nor are they involved in pathology modulation. **(E)** OPCs react by proliferating. Myelin decay and phagocytic clearance allow occasional remyelination, but vastly myelin debris remains present. **(F)** Clearance of myelin debris and remyelination are insufficient; damaged myelin persists, and finally axonal damage occurs.

Effective tissue repair by remyelination after myelin damage requires clearance of old myelin, activation of OPCs, and their subsequent differentiation into myelin-forming oligodendrocytes (Franklin & ffrench-Constant, 2008). Besides limited myelin debris clearance, OPCs became activated late on subsequent to myelin damage –but not early on in response to oligodendrocyte ablation, acquired a ramified morphology, proliferated within and likely migrated into areas of myelin damage (Sim et al., 2002). This precursor activation is suspected to be indirect and to rely on microglial and astrocytic signalling in response to myelin defects (Levine & Reynolds, 1999; Glezer et al., 2006; Rhodes et al., 2006). Although OPCs were activated upon damage, remyelination remained a sparse event in most tissues investigated (Fig. 4-1 E). This lack of remyelination is possibly due to the unavailability of denuded axons and the inhibitory properties of myelin debris on OPC differentiation (Miller, 1999; Kotter et al., 2006; Syed et al., 2008; Baer et al., 2009).

Subsequently, with persistence of myelin damage, and both inefficient myelin debris clearance and remyelination, axonal damage commenced (Fig. 4-1 D). Axonal transport and axoskeletal organisation became increasingly impaired secondary to oligodendroglial cell death and myelin defects, although axonal transection as indicated by axonal terminal spheroids could not be observed. This axonal impairment is independent of adaptive immune system functions, since both myelin disruptions and axonal damage were identical in an immune-deficient mouse strain. This indicates that axons degenerate independent of adaptive immune cells when debarred from functional oligodendrocytes for extended periods, and is in line with the view that myelinating glia provide vital trophic support for the underlying axons (Nave & Trapp, 2008; Nave, 2010b).

In summary, the model is characterised by early, fast and efficient loss of adult oligodendrocytes, residual myelin subject to decay, inefficient myelin debris clearance and repair, and consequent axonal damage; all this occurs in the absence of extensive inflammation and is unaltered by the adaptive immune system (Fig. 4-1).

Secondary axonal damage following genetic ablation of oligodendrocytes

Axonal impairment in demyelinating diseases is thought to be the main clinical correlate, with axonal loss being the major cause of irreversible disability. In mouse models axonal impairment is well known and most prominent in inflammatory demyelination, and mostly linked to nonspecific damage caused by the inflammatory process. However, the impact of chronic loss of myelin on the maintenance of axonal function and integrity has meanwhile come to be considered a major factor, although debated (DeLuca et al., 2006; Dutta & Trapp, 2007; Trapp & Nave, 2008).

Following genetically-mediated cell death of myelinating oligodendrocytes in this mouse model, accumulating axonal damage was observed, especially in areas of pronounced myelin damage and vacuolation with abundant residual myelin debris and marginal repair. Axonal deficiencies included axonal transport defects, cytoskeletal reorganisation or breakdown, axonal atrophy, and loss of domain organisation, but not axonal transection or loss. The latter were often attributed to inflammatory-mediated axonal damage and especially transection was linked with mechanisms of adaptive immunity (Babbe et al., 2000; Dutta & Trapp, 2007; Sobottka et al., 2009). Their absence in the model described here is therefore not surprising, given that lymphocytes are absent from CNS tissue and not involved in the modulation of the disease.

Defective axonal transport, disruption of the axonal cytoskeleton, loss of nodal organization, and axon atrophy on the other hand are thought to be caused by a variety of different factors and are likely multifactorial. Loss of axonal compartmentalisation due to the loss of myelin and the axo-glial junction leads to uncontrolled distribution of ion channels, and therefore failure in saltatory conduction with ultimately higher energy demands on the axon (Einheber et al., 2006; Howell et al., 2006). Additional alterations of axonal energy metabolism are thought to nocuously contribute, potentially accumulating in virtual hypoxia and axonopathy. These additional insults might comprise: impaired mitochondrial function, Na^{+} influx, Ca^{++} release or influx, overactivation of glutamate receptors but also lack of metabolic supply due to impaired axonal transport or loss of myelinating glia (Trapp & Stys, 2009; Nave, 2010b).

Activated microglia and astrocytes –besides their role in attraction of detrimental inflammatory components– have been implicated in axonal impairment via inflammatory mediators affecting axonal metabolism, mitochondrial function, and transport (Lu et al., 2000; Dutta et al., 2006; De Vos et al., 2008). Additionally, microglial activation has been shown to precede axonal phenotypes in myelin gene defect-mediated axonal impairment (Yool et al., 2001; Lappe-Siefke et al., 2003). However, several observations lead one to hypothesise that other factors contribute substantially to the observed axonal degeneration in the model presented here: the late presence of astroglial and microglial activation; the vast amount of residual myelin still associated with axons and potentially protecting the underlying axon from inflammatory insults (Dutta & Trapp, 2007); and the lack of correlation between signs of axonal damage and the presence of activated microglia/astrocytes. Defective axonal transport might be an important factor in the observed axonal damage, as it is crucial both for local axonal metabolism as well as for long-range survival signalling (Coleman, 2005). Failure of axonal transport might be due to axoskeletal disorganisation, or inflammatory mediators (De Vos et al., 2008; Morfini et al., 2009), but might in the present model also be caused sterically by myelin vacuoles constricting axonal volume. Additionally, the long-term absence of contact with

metabolically active oligodendrocytes that potentially provide trophic support for the axon likely contributes to axonal damage (Nave & Trapp, 2008; Nave, 2010b).

Although remyelination will always be the final goal to fully restore axonal function after demyelinating insults (Irvine & Blakemore, 2008; Bruce et al., 2010), the model presented here could prove to be valuable in further dissecting potentially harmful factors causing axonal impairment. Additionally, it has the potential to allow investigation of strategies aiming at neuroprotection in demyelinating diseases and especially MS, as the model lacks strong and adaptive inflammation and might therefore better reflect chronic neurologic impairment during the progressive phase of the disease (Wilkins & Scolding, 2008).

In addition, neuroprotection might be key to full recovery following demyelination due to disease or injury as well as in the present model. Maintaining axonal structure as well as functionality for prolonged periods is likely critical, as remyelination by OPCs might depend on axonal activity (Bruce et al., 2010), and protecting axons from injury beyond reversal therefore maintaining their capacity for remyelination (Crawford et al., 2009) might be crucial. Neuroprotection maintaining normal axonal activity and structure might therefore ideally complement fostering of damage clearance and repair by increasing the time span in which remyelination can occur.

Remyelination following genetically-mediated ablation of adult oligodendrocytes

Remyelination found subsequent to ablation of myelinating glia was sparse in most tissues. In the majority of areas analysed, residual vacuolated myelin still associated with axons, often exhibiting signs of impairment, and widespread myelin debris dominated the picture. Completely denuded axons were rare and remyelinated fibres scarce. Additionally, proliferative OPCs could be found in most damaged areas at end stage, but not immediately upon oligodendrocyte ablation. Tissue vacuolation, presence of myelin debris and severe axon pathology was most prominent in areas containing large, heavily myelinated axons packed in dense white matter tracts such as the cortico-spinal tracts in the brain stem or spinal cord, or deep cerebellar white matter.

In contrast, the corpus callosum showed only little vacuole load or myelin debris, and few phagocytes. This was accompanied by substantial remyelination but no accumulation of proliferative OPCs. Various reasons might account for the low impairment and relatively effective repair, and these factors may be interrelated: 1) Corpus callosal axons are almost exclusively small diameter axons resulting in comparably thin myelin sheaths and short internodes, and the degree of myelination is rather small. There might thus be much less myelin debris generated after cell death of myelinating oligodendrocytes, and the debris would be dispersed within the fibre tracts, probably

aiding myelin clearance and/or being more permissive for OPC differentiation. Additionally, the corpus callosum is marked by a very high density of oligodendrocytes; therefore the amount of myelin associated with a single oligodendrocyte might be small. 2) For those small calibre axons being size-wise at the edge of necessity to be myelinated, demyelination might bear less detrimental consequences, resulting in less impairment and finally maintained capacity to be remyelinated. 3) The corpus callosum's localisation lying between the OPC-rich grey matter of the frontal cortex and the neuro- and gliogenic subventricular zone might provide unique availability of remyelinating precursor cells. The subventricular zone has been shown to be altered in its dynamics upon genetically-mediated ablation of oligodendrocytes, and might increase its supply of oligodendroglial lineage cells (Cristina Porcheri, unpublished data). Additionally, although proliferative OPCs were not increased within the corpus callosum, an increase in Sox10+ cells not yet reaching physiological levels suggests that OPCs multiply in the surrounding parenchyma and afterwards migrate into the corpus callosum to differentiate, rather than proliferative expansion within the tissue already finished being the source of cell number recovery.

The picture found in most other white and mixed matter tissues, including the morphologically quite similar anterior commissure, is rather the contrary. Tissue appearance is dominated by pronounced myelin and axonal damage, and increased OPC proliferation, but a lack of remyelination; culminating in the spinal cord's white matter with extensive damage and no OPC activation. This pathology clearly demonstrates that remyelination largely fails in this model.

Both remyelination and myelin debris clearance fail

With the obvious lack of remyelination in the absence of severe inflammation and primary confounding effects on other cell types, the model presented here offers novel opportunities to study remyelination failure. It is generally conceivable, that remyelination in this model might occur at later times exceeding the possible time frame of analysis, assuming that both survival and axonal preservation might be increased. However, given that in principle widespread extensive remyelination in the CNS is possible, efficient, and rather immediate (Chari & Blakemore, 2002; Franklin, 2002; Duncan et al., 2009), the reasons for the failure of timely remyelination in this mouse model might provide crucial insight into the underlying mechanisms. Considering the absence of an adaptive immune response and generally moderate inflammatory activity, a variety of inflammation-linked factors that are likely involved in remyelination failure in MS (Franklin & ffrench-Constant, 2008) can be excluded. Additionally, OPCs are found within damaged tissues and are proliferative despite very sparse remyelination. Although it cannot be estimated whether the present OPCs are

sufficient for complete recovery, they should at least be capable of substantial repair, and a failure in OPC activation and recruitment is therefore unlikely (Franklin & ffrench-Constant, 2008).

Remyelination failure is therefore presumably a failure in OPC differentiation into myelinating oligodendrocytes. Although axonal signals blocking oligodendroglial differentiation or lacking pro-differentiation signals have been demonstrated to play a role in remyelination failure (Franklin & ffrench-Constant, 2008; Syed et al., 2011), their contribution to remyelination failure in the model presented here is likely subordinate, given the vast amount of residual, defective myelin still covering most of the axonal surfaces.

Failure of remyelination can therefore be attributed to a failure in the initial step necessary for myelin restoration, the clearance of the old myelin –the myelin debris. Residual myelin might sterically inhibit axo-glial contact and mask axonal signals necessary for differentiation (Coman et al., 2005; Franklin & Kotter, 2008; Bruce et al., 2010; Taveggia et al., 2010). Additionally, myelin debris is inhibitory to OPC differentiation (Kotter et al., 2005; Kotter et al., 2006; Baer et al., 2009). Both factors are capable of suppressing remyelination and are found within damaged tissues. In general, tissue debris does not linger for long periods after CNS damage due to efficient removal by phagocytes (Neumann et al., 2009). Brisk and efficient debris clearance followed by thorough remyelination is a hallmark of toxin-induced demyelination (Zhao et al., 2006); and also in inflammatory demyelination, myelin debris is removed fast and efficiently (Barnett & Prineas, 2004; Frohman et al., 2006; Rodriguez, 2007). However, myelin debris associated with Wallerian degeneration can persist for long time periods, and debris persistence has been associated with a lack of inflammation and BBB opening (Miklossy & Van der Loos, 1991; Vargas & Barres, 2007).

Debris clearance within the CNS is normally executed by microglia, which show remarkable motility that enables them to monitor the surrounding parenchyma and phagocytose small debris or budded vesicular structures as they are arising during apoptosis (Neumann et al., 2009). This baseline phagocytic activity might be sufficient to clear the remnants of oligodendroglial cell bodies after genetic induction of cell death, but not the vast amount of myelin debris arising thereafter. Although microglia react extremely fast to CNS insults (Neumann et al., 2009), microglial activation after genetically-mediated cell death of adult oligodendrocytes was generally slow and appeared progressively along with myelin decay and vacuolation. Besides limited phagocytic capacities of microglia in comparison to blood-borne macrophages, and the dependency of effective CNS debris clearance and remyelination on the latter (Mosley & Cuzner, 1996; Popovich et al., 1999; Kotter et al., 2001), my results indicate that myelin remaining behind after oligodendroglial cell death does not exhibit any signal aiming at its phagocytosis and that these stimuli only arise with progressive decay

of myelin sheaths. Additionally, it is imaginable that large pieces of myelin debris might not be capable of being phagocytosed without further breakdown, and that additional inflammatory mediators, such as antibody/complement-mediated lysis (Vargas et al., 2010), might prove beneficial in this regard. Whether increased activation of microglial phagocytosis alone would be sufficient to facilitate efficient debris clearance and remyelination still needs to be elucidated.

Inflammation and its role following genetically-mediated ablation of oligodendrocytes

Adaptive immunity is neither present nor involved in the phenotype following genetically-mediated ablation of oligodendrocytes. The BBB is intact and no prominent extravasation of blood-borne macrophages is detectable. Furthermore, although CNS-resident cells capable of mediating or participating in an immune response –namely astrocytes and microglia– are activated, the lack of an effect on other immune components indicates that the pathological changes are not sufficient to induce a pronounced inflammatory response. In the case of microglia, this activation might reflect a phagocytic reaction without inflammation rather than an inflammatory trigger (Neumann et al., 2009), although the exact level of microglial and astrocytic activation and inflammatory contribution needs to be evaluated. Therefore, oligodendroglial cell death and subsequent appearance of myelin damage and debris does not deploy a pronounced inflammation of affected nervous tissues in the presented mouse model, in contrast to what has been suspected underlying primary demyelinating MS lesion (Barnett et al., 2006). The difference between non-inflammatory MS lesions and the mouse model presented here is further emphasised by the presence of large amounts of myelin debris in the mouse model, which is not seen in type III/IV lesions (Lassmann et al., 2001). This suggests that additional factors are involved in the appearance of these lesion types. However, additional systemic inflammatory insults might initiate an adaptive immune response directed towards CNS components, as an exacerbated disease course together with T-cells reactive to MOG was found, when additionally to genetic induction of glial cell death a systemic inflammation was triggered using complete Freund's adjuvant (Porcheri, Esposito & Pohl, unpublished data).

Overall, inflammation in the mouse model presented here is minimal, and seems to be insufficient to promote myelin debris clearance and efficient remyelination –two necessary steps for full recovery that are tightly linked with inflammatory processes (Foote & Blakemore, 2005; Hohlfeld, 2007; Franklin & ffrench-Constant, 2008). This model therefore allows one to study the amount of inflammation necessary for and beneficial to remyelination, and the factors involved in fine-tuning an inflammatory response supporting beneficial phagocytic clearance while minimising neurotoxic effects of inflammation (Diemel et al., 1998; Kotter et al., 2001; Neumann et al., 2009; Edgar et al., 2010). The balance between sufficient inflammation to promote fast myelin clearance while avoiding

detrimental bystander effects on the underlying axons (Papadopoulos et al., 2006) might be a fine line, given that in the short-term neuroinflammation is more deleterious than demyelination itself (Edgar et al., 2010). Additionally, especially chronic demyelination leads to axonal damage (Lindner et al., 2009) and therefore axons might allow remyelination only within a distinct time window before impairment interferes with remyelination and functional restoration (Crawford et al., 2009). Therefore, neuroprotective strategies might provide useful support during this process, as intact axons probably retain their myelination capacity throughout life (Setzu et al., 2004).

In summary, the model will likely provide valuable additional insights into the mechanisms underlying demyelination and especially inflammatory-driven demyelinating diseases, given that it is in its lack of beneficial inflammation so much contrary to existing models, where detrimental inflammation often dominates the picture.

Suitability of MRI methods to monitor pathologies underlying demyelination

Although MRI has proven to be a valuable imaging method to diagnose and monitor demyelinating diseases and in particular MS, the correlation between radiological MRI findings and underlying distinct tissue pathologies is not entirely clear (Barkhof, 2002). Therefore an MRI fingerprint of the mouse model presented here was compiled, to compare MRI findings resulting from non-inflammatory neurodegenerative processes following induction of oligodendroglial cell death to those found in inflammatory demyelination.

Hyperintense T2-lesions were associated in EAE with demyelination, inflammation and infiltration of immune cells (Nessler et al., 2007; Serres et al., 2009) and are generally considered an MRI hallmark of MS (Fazekas et al., 1999). Despite negligible inflammatory contribution in the present study, affected CNS tissues showed pronounced T2 hyperintensities with progression of tissue disruption, which can be attributed to the observed myelin vacuolation. Additionally, no infiltration of blood-borne macrophages could be detected using USPIO-enhanced MRI (Dousset et al., 1999a; Rausch et al., 2003; Ladewig et al., 2009). These findings support the view that alterations of T2 relaxation times can reflect a variety of pathological changes independent of inflammatory processes, such as demyelination, axonal loss or gliosis (Bruck et al., 1997; van Walderveen et al., 1998; van Waesberghe et al., 1999). T2 MRI therefore might be a valuable readout to monitor general nervous tissue pathology and diagnose CNS demyelinating diseases, but it exhibits limitations in detailed analysis of possible detrimental mechanisms underlying the disease.

Differential insights into pathological changes in tissues subjected to myelin damage might be provided by advanced MRI methods such as DTI or MTI. Analysis of DTI parameters revealed

decreased fractional anisotropy in areas of pronounced white matter damage after oligodendroglial ablation, and can be attributed to general structural tissue disruptions. Although assessment of fractional anisotropy is considered to be exquisitely sensitive to white matter pathologies, axonal and myelin damage cannot be discriminated. Analysis of directional diffusion coefficients revealed a clear decrease in axial, fibre parallel diffusivity, but only a trend in increase of radial, fibre perpendicular diffusitivity. Decrease in axial diffusitivity has been associated with axon degeneration, injury and axocytoskeleletal defects in demyelination (Arfanakis et al., 2002; Song et al., 2003; Sun et al., 2006; Budde et al., 2009), while increases in radial diffusitivity has been associated with dysmyelination and loss of myelin (Song et al., 2002; Song et al., 2005). These interpretations are in line with the axonal impairment found in the presence of disrupted and vacuolated, but still present myelin in the areas of pronounced damage after oligodendroglial cell death. DTI therefore provides a non-invasive imaging method that would allow for following of improvements in both axon protection and clearance of residual myelin longitudinally within one animal, as well as a potentially powerful radiological tool to dissect white matter pathology.

MTI is considered to represent predominantly a measure of myelin integrity, although inflammatory events, such as oedema formation, preceding demyelination might contribute to reductions in MTR (Gareau et al., 2000; Schmierer et al., 2004; Serres et al., 2009). Loss of MTR in affected regions found in the present mouse model at end stage might reflect both loss of macromolecular integrity by myelin decay as well as increase in tissue vacuolation, and the minor decrease reaching significance only in brainstem regions might be based on substantial residual myelin debris largely comprised of rather bulky fragments. Concluding, both sensitivity towards the pathology in this mouse model, and image resolution of MTI might be borderline and limiting its use, despite its auspicious potential in clinical use.

Summarising, a well chosen combination of MRI readouts is potentially well suited for monitoring demyelination and dissect underlying pathological processes, in MS as well as in mouse models thereof.

Advantages and potential future applications of the mouse model

The mouse model of demyelination I generated and described in this work has many advantages over existing research models, and is unique in its way of generating a single, temporally well defined insult to oligodendrocytes without potentially confounding effects on other cell types, including neurons or their axons as well as the immune system. In contrast, it does not provide an accurate facsimile of human demyelinating diseases but likely provides useful insights into their underlying mechanisms.

The cellular specificity of the model together with the defined clinical course allows studying the time sequence of events following cell death of myelinating glia and demyelination on a systemic scale, a possibility lacking until now (Trapp & Nave, 2008). Current genetic, injury, toxin-mediated, or inflammatory models used to study demyelination were either derogated by a diffuse and unsynchronised onset, a lack of cell type specificity, or both, resulting in complications when seeking to dissect distinct underlying factors.

Besides its novel mode of triggering demyelination, the consequent pathology of the mouse model turned out to be surprising and unique. The abundant myelin debris remaining after oligodendroglial cell death, gradually decaying in amount over time, allows for studying the consequences of impaired myelin debris clearance and the key factors involved in the absence of initial axonal impairment or inflammatory insults. Strategies to promote and speed up myelin debris clearance will provide valuable insights into the regulatory mechanisms of this process which is so vital preceding remyelination and repair (Neumann et al., 2009). Especially, the model will allow compiling of a microglial activation profile during debris clearance uninfluenced by modulating inflammatory mediators, which should deepen our understanding of how and whether phagocytic clearance of defective myelin is providing harmful insults to the associated axon (Trapp & Nave, 2008). This in turn will facilitate our understanding of axonal impairment consequent to loss of myelin and provide further insight into the axo-glial interdependency pointed out once more by the observed axonal damage in this model. Furthermore, the model provides unique opportunities to fine-tune necessary neuroprotective strategies aiming to counteract the deficiencies in trophic supply and the detrimental insults to axons following loss of myelin, and to tackle problems of axonal survival in chronically demyelinated situations –a mechanism of great concern and up to now without treatment perspective in secondary progressive MS (Wilkins & Scolding, 2008). Enhanced axonal preservation in combination with improved myelin clearance is likely key to promote remyelination in the mouse model presented here, but not less so in situations following disease or injury (Vargas & Barres, 2007; Nielsen et al., 2009).

Additionally, a focal model using similar mechanisms of oligodendrocyte ablation within a defined area might prove useful in understanding certain aspects of the underlying pathology as well as to monitor the subsequent events for extended periods and would allow for better comparison with models of focal toxin use (Blakemore & Franklin, 2008). Unfortunately, focal injections of TAM have proven to be fruitless, resulting in rather sparse, distributed recombination of single cells rather than a locally defined insult (data not shown). In addition, titrating recombination efficiency by altered TAM injection paradigms to obtain locally distributed and alleviated damage turned out to be futile,

resulting in either only little reduction of recombination efficiency or no recombination at all (data not shown).

Ultimately, the model will contribute to our understanding of the cascade of events subsequent to demyelination originating in the oligodendrocytes and ideally ending in full remyelination, being so clearly different from currently established models. This model might be of particular interest, not because it fails in remyelination, but because the failure originates in the primary event of white matter repair, the clearance of damaged myelin, and is therefore unique amongst demyelinating mouse models. In addition, the regional differences in tissue damage, debris clearance and repair between the different CNS tissues and understanding the causative factorial cellular interplay might prove to be key to further understanding of the dynamics and regulation of remyelination and repair following myelin damage.

In summary, I present in this work a highly reproducible animal model of induced cell death of oligodendrocytes that has ample potential to promote our understanding of axo-glial interactions, demyelination, myelin clearance and subsequent remyelination, and reveals some potential uses to investigate treatment strategies aiming to ameliorate myelin diseases.

References

Adornato, B., and Lampert, P. (1971). Status spongiosus of nervous tissue. Electron microscopic studies. Acta Neuropathol *19*, 271-289.

Akassoglou, K., Bauer, J., Kassiotis, G., Pasparakis, M., Lassmann, H., Kollias, G., and Probert, L. (1998). Oligodendrocyte apoptosis and primary demyelination induced by local TNF/p55TNF receptor signaling in the central nervous system of transgenic mice: models for multiple sclerosis with primary oligodendrogliopathy. Am J Pathol *153*, 801-813.

Andlin-Sobocki, P., Jonsson, B., Wittchen, H.U., and Olesen, J. (2005). Cost of disorders of the brain in Europe. Eur J Neurol *12 Suppl 1*, 1-27.

Anyanwu, E.C., and Kanu, I. (2007). Biochemical impedance on intracellular functions of vitamin B12 in chronic toxigenic mold exposures. ScientificWorldJournal *7*, 1649-1657.

Arfanakis, K., Hermann, B.P., Rogers, B.P., Carew, J.D., Seidenberg, M., and Meyerand, M.E. (2002). Diffusion tensor MRI in temporal lobe epilepsy. Magn Reson Imaging *20*, 511-519.

Arroyo, E.J., Sirkowski, E.E., Chitale, R., and Scherer, S.S. (2004). Acute demyelination disrupts the molecular organization of peripheral nervous system nodes. J Comp Neurol *479*, 424-434.

Audoin, B., Guye, M., Reuter, F., Au Duong, M.V., Confort-Gouny, S., Malikova, I., Soulier, E., Viout, P., Cherif, A.A., Cozzone, P.J., Pelletier, J., and Ranjeva, J.P. (2007). Structure of WM bundles constituting the working memory system in early multiple sclerosis: a quantitative DTI tractography study. Neuroimage *36*, 1324-1330.

Babbe, H., Roers, A., Waisman, A., Lassmann, H., Goebels, N., Hohlfeld, R., Friese, M., Schroder, R., Deckert, M., Schmidt, S., Ravid, R., and Rajewsky, K. (2000). Clonal expansions of CD8(+) T cells dominate the T cell infiltrate in active multiple sclerosis lesions as shown by micromanipulation and single cell polymerase chain reaction. J Exp Med *192*, 393-404.

Baer, A.S., Syed, Y.A., Kang, S.U., Mitteregger, D., Vig, R., Ffrench-Constant, C., Franklin, R.J., Altmann, F., Lubec, G., and Kotter, M.R. (2009). Myelin-mediated inhibition of oligodendrocyte precursor differentiation can be overcome by pharmacological modulation of Fyn-RhoA and protein kinase C signalling. Brain *132*, 465-481.

Bakshi, R., Thompson, A.J., Rocca, M.A., Pelletier, D., Dousset, V., Barkhof, F., Inglese, M., Guttmann, C.R., Horsfield, M.A., and Filippi, M. (2008). MRI in multiple sclerosis: current status and future prospects. Lancet Neurol *7*, 615-625.

Barbin, G., Aigrot, M.S., Charles, P., Foucher, A., Grumet, M., Schachner, M., Zalc, B., and Lubetzki, C. (2004). Axonal cell-adhesion molecule L1 in CNS myelination. Neuron Glia Biol *1*, 65-72.

Barkhof, F. (2002). The clinico-radiological paradox in multiple sclerosis revisited. Curr Opin Neurol *15*, 239-245.

Barnett, M.H., and Prineas, J.W. (2004). Relapsing and remitting multiple sclerosis: pathology of the newly forming lesion. Ann Neurol *55*, 458-468.

Barnett, M.H., Henderson, A.P., and Prineas, J.W. (2006). The macrophage in MS: just a scavenger after all? Pathology and pathogenesis of the acute MS lesion. Mult Scler *12*, 121-132.

Barnett, M.H., and Sutton, I. (2006). The pathology of multiple sclerosis: a paradigm shift. Curr Opin Neurol *19*, 242-247.

Barnett, M.H., Parratt, J.D., Pollard, J.D., and Prineas, J.W. (2009). MS: is it one disease? Int MS J *16*, 57-65.

Barres, B.A., Hart, I.K., Coles, H.S., Burne, J.F., Voyvodic, J.T., Richardson, W.D., and Raff, M.C. (1992). Cell death and control of cell survival in the oligodendrocyte lineage. Cell *70*, 31-46.

Barres, B.A., and Raff, M.C. (1993). Proliferation of oligodendrocyte precursor cells depends on electrical activity in axons. Nature *361*, 258-260.

Basser, P.J., Mattiello, J., and LeBihan, D. (1994). MR diffusion tensor spectroscopy and imaging. Biophys J *66*, 259-267.

Baumann, N., and Pham-Dinh, D. (2001). Biology of oligodendrocyte and myelin in the mammalian central nervous system. Physiol Rev *81*, 871-927.

Baxter, A.G. (2007). The origin and application of experimental autoimmune encephalomyelitis. Nat Rev Immunol *7*, 904-912.

Beer, S., and Kesselring, J. (1994). High prevalence of multiple sclerosis in Switzerland. Neuroepidemiology *13*, 14-18.

Benes, F.M., Turtle, M., Khan, Y., and Farol, P. (1994). Myelination of a key relay zone in the hippocampal formation occurs in the human brain during childhood, adolescence, and adulthood. Arch Gen Psychiatry *51*, 477-484.

Bengtsson, S.L., Nagy, Z., Skare, S., Forsman, L., Forssberg, H., and Ullen, F. (2005). Extensive piano practicing has regionally specific effects on white matter development. Nat Neurosci *8*, 1148-1150.

Bergles, D.E., Roberts, J.D., Somogyi, P., and Jahr, C.E. (2000). Glutamatergic synapses on oligodendrocyte precursor cells in the hippocampus. Nature *405*, 187-191.

Bhat, M.A. (2003). Molecular organization of axo-glial junctions. Current Opinion in Neurobiology *13*, 552-559.

Birgbauer, E., Rao, T.S., and Webb, M. (2004). Lysolecithin induces demyelination in vitro in a cerebellar slice culture system. J Neurosci Res *78*, 157-166.

Bjartmar, C., Hildebrand, C., and Loinder, K. (1994). Morphological heterogeneity of rat oligodendrocytes: electron microscopic studies on serial sections. Glia *11*, 235-244.

Bjartmar, C., Kidd, G., Mork, S., Rudick, R., and Trapp, B.D. (2000). Neurological disability correlates with spinal cord axonal loss and reduced N-acetyl aspartate in chronic multiple sclerosis patients. Ann Neurol *48*, 893-901.

Blakemore, W.F. (1972). Observations on oligodendrocyte degeneration, the resolution of status spongiosus and remyelination in cuprizone intoxication in mice. J Neurocytol *1*, 413-426.

Blakemore, W.F. (1974). Pattern of remyelination in the CNS. Nature *249*, 577-578.

Blakemore, W.F., and Franklin, R.J. (2008). Remyelination in experimental models of toxin-induced demyelination. Curr Top Microbiol Immunol *318*, 193-212.

Boespflug-Tanguy, O., Labauge, P., Fogli, A., and Vaurs-Barriere, C. (2008). Genes involved in leukodystrophies: a glance at glial functions. Curr Neurol Neurosci Rep *8*, 217-229.

Bradl, M., and Linington, C. (1996). Animal models of demyelination. Brain Pathol *6*, 303-311.

Brady, S.T., Witt, A.S., Kirkpatrick, L.L., de Waegh, S.M., Readhead, C., Tu, P.H., and Lee, V.M. (1999). Formation of compact myelin is required for maturation of the axonal cytoskeleton. J Neurosci *19*, 7278-7288.

Bray, P.F., Luka, J., Culp, K.W., and Schlight, J.P. (1992). Antibodies against Epstein-Barr nuclear antigen (EBNA) in multiple sclerosis CSF, and two pentapeptide sequence identities between EBNA and myelin basic protein. Neurology *42*, 1798-1804.

Brill, M.H., Waxman, S.G., Moore, J.W., and Joyner, R.W. (1977). Conduction velocity and spike configuration in myelinated fibres: computed dependence on internode distance. J Neurol Neurosurg Psychiatry *40*, 769-774.

Brinkmann, B.G., Agarwal, A., Sereda, M.W., Garratt, A.N., Muller, T., Wende, H., Stassart, R.M., Nawaz, S., Humml, C., Velanac, V., Radyushkin, K., Goebbels, S., Fischer, T.M., Franklin, R.J., Lai, C., Ehrenreich, H., Birchmeier, C., Schwab, M.H., and Nave, K.A. (2008). Neuregulin-1/ErbB signaling serves distinct functions in myelination of the peripheral and central nervous system. Neuron *59*, 581-595.

Brocard, J., Warot, X., Wendling, O., Messaddeq, N., Vonesch, J.L., Chambon, P., and Metzger, D. (1997). Spatio-temporally controlled site-specific somatic mutagenesis in the mouse. Proc Natl Acad Sci U S A *94*, 14559-14563.

Brockschnieder, D., Lappe-Siefke, C., Goebbels, S., Boesl, M.R., Nave, K.A., and Riethmacher, D. (2004). Cell depletion due to diphtheria toxin fragment A after Cre-mediated recombination. Mol Cell Biol *24*, 7636-7642.

Brockschnieder, D., Pechmann, Y., Sonnenberg-Riethmacher, E., and Riethmacher, D. (2006). An improved mouse line for Cre-induced cell ablation due to diphtheria toxin A, expressed from the Rosa26 locus. Genesis *44*, 322-327.

Brown, G.C., and Borutaite, V. (2002). Nitric oxide inhibition of mitochondrial respiration and its role in cell death. Free Radic Biol Med *33*, 1440-1450.

Bruce, C.C., Zhao, C., and Franklin, R.J.M. (2010). Remyelination -- An effective means of neuroprotection. Hormones and Behavior *57*, 56-62.

Brück (2007). New insights into the pathology of multiple sclerosis: towards a unified concept? J Neurol *254*, I/3-I/9.

Bruck, W., Bitsch, A., Kolenda, H., Bruck, Y., Stiefel, M., and Lassmann, H. (1997). Inflammatory central nervous system demyelination: correlation of magnetic resonance imaging findings with lesion pathology. Ann Neurol *42*, 783-793.

Budde, M.D., Xie, M., Cross, A.H., and Song, S.K. (2009). Axial diffusivity is the primary correlate of axonal injury in the experimental autoimmune encephalomyelitis spinal cord: a quantitative pixelwise analysis. J Neurosci *29*, 2805-2813.

Bunge, M.B., Bunge, R.P., and Ris, H. (1961). Ultrastructural study of remyelination in an experimental lesion in adult cat spinal cord. J Biophys Biochem Cytol *10*, 67-94.

Bunge, M.B., Bunge, R.P., and Pappas, G.D. (1962). Electron microscopic demonstration of connections between glia and myelin sheaths in the developing mammalian central nervous system. J Cell Biol *12*, 448-453.

Butt, A.M., and Ransom, B.R. (1989). Visualization of oligodendrocytes and astrocytes in the intact rat optic nerve by intracellular injection of lucifer yellow and horseradish peroxidase. Glia *2*, 470-475.

Caley, D.W., and Butler, A.B. (1974). Formation of central and peripheral myelin sheaths in the rat: an electron microscopic study. Am J Anat *140*, 339-347.

Carswell, R. (1838). Pathological Anatomy: Illustrations of the Elementry Forms of Disease. London: Longman, Orme, Brown, Green and Longman.

Cerghet, M., Bessert, D.A., Nave, K.A., and Skoff, R.P. (2001). Differential expression of apoptotic markers in jimpy and in Plp overexpressors: evidence for different apoptotic pathways. J Neurocytol *30*, 841-855.

Chance, P.F. (2001). Molecular basis of hereditary neuropathies. Phys Med Rehabil Clin N Am *12*, 277-291.

Chandran, S., Hunt, D., Joannides, A., Zhao, C., Compston, A., and Franklin, R.J. (2008). Myelin repair: the role of stem and precursor cells in multiple sclerosis. Philos Trans R Soc Lond B Biol Sci *363*, 171-183.

Chang, A., Nishiyama, A., Peterson, J., Prineas, J., and Trapp, B.D. (2000). NG2-positive oligodendrocyte progenitor cells in adult human brain and multiple sclerosis lesions. J Neurosci *20*, 6404-6412.

Chang, A., Tourtellotte, W.W., Rudick, R., and Trapp, B.D. (2002). Premyelinating oligodendrocytes in chronic lesions of multiple sclerosis. N Engl J Med *346*, 165-173.

Charcot, J.-M. (1868). Histologie de la sclerose en plaques. Gazette des hopitaux, Paris, 554-555.

Chari, D.M., and Blakemore, W.F. (2002). Efficient recolonisation of progenitor-depleted areas of the CNS by adult oligodendrocyte progenitor cells. Glia *37*, 307-313.

Charil, A., Yousry, T.A., Rovaris, M., Barkhof, F., De Stefano, N., Fazekas, F., Miller, D.H., Montalban, X., Simon, J.H., Polman, C., and Filippi, M. (2006). MRI and the diagnosis of multiple sclerosis: expanding the concept of "no better explanation". Lancet Neurol *5*, 841-852.

Charles, P., Reynolds, R., Seilhean, D., Rougon, G., Aigrot, M.S., Niezgoda, A., Zalc, B., and Lubetzki, C. (2002). Re-expression of PSA-NCAM by demyelinated axons: an inhibitor of remyelination in multiple sclerosis? Brain *125*, 1972-1979.

Chen, S., Rio, C., Ji, R.R., Dikkes, P., Coggeshall, R.E., Woolf, C.J., and Corfas, G. (2003). Disruption of ErbB receptor signaling in adult non-myelinating Schwann cells causes progressive sensory loss. Nat Neurosci *6*, 1186-1193.

Chen, Z., Ma, Z., Wang, Y., Li, Y., Lu, H., Fu, S., Hang, Q., and Lu, P.H. (2010). Oligodendrocyte-spinal cord explant co-culture: an in vitro model for the study of myelination. Brain Res *1309*, 9-18.

Coleman, M. (2005). Axon degeneration mechanisms: commonality amid diversity. Nat Rev Neurosci *6*, 889-898.

Coles, A.J., Wing, M.G., Molyneux, P., Paolillo, A., Davie, C.M., Hale, G., Miller, D., Waldmann, H., and Compston, A. (1999). Monoclonal antibody treatment exposes three mechanisms underlying the clinical course of multiple sclerosis. Ann Neurol *46*, 296-304.

Collier, R.J. (1975). Diphtheria toxin: mode of action and structure. Bacteriol Rev *39*, 54-85.

Collier, R.J. (2001). Understanding the mode of action of diphtheria toxin: a perspective on progress during the 20th century. Toxicon *39*, 1793-1803.

Colognato, H., Baron, W., Avellana-Adalid, V., Relvas, J.B., Baron-Van Evercooren, A., Georges-Labouesse, E., and ffrench-Constant, C. (2002). CNS integrins switch growth factor signalling to promote target-dependent survival. Nat Cell Biol *4*, 833-841.

Colognato, H., and ffrench-Constant, C. (2004). Mechanisms of glial development. Curr Opin Neurobiol *14*, 37-44.

Colognato, H., ffrench-Constant, C., and Feltri, M.L. (2005). Human diseases reveal novel roles for neural laminins. Trends Neurosci *28*, 480-486.

Coman, I., Barbin, G., Charles, P., Zalc, B., and Lubetzki, C. (2005). Axonal signals in central nervous system myelination, demyelination and remyelination. J Neurol Sci *233*, 67-71.

Compston, A., and Coles, A. (2002). Multiple sclerosis. The Lancet *359*, 1221-1231.

Compston, A., and Coles, A. (2008). Multiple sclerosis. Lancet *372*, 1502-1517.

Court, F.A., Sherman, D.L., Pratt, T., Garry, E.M., Ribchester, R.R., Cottrell, D.F., Fleetwood-Walker, S.M., and Brophy, P.J. (2004). Restricted growth of Schwann cells lacking Cajal bands slows conduction in myelinated nerves. Nature *431*, 191-195.

Craner, M.J., Lo, A.C., Black, J.A., and Waxman, S.G. (2003). Abnormal sodium channel distribution in optic nerve axons in a model of inflammatory demyelination. Brain *126*, 1552-1561.

Craner, M.J., Newcombe, J., Black, J.A., Hartle, C., Cuzner, M.L., and Waxman, S.G. (2004). Molecular changes in neurons in multiple sclerosis: altered axonal expression of Nav1.2 and Nav1.6 sodium channels and Na+/Ca2+ exchanger. Proc Natl Acad Sci U S A *101*, 8168-8173.

Crang, A.J., Gilson, J., and Blakemore, W.F. (1998). The demonstration by transplantation of the very restricted remyelinating potential of post-mitotic oligodendrocytes. J Neurocytol *27*, 541-553.

Crawford, D.K., Mangiardi, M., Xia, X., Lopez-Valdes, H.E., and Tiwari-Woodruff, S.K. (2009). Functional recovery of callosal axons following demyelination: a critical window. Neuroscience *164*, 1407-1421.

Croxford, A.L., Kurschus, F.C., and Waisman, A. (2011). Mouse models for multiple sclerosis: historical facts and future implications. Biochim Biophys Acta *1812*, 177-183.

Cruveilhier (1841). L'anatomie pathologique du corps humain; description avec figures lithographiées et coloriées: diverses alterations morbides dont le corps humain est susceptible. Ballière, Paris *2(32)*, 19-24.

Curtis, R., Cohen, J., Fok-Seang, J., Hanley, M.R., Gregson, N.A., Reynolds, R., and Wilkin, G.P. (1988). Development of macroglial cells in rat cerebellum. I. Use of antibodies to follow early in vivo development and migration of oligodendrocytes. J Neurocytol *17*, 43-54.

Dawson, M.R., Polito, A., Levine, J.M., and Reynolds, R. (2003). NG2-expressing glial progenitor cells: an abundant and widespread population of cycling cells in the adult rat CNS. Mol Cell Neurosci *24*, 476-488.

De Vos, K.J., Grierson, A.J., Ackerley, S., and Miller, C.C. (2008). Role of axonal transport in neurodegenerative diseases. Annu Rev Neurosci *31*, 151-173.

DeLuca, G.C., Williams, K., Evangelou, N., Ebers, G.C., and Esiri, M.M. (2006). The contribution of demyelination to axonal loss in multiple sclerosis. Brain *129*, 1507-1516.

Diemel, L.T., Copelman, C.A., and Cuzner, M.L. (1998). Macrophages in CNS remyelination: friend or foe? Neurochem Res *23*, 341-347.

Dousset, V., Delalande, C., Ballarino, L., Quesson, B., Seilhan, D., Coussemacq, M., Thiaudiere, E., Brochet, B., Canioni, P., and Caille, J.M. (1999a). In vivo macrophage activity imaging in the central nervous system detected by magnetic resonance. Magn Reson Med *41*, 329-333.

Dousset, V., Gomez, C., Petry, K.G., Delalande, C., and Caille, J.M. (1999b). Dose and scanning delay using USPIO for central nervous system macrophage imaging. MAGMA *8*, 185-189.

Duncan, I.D., Brower, A., Kondo, Y., Curlee, J.F., Jr., and Schultz, R.D. (2009). Extensive remyelination of the CNS leads to functional recovery. Proc Natl Acad Sci U S A *106*, 6832-6836.

Dutta, R., McDonough, J., Yin, X., Peterson, J., Chang, A., Torres, T., Gudz, T., Macklin, W.B., Lewis, D.A., Fox, R.J., Rudick, R., Mirnics, K., and Trapp, B.D. (2006). Mitochondrial dysfunction as a cause of axonal degeneration in multiple sclerosis patients. Ann Neurol *59*, 478-489.

Dutta, R., and Trapp, B.D. (2007). Pathogenesis of axonal and neuronal damage in multiple sclerosis. Neurology *68*, S22-31; discussion S43-54.

Edgar, J.M., McLaughlin, M., Yool, D., Zhang, S.C., Fowler, J.H., Montague, P., Barrie, J.A., McCulloch, M.C., Duncan, I.D., Garbern, J., Nave, K.A., and Griffiths, I.R. (2004). Oligodendroglial modulation of fast axonal transport in a mouse model of hereditary spastic paraplegia. J Cell Biol *166*, 121-131.

Edgar, J.M., McLaughlin, M., Werner, H.B., McCulloch, M.C., Barrie, J.A., Brown, A., Faichney, A.B., Snaidero, N., Nave, K.A., and Griffiths, I.R. (2009). Early ultrastructural defects of axons and axon-glia junctions in mice lacking expression of Cnp1. Glia *57*, 1815-1824.

Edgar, J.M., and Nave, K.A. (2009). The role of CNS glia in preserving axon function. Curr Opin Neurobiol *19*, 498-504.

Edgar, J.M., McCulloch, M.C., Montague, P., Brown, A.M., Thilemann, S., Pratola, L., Gruenenfelder, F.I., Griffiths, I.R., and Nave, K.A. (2010). Demyelination and axonal preservation in a transgenic mouse model of Pelizaeus-Merzbacher disease. EMBO Mol Med *2*, 42-50.

Einheber, S., Bhat, M.A., and Salzer, J.L. (2006). Disrupted Axo-Glial Junctions Result in Accumulation of Abnormal Mitochondria at Nodes of Ranvier. Neuron Glia Biol *2*, 165-174.

Ellis, E. (2006). Corrected Formulation for Spurr Low Viscosity Embedding Medium Using The Replacement Epoxide ERL 4221. Microscopy and Microanalysis *12*, 288-289.

Emery, B. (2010). Regulation of oligodendrocyte differentiation and myelination. Science *330*, 779-782.

Epinat, J.C., and Gilmore, T.D. (1999). In vitro-translated diphtheria toxin A chain inhibits translation in wheat germ extracts: analysis of biologically active, caspase-3-resistant diphtheria toxin mutants. Biochim Biophys Acta *1472*, 34-41.

Evangelou, N., Esiri, M.M., Smith, S., Palace, J., and Matthews, P.M. (2000). Quantitative pathological evidence for axonal loss in normal appearing white matter in multiple sclerosis. Ann Neurol *47*, 391-395.

Fancy, S.P., Kotter, M.R., Harrington, E.P., Huang, J.K., Zhao, C., Rowitch, D.H., and Franklin, R.J. (2010). Overcoming remyelination failure in multiple sclerosis and other myelin disorders. Exp Neurol *225*, 18-23.

Faust, P.L., Kaye, E.M., and Powers, J.M. (2010). Myelin lesions associated with lysosomal and peroxisomal disorders. Expert Rev Neurother *10*, 1449-1466.

Fazekas, F., Barkhof, F., Filippi, M., Grossman, R.I., Li, D.K., McDonald, W.I., McFarland, H.F., Paty, D.W., Simon, J.H., Wolinsky, J.S., and Miller, D.H. (1999). The contribution of magnetic resonance imaging to the diagnosis of multiple sclerosis. Neurology *53*, 448-456.

Feil, R., Wagner, J., Metzger, D., and Chambon, P. (1997). Regulation of Cre recombinase activity by mutated estrogen receptor ligand-binding domains. Biochem Biophys Res Commun *237*, 752-757.

Felts, P.A., Woolston, A.M., Fernando, H.B., Asquith, S., Gregson, N.A., Mizzi, O.J., and Smith, K.J. (2005). Inflammation and primary demyelination induced by the intraspinal injection of lipopolysaccharide. Brain *128*, 1649-1666.

Ferguson, B., Matyszak, M.K., Esiri, M.M., and Perry, V.H. (1997). Axonal damage in acute multiple sclerosis lesions. Brain *120 (Pt 3)*, 393-399.

Fex Svenningsen, A., Shan, W.S., Colman, D.R., and Pedraza, L. (2003). Rapid method for culturing embryonic neuron-glial cell cocultures. J Neurosci Res *72*, 565-573.

ffrench-Constant, C., and Raff, M.C. (1986). Proliferating bipotential glial progenitor cells in adult rat optic nerve. Nature *319*, 499-502.

Fields, R.D. (2005). Myelination: an overlooked mechanism of synaptic plasticity? Neuroscientist *11*, 528-531.

Filippi, M., and Agosta, F. (2009). Magnetic resonance techniques to quantify tissue damage, tissue repair, and functional cortical reorganization in multiple sclerosis. Prog Brain Res *175*, 465-482.

Fischer, C.A., and Morell, P. (1974). Turnover of proteins in myelin and myelin-like material of mouse brain. Brain Res *74*, 51-65.

Foote, A.K., and Blakemore, W.F. (2005). Inflammation stimulates remyelination in areas of chronic demyelination. Brain *128*, 528-539.

Franklin, R.J. (2002). Why does remyelination fail in multiple sclerosis? Nat Rev Neurosci *3*, 705-714.

Franklin, R.J., and ffrench-Constant, C. (2008). Remyelination in the CNS: from biology to therapy. Nat Rev Neurosci *9*, 839-855.

Franklin, R.J., and Kotter, M.R. (2008). The biology of CNS remyelination: the key to therapeutic advances. J Neurol *255 Suppl 1*, 19-25.

Friede, R.L. (1972). Control of myelin formation by axon caliber (with a model of the control mechanism). J Comp Neurol *144*, 233-252.

Friese, M.A., Montalban, X., Willcox, N., Bell, J.I., Martin, R., and Fugger, L. (2006). The value of animal models for drug development in multiple sclerosis. Brain *129*, 1940-1952.

Frohman, E.M., Racke, M.K., and Raine, C.S. (2006). Multiple sclerosis--the plaque and its pathogenesis. N Engl J Med *354*, 942-955.

Garbern, J. (2007). Pelizaeus-Merzbacher disease: Genetic and cellular pathogenesis. Cellular and Molecular Life Sciences *64*, 50-65.

Garcia-Fresco, G.P., Sousa, A.D., Pillai, A.M., Moy, S.S., Crawley, J.N., Tessarollo, L., Dupree, J.L., and Bhat, M.A. (2006). Disruption of axo-glial junctions causes cytoskeletal disorganization and degeneration of Purkinje neuron axons. Proc Natl Acad Sci U S A *103*, 5137-5142.

Gareau, P.J., Rutt, B.K., Karlik, S.J., and Mitchell, J.R. (2000). Magnetization transfer and multicomponent T2 relaxation measurements with histopathologic correlation in an experimental model of MS. J Magn Reson Imaging *11*, 586-595.

Gaughwin, P.M., Caldwell, M.A., Anderson, J.M., Schwiening, C.J., Fawcett, J.W., Compston, D.A., and Chandran, S. (2006). Astrocytes promote neurogenesis from oligodendrocyte precursor cells. Eur J Neurosci *23*, 945-956.

Genoud, S., Lappe-Siefke, C., Goebbels, S., Radtke, F., Aguet, M., Scherer, S.S., Suter, U., Nave, K.A., and Mantei, N. (2002). Notch1 control of oligodendrocyte differentiation in the spinal cord. J Cell Biol *158*, 709-718.

Geren, B.B., and Raskind, J. (1953). Development of the Fine Structure of the Myelin Sheath in Sciatic Nerves of Chick Embryos. Proc Natl Acad Sci U S A *39*, 880-884.

Glezer, I., Lapointe, A., and Rivest, S. (2006). Innate immunity triggers oligodendrocyte progenitor reactivity and confines damages to brain injuries. FASEB J *20*, 750-752.

Glickstein, M. (2006). Golgi and Cajal: The neuron doctrine and the 100th anniversary of the 1906 Nobel Prize. Curr Biol *16*, R147-151.

Gold, R., Linington, C., and Lassmann, H. (2006). Understanding pathogenesis and therapy of multiple sclerosis via animal models: 70 years of merits and culprits in experimental autoimmune encephalomyelitis research. Brain *129*, 1953-1971.

Griffiths, I., Klugmann, M., Anderson, T., Yool, D., Thomson, C., Schwab, M.H., Schneider, A., Zimmermann, F., McCulloch, M., Nadon, N., and Nave, K.A. (1998). Axonal swellings and degeneration in mice lacking the major proteolipid of myelin. Science *280*, 1610-1613.

Gruenenfelder, F.I., Thomson, G., Penderis, J., and Edgar, J.M. (2011). Axon–glial interaction in the CNS: what we have learned from mouse models of Pelizaeus–Merzbacher disease. Journal of Anatomy, no-no.

Gyllensten, L., and Malmfors, T. (1963). Myelinization of the optic nerve and its dependence on visual function--a quantitative investigation in mice. J Embryol Exp Morphol *11*, 255-266.

Hawkins, B.T., and Egleton, R.D. (2006). Fluorescence imaging of blood-brain barrier disruption. J Neurosci Methods *151*, 262-267.

Hemmer, B., Archelos, J.J., and Hartung, H.P. (2002). New concepts in the immunopathogenesis of multiple sclerosis. Nat Rev Neurosci *3*, 291-301.

Hennig, J., Nauerth, A., and Friedburg, H. (1986). RARE imaging: a fast imaging method for clinical MR. Magn Reson Med *3*, 823-833.

Hohlfeld, R. (2007). Does Inflammation Stimulate Remyelination? J Neurol *254*, I/47-I/54.

Horner, P.J., Power, A.E., Kempermann, G., Kuhn, H.G., Palmer, T.D., Winkler, J., Thal, L.J., and Gage, F.H. (2000). Proliferation and differentiation of progenitor cells throughout the intact adult rat spinal cord. J Neurosci *20*, 2218-2228.

Hosking, M.P., and Lane, T.E. (2009). The Biology of Persistent Infection: Inflammation and Demyelination following Murine Coronavirus Infection of the Central Nervous System. Curr Immunol Rev *5*, 267-276.

Howell, O.W., Palser, A., Polito, A., Melrose, S., Zonta, B., Scheiermann, C., Vora, A.J., Brophy, P.J., and Reynolds, R. (2006). Disruption of neurofascin localization reveals early changes preceding demyelination and remyelination in multiple sclerosis. Brain *129*, 3173-3185.

Huang, J.K., Phillips, G.R., Roth, A.D., Pedraza, L., Shan, W., Belkaid, W., Mi, S., Fex-Svenningsen, A., Florens, L., Yates, J.R., 3rd, and Colman, D.R. (2005). Glial membranes at the node of Ranvier prevent neurite outgrowth. Science *310*, 1813-1817.

Hyden, H., and Pigon, A. (1960). A cytophysiological study of the functional relationship between oliodendroglial cells and nerve cells of Deiters' nucleus. J Neurochem *6*, 57-72.

Irvine, K.A., and Blakemore, W.F. (2008). Remyelination protects axons from demyelination-associated axon degeneration. Brain *131*, 1464-1477.

Ishibashi, T., Dakin, K.A., Stevens, B., Lee, P.R., Kozlov, S.V., Stewart, C.L., and Fields, R.D. (2006). Astrocytes promote myelination in response to electrical impulses. Neuron *49*, 823-832.

Itoh, K., Stevens, B., Schachner, M., and Fields, R.D. (1995). Regulated expression of the neural cell adhesion molecule L1 by specific patterns of neural impulses. Science *270*, 1369-1372.

Ivanova, A., Signore, M., Caro, N., Greene, N.D., Copp, A.J., and Martinez-Barbera, J.P. (2005). In vivo genetic ablation by Cre-mediated expression of diphtheria toxin fragment A. Genesis *43*, 129-135.

Jalabi, W., Boehm, N., Grucker, D., and Ghandour, M.S. (2005). Recovery of myelin after induction of oligodendrocyte cell death in postnatal brain. J Neurosci *25*, 2885-2894.

Jessen, K.R., and Mirsky, R. (2005). The origin and development of glial cells in peripheral nerves. Nat Rev Neurosci *6*, 671-682.

Juraska, J.M., and Kopcik, J.R. (1988). Sex and environmental influences on the size and ultrastructure of the rat corpus callosum. Brain Res *450*, 1-8.

Karadottir, R., Hamilton, N.B., Bakiri, Y., and Attwell, D. (2008). Spiking and nonspiking classes of oligodendrocyte precursor glia in CNS white matter. Nat Neurosci *11*, 450-456.

Kassmann, C.M., Lappe-Siefke, C., Baes, M., Brugger, B., Mildner, A., Werner, H.B., Natt, O., Michaelis, T., Prinz, M., Frahm, J., and Nave, K.A. (2007). Axonal loss and neuroinflammation caused by peroxisome-deficient oligodendrocytes. Nat Genet *39*, 969-976.

Kassmann, C.M., and Nave, K.A. (2008). Oligodendroglial impact on axonal function and survival - a hypothesis. Curr Opin Neurol *21*, 235-241.

Keirstead, H.S., and Blakemore, W.F. (1997). Identification of post-mitotic oligodendrocytes incapable of remyelination within the demyelinated adult spinal cord. J Neuropathol Exp Neurol *56*, 1191-1201.

Kessaris, N., Fogarty, M., Iannarelli, P., Grist, M., Wegner, M., and Richardson, W.D. (2006). Competing waves of oligodendrocytes in the forebrain and postnatal elimination of an embryonic lineage. Nat Neurosci *9*, 173-179.

King, A.E., Dickson, T.C., Blizzard, C.A., Woodhouse, A., Foster, S.S., Chung, R.S., and Vickers, J.C. (2009). Neuron-glia interactions underlie ALS-like axonal cytoskeletal pathology. Neurobiol Aging.

Kipp, M., Clarner, T., Dang, J., Copray, S., and Beyer, C. (2009). The cuprizone animal model: new insights into an old story. Acta Neuropathol *118*, 723-736.

Kirby, B.B., Takada, N., Latimer, A.J., Shin, J., Carney, T.J., Kelsh, R.N., and Appel, B. (2006). In vivo time-lapse imaging shows dynamic oligodendrocyte progenitor behavior during zebrafish development. Nat Neurosci *9*, 1506-1511.

Kirschner, D.A., and Ganser, A.L. (1980). Compact myelin exists in the absence of basic protein in the shiverer mutant mouse. Nature *283*, 207-210.

Klugmann, M., Schwab, M.H., Puhlhofer, A., Schneider, A., Zimmermann, F., Griffiths, I.R., and Nave, K.A. (1997). Assembly of CNS myelin in the absence of proteolipid protein. Neuron *18*, 59-70.

Knapp, P.E., Bartlett, W.P., Williams, L.A., Yamada, M., Ikenaka, K., and Skoff, R.P. (1999). Programmed cell death without DNA fragmentation in the jimpy mouse: secreted factors can enhance survival. Cell Death Differ *6*, 136-145.

Knobler, R.L., Lampert, P.W., and Oldstone, M.B. (1982). Virus persistence and recurring demyelination produced by a temperature-sensitive mutant of MHV-4. Nature *298*, 279-280.

Kondo, T., and Raff, M. (2000). Oligodendrocyte precursor cells reprogrammed to become multipotential CNS stem cells. Science *289*, 1754-1757.

Kornek, B., Storch, M.K., Weissert, R., Wallstroem, E., Stefferl, A., Olsson, T., Linington, C., Schmidbauer, M., and Lassmann, H. (2000). Multiple sclerosis and chronic autoimmune encephalomyelitis: a comparative quantitative study of axonal injury in active, inactive, and remyelinated lesions. Am J Pathol *157*, 267-276.

Kotter, M.R., Setzu, A., Sim, F.J., Van Rooijen, N., and Franklin, R.J. (2001). Macrophage depletion impairs oligodendrocyte remyelination following lysolecithin-induced demyelination. Glia *35*, 204-212.

Kotter, M.R., Zhao, C., van Rooijen, N., and Franklin, R.J. (2005). Macrophage-depletion induced impairment of experimental CNS remyelination is associated with a reduced oligodendrocyte progenitor cell response and altered growth factor expression. Neurobiol Dis *18*, 166-175.

Kotter, M.R., Li, W.W., Zhao, C., and Franklin, R.J. (2006). Myelin impairs CNS remyelination by inhibiting oligodendrocyte precursor cell differentiation. J Neurosci *26*, 328-332.

Krämer-Albers, E.-M., Bretz, N., Tenzer, S., Winterstein, C., Möbius, W., Berger, H., Nave, K.-A., Schild, H., and Trotter, J. (2007). Oligodendrocytes secrete exosomes containing major myelin and stress-protective proteins: Trophic support for axons? PROTEOMICS - CLINICAL APPLICATIONS *1*, 1446-1461.

Kuhlmann, T., Miron, V., Cui, Q., Wegner, C., Antel, J., and Bruck, W. (2008). Differentiation block of oligodendroglial progenitor cells as a cause for remyelination failure in chronic multiple sclerosis. Brain *131*, 1749-1758.

Ladewig, G., Jestaedt, L., Misselwitz, B., Solymosi, L., Toyka, K., Bendszus, M., and Stoll, G. (2009). Spatial diversity of blood-brain barrier alteration and macrophage invasion in experimental autoimmune encephalomyelitis: a comparative MRI study. Exp Neurol *220*, 207-211.

Laemmli, U.K. (1970). Cleavage of structural proteins during the assembly of the head of bacteriophage T4. Nature *227*, 680-685.

Lappe-Siefke, C., Goebbels, S., Gravel, M., Nicksch, E., Lee, J., Braun, P.E., Griffiths, I.R., and Nave, K.A. (2003). Disruption of Cnp1 uncouples oligodendroglial functions in axonal support and myelination. Nat Genet *33*, 366-374.

Lassmann, H., Bruck, W., and Lucchinetti, C. (2001). Heterogeneity of multiple sclerosis pathogenesis: implications for diagnosis and therapy. Trends Mol Med *7*, 115-121.

Lassmann, H. (2003). Hypoxia-like tissue injury as a component of multiple sclerosis lesions. J Neurol Sci *206*, 187-191.

Lassmann, H. (2008). Models of multiple sclerosis: new insights into pathophysiology and repair. Curr Opin Neurol *21*, 242-247.

Laursen, L.S., Chan, C.W., and ffrench-Constant, C. (2009). An integrin-contactin complex regulates CNS myelination by differential Fyn phosphorylation. J Neurosci *29*, 9174-9185.

Le Bihan, D., Mangin, J.F., Poupon, C., Clark, C.A., Pappata, S., Molko, N., and Chabriat, H. (2001). Diffusion tensor imaging: concepts and applications. J Magn Reson Imaging *13*, 534-546.

Lee, P., Morley, G., Huang, Q., Fischer, A., Seiler, S., Horner, J.W., Factor, S., Vaidya, D., Jalife, J., and Fishman, G.I. (1998). Conditional lineage ablation to model human diseases. Proc Natl Acad Sci U S A *95*, 11371-11376.

Leist, T.P., and Marks, S. (2010). Magnetic resonance imaging and treatment effects of multiple sclerosis therapeutics. Neurology *74 Suppl 1*, S54-61.

Leone, D.P., Genoud, S., Atanasoski, S., Grausenburger, R., Berger, P., Metzger, D., Macklin, W.B., Chambon, P., and Suter, U. (2003). Tamoxifen-inducible glia-specific Cre mice for somatic mutagenesis in oligodendrocytes and Schwann cells. Mol Cell Neurosci *22*, 430-440.

Levine, J.M., and Reynolds, R. (1999). Activation and proliferation of endogenous oligodendrocyte precursor cells during ethidium bromide-induced demyelination. Exp Neurol *160*, 333-347.

Levine, J.M., Reynolds, R., and Fawcett, J.W. (2001). The oligodendrocyte precursor cell in health and disease. Trends Neurosci *24*, 39-47.

Li, Q., Brus-Ramer, M., Martin, J.H., and McDonald, J.W. (2010). Electrical stimulation of the medullary pyramid promotes proliferation and differentiation of oligodendrocyte progenitor cells in the corticospinal tract of the adult rat. Neurosci Lett *479*, 128-133.

Lindner, M., Fokuhl, J., Linsmeier, F., Trebst, C., and Stangel, M. (2009). Chronic toxic demyelination in the central nervous system leads to axonal damage despite remyelination. Neurosci Lett *453*, 120-125.

Lisak, R.P. (2007). Neurodegeneration in multiple sclerosis: defining the problem. Neurology *68*, S5-12; discussion S43-54.

Lovas, G., Szilagyi, N., Majtenyi, K., Palkovits, M., and Komoly, S. (2000). Axonal changes in chronic demyelinated cervical spinal cord plaques. Brain *123 (Pt 2)*, 308-317.

Lu, F., Selak, M., O'Connor, J., Croul, S., Lorenzana, C., Butunoi, C., and Kalman, B. (2000). Oxidative damage to mitochondrial DNA and activity of mitochondrial enzymes in chronic active lesions of multiple sclerosis. J Neurol Sci *177*, 95-103.

Lublin, F.D., and Reingold, S.C. (1996). Defining the clinical course of multiple sclerosis: results of an international survey. National Multiple Sclerosis Society (USA) Advisory Committee on Clinical Trials of New Agents in Multiple Sclerosis. Neurology *46*, 907-911.

Lucchinetti, C., Bruck, W., Parisi, J., Scheithauer, B., Rodriguez, M., and Lassmann, H. (2000). Heterogeneity of multiple sclerosis lesions: implications for the pathogenesis of demyelination. Ann Neurol *47*, 707-717.

Ludwin, S.K. (1980). Chronic demyelination inhibits remyelination in the central nervous system. An analysis of contributing factors. Lab Invest *43*, 382-387.

Ludwin, S.K., and Maitland, M. (1984). Long-term remyelination fails to reconstitute normal thickness of central myelin sheaths. J Neurol Sci *64*, 193-198.

Luskin, M.B., Pearlman, A.L., and Sanes, J.R. (1988). Cell lineage in the cerebral cortex of the mouse studied in vivo and in vitro with a recombinant retrovirus. Neuron *1*, 635-647.

Mallon, B.S., Shick, H.E., Kidd, G.J., and Macklin, W.B. (2002). Proteolipid promoter activity distinguishes two populations of NG2-positive cells throughout neonatal cortical development. J Neurosci *22*, 876-885.

Marrie, R.A. (2004). Environmental risk factors in multiple sclerosis aetiology. Lancet Neurol *3*, 709-718.

Martini, R., Mohajeri, M.H., Kasper, S., Giese, K.P., and Schachner, M. (1995). Mice doubly deficient in the genes for P0 and myelin basic protein show that both proteins contribute to the formation of the major dense line in peripheral nerve myelin. J Neurosci *15*, 4488-4495.

Martino, G., Furlan, R., Brambilla, E., Bergami, A., Ruffini, F., Gironi, M., Poliani, P.L., Grimaldi, L.M., and Comi, G. (2000). Cytokines and immunity in multiple sclerosis: the dual signal hypothesis. J Neuroimmunol *109*, 3-9.

Mason, J.L., Langaman, C., Morell, P., Suzuki, K., and Matsushima, G.K. (2001). Episodic demyelination and subsequent remyelination within the murine central nervous system: changes in axonal calibre. Neuropathol Appl Neurobiol *27*, 50-58.

Mason, J.L., Toews, A., Hostettler, J.D., Morell, P., Suzuki, K., Goldman, J.E., and Matsushima, G.K. (2004). Oligodendrocytes and progenitors become progressively depleted within chronically demyelinated lesions. Am J Pathol *164*, 1673-1682.

Matsushima, G.K., and Morell, P. (2001). The neurotoxicant, cuprizone, as a model to study demyelination and remyelination in the central nervous system. Brain Pathol *11*, 107-116.

Matthaei, I., Polman, C.H., de Groot, C.J., Dijkstra, C.D., Koetsier, J.C., and Sminia, T. (1989). Observer agreement in the assessment of clinical signs in experimental allergic encephalomyelitis. J Neuroimmunol *23*, 25-28.

McMahon, E.J., Suzuki, K., and Matsushima, G.K. (2002). Peripheral macrophage recruitment in cuprizone-induced CNS demyelination despite an intact blood-brain barrier. J Neuroimmunol *130*, 32-45.

Mendel, I., Kerlero de Rosbo, N., and Ben-Nun, A. (1995). A myelin oligodendrocyte glycoprotein peptide induces typical chronic experimental autoimmune encephalomyelitis in H-2b mice: fine specificity and T cell receptor V beta expression of encephalitogenic T cells. Eur J Immunol *25*, 1951-1959.

Menn, B., Garcia-Verdugo, J.M., Yaschine, C., Gonzalez-Perez, O., Rowitch, D., and Alvarez-Buylla, A. (2006). Origin of oligodendrocytes in the subventricular zone of the adult brain. J Neurosci *26*, 7907-7918.

Merkler, D., Ernsting, T., Kerschensteiner, M., Bruck, W., and Stadelmann, C. (2006). A new focal EAE model of cortical demyelination: multiple sclerosis-like lesions with rapid resolution of inflammation and extensive remyelination. Brain *129*, 1972-1983.

Messing, A., Behringer, R.R., Hammang, J.P., Palmiter, R.D., Brinster, R.L., and Lemke, G. (1992). P0 promoter directs expression of reporter and toxin genes to Schwann cells of transgenic mice. Neuron *8*, 507-520.

Mi, S., Miller, R.H., Lee, X., Scott, M.L., Shulag-Morskaya, S., Shao, Z., Chang, J., Thill, G., Levesque, M., Zhang, M., Hession, C., Sah, D., Trapp, B., He, Z., Jung, V., McCoy, J.M., and Pepinsky, R.B. (2005). LINGO-1 negatively regulates myelination by oligodendrocytes. Nat Neurosci *8*, 745-751.

Mi, S., Miller, R.H., Tang, W., Lee, X., Hu, B., Wu, W., Zhang, Y., Shields, C.B., Miklasz, S., Shea, D., Mason, J., Franklin, R.J., Ji, B., Shao, Z., Chedotal, A., Bernard, F., Roulois, A., Xu, J., Jung, V., and Pepinsky, B. (2009). Promotion of central nervous system remyelination by induced differentiation of oligodendrocyte precursor cells. Ann Neurol *65*, 304-315.

Michailov, G.V., Sereda, M.W., Brinkmann, B.G., Fischer, T.M., Haug, B., Birchmeier, C., Role, L., Lai, C., Schwab, M.H., and Nave, K.A. (2004). Axonal neuregulin-1 regulates myelin sheath thickness. Science *304*, 700-703.

Middlebrook, J.L., and Dorland, R.B. (1977). Differential chemical protection of mammalian cells from the exotoxins of Corynebacterium diphtheriae and Pseudomonas aeruginosa. Infect Immun *16*, 232-239.

Miklossy, J., and Van der Loos, H. (1991). The long-distance effects of brain lesions: visualization of myelinated pathways in the human brain using polarizing and fluorescence microscopy. J Neuropathol Exp Neurol *50*, 1-15.

Miller, R.H. (1999). Contact with central nervous system myelin inhibits oligodendrocyte progenitor maturation. Dev Biol *216*, 359-368.

Miller, R.H., and Fyffe-Maricich, S.L. (2010). Restoring the balance between disease and repair in multiple sclerosis: insights from mouse models. Dis Model Mech *3*, 535-539.

Mix, E., Meyer-Rienecker, H., Hartung, H.P., and Zettl, U.K. (2010). Animal models of multiple sclerosis--potentials and limitations. Prog Neurobiol *92*, 386-404.

Mombaerts, P., Iacomini, J., Johnson, R.S., Herrup, K., Tonegawa, S., and Papaioannou, V.E. (1992). RAG-1-deficient mice have no mature B and T lymphocytes. Cell *68*, 869-877.

Morell, P., Quarles, R.H., and Norton, W.T. (1994). Myelin Formation, Structure and Biochemistry. In: *Basic Neurochemistry*, edited by Siegel GJ, Agranoff BW, Albers RW and Molinoff PB. New York: Raven, 117-143.

Morell, P., Barrett, C.V., Mason, J.L., Toews, A.D., Hostettler, J.D., Knapp, G.W., and Matsushima, G.K. (1998). Gene expression in brain during cuprizone-induced demyelination and remyelination. Mol Cell Neurosci *12*, 220-227.

Morfini, G.A., Burns, M., Binder, L.I., Kanaan, N.M., LaPointe, N., Bosco, D.A., Brown, R.H., Jr., Brown, H., Tiwari, A., Hayward, L., Edgar, J., Nave, K.A., Garberrn, J., Atagi, Y., Song, Y., Pigino, G., and Brady, S.T. (2009). Axonal transport defects in neurodegenerative diseases. J Neurosci *29*, 12776-12786.

Mosley, K., and Cuzner, M.L. (1996). Receptor-mediated phagocytosis of myelin by macrophages and microglia: effect of opsonization and receptor blocking agents. Neurochem Res *21*, 481-487.

Nait-Oumesmar, B., Decker, L., Lachapelle, F., Avellana-Adalid, V., Bachelin, C., and Van Evercooren, A.B. (1999). Progenitor cells of the adult mouse subventricular zone proliferate, migrate and differentiate into oligodendrocytes after demyelination. Eur J Neurosci *11*, 4357-4366.

Nave, K.A., and Salzer, J.L. (2006). Axonal regulation of myelination by neuregulin 1. Curr Opin Neurobiol *16*, 492-500.

Nave, K.A., and Trapp, B.D. (2008). Axon-glial signaling and the glial support of axon function. Annu Rev Neurosci *31*, 535-561.

Nave, K.A. (2010a). Myelination and support of axonal integrity by glia. Nature *468*, 244-252.

Nave, K.A. (2010b). Myelination and the trophic support of long axons. Nat Rev Neurosci *11*, 275-283.

Nessler, S., Boretius, S., Stadelmann, C., Bittner, A., Merkler, D., Hartung, H.P., Michaelis, T., Bruck, W., Frahm, J., Sommer, N., and Hemmer, B. (2007). Early MRI changes in a mouse model of multiple sclerosis are predictive of severe inflammatory tissue damage. Brain *130*, 2186-2198.

Neumann, H., Kotter, M.R., and Franklin, R.J. (2009). Debris clearance by microglia: an essential link between degeneration and regeneration. Brain *132*, 288-295.

Nielsen, H.H., Ladeby, R., Fenger, C., Toft-Hansen, H., Babcock, A.A., Owens, T., and Finsen, B. (2009). Enhanced Microglial Clearance of Myelin Debris in T Cell-Infiltrated Central Nervous System. Journal of Neuropathology & Experimental Neurology *68*, 845-856 810.1097/NEN.1090b1013e3181ae0236.

Norton, W.T., and Poduslo, S.E. (1973). Myelination in rat brain: changes in myelin composition during brain maturation. J Neurochem *21*, 759-773.

Nunes, M.C., Roy, N.S., Keyoung, H.M., Goodman, R.R., McKhann, G., 2nd, Jiang, L., Kang, J., Nedergaard, M., and Goldman, S.A. (2003). Identification and isolation of multipotential neural progenitor cells from the subcortical white matter of the adult human brain. Nat Med *9*, 439-447.

Ogunshola, O.O., Djonov, V., Staudt, R., Vogel, J., and Gassmann, M. (2006). Chronic excessive erythrocytosis induces endothelial activation and damage in mouse brain. Am J Physiol Regul Integr Comp Physiol *290*, R678-684.

Oksenberg, J.R., Barcellos, L.F., Cree, B.A., Baranzini, S.E., Bugawan, T.L., Khan, O., Lincoln, R.R., Swerdlin, A., Mignot, E., Lin, L., Goodin, D., Erlich, H.A., Schmidt, S., Thomson, G., Reich, D.E., Pericak-Vance, M.A., Haines, J.L., and Hauser, S.L. (2004). Mapping multiple sclerosis susceptibility to the HLA-DR locus in African Americans. Am J Hum Genet *74*, 160-167.

Olson, J.K., Croxford, J.L., Calenoff, M.A., Dal Canto, M.C., and Miller, S.D. (2001). A virus-induced molecular mimicry model of multiple sclerosis. J Clin Invest *108*, 311-318.

Omlin, F.X. (1997). Optic disc and optic nerve of the blind cape mole-rat (Georychus capensis): a proposed model for naturally occurring reactive gliosis. Brain Res Bull *44*, 627-632.

Orthmann-Murphy, J.L., Abrams, C.K., and Scherer, S.S. (2008). Gap junctions couple astrocytes and oligodendrocytes. J Mol Neurosci *35*, 101-116.

Paivalainen, S., Nissinen, M., Honkanen, H., Lahti, O., Kangas, S.M., Peltonen, J., Peltonen, S., and Heape, A.M. (2008). Myelination in mouse dorsal root ganglion/Schwann cell cocultures. Mol Cell Neurosci *37*, 568-578.

Papadopoulos, D., Pham-Dinh, D., and Reynolds, R. (2006). Axon loss is responsible for chronic neurological deficit following inflammatory demyelination in the rat. Exp Neurol *197*, 373-385.

Pappenheimer, A.M., Jr., Harper, A.A., Moynihan, M., and Brockes, J.P. (1982). Diphtheria toxin and related proteins: effect of route of injection on toxicity and the determination of cytotoxicity for various cultured cells. J Infect Dis *145*, 94-102.

Paus, T., Zijdenbos, A., Worsley, K., Collins, D.L., Blumenthal, J., Giedd, J.N., Rapoport, J.L., and Evans, A.C. (1999). Structural maturation of neural pathways in children and adolescents: in vivo study. Science *283*, 1908-1911.

Peles, E., and Salzer, J.L. (2000). Molecular domains of myelinated axons. Curr Opin Neurobiol *10*, 558-565.

Penderis, J., Shields, S.A., and Franklin, R.J. (2003). Impaired remyelination and depletion of oligodendrocyte progenitors does not occur following repeated episodes of focal demyelination in the rat central nervous system. Brain *126*, 1382-1391.

Perier, O., and Gregoire, A. (1965). Electron microscopic features of multiple sclerosis lesions. Brain *88*, 937-952.

Piaton, G., Gould, R.M., and Lubetzki, C. (2010). Axon-oligodendrocyte interactions during developmental myelination, demyelination and repair. J Neurochem *114*, 1243-1260.

Polman, C.H., Reingold, S.C., Edan, G., Filippi, M., Hartung, H.P., Kappos, L., Lublin, F.D., Metz, L.M., McFarland, H.F., O'Connor, P.W., Sandberg-Wollheim, M., Thompson, A.J., Weinshenker, B.G., and Wolinsky, J.S. (2005). Diagnostic criteria for multiple sclerosis: 2005 revisions to the "McDonald Criteria". Ann Neurol *58*, 840-846.

Popko, B. (2010). Myelin maintenance: axonal support required. Nat Neurosci *13*, 275-277.

Popovich, P.G., Guan, Z., Wei, P., Huitinga, I., van Rooijen, N., and Stokes, B.T. (1999). Depletion of hematogenous macrophages promotes partial hindlimb recovery and neuroanatomical repair after experimental spinal cord injury. Exp Neurol *158*, 351-365.

Pratt, R.W., and Weimer, L.H. (2005). Medication and toxin-induced peripheral neuropathy. Semin Neurol *25*, 204-216.

Prayoonwiwat, N., and Rodriguez, M. (1993). The potential for oligodendrocyte proliferation during demyelinating disease. J Neuropathol Exp Neurol *52*, 55-63.

Price, J., and Thurlow, L. (1988). Cell lineage in the rat cerebral cortex: a study using retroviral-mediated gene transfer. Development *104*, 473-482.

Pugliatti, M., Sotgiu, S., and Rosati, G. (2002). The worldwide prevalence of multiple sclerosis. Clinical Neurology and Neurosurgery *104*, 182-191.

Raine, C.S., and Wu, E. (1993). Multiple sclerosis: remyelination in acute lesions. J Neuropathol Exp Neurol *52*, 199-204.

Rasband, M.N., Tayler, J., Kaga, Y., Yang, Y., Lappe-Siefke, C., Nave, K.A., and Bansal, R. (2005). CNP is required for maintenance of axon-glia interactions at nodes of Ranvier in the CNS. Glia *50*, 86-90.

Ratering, D., Baltes, C., Nordmeyer-Massner, J., Marek, D., and Rudin, M. (2008). Performance of a 200-MHz cryogenic RF probe designed for MRI and MRS of the murine brain. Magn Reson Med *59*, 1440-1447.

Rausch, M., Sauter, A., Frohlich, J., Neubacher, U., Radu, E.W., and Rudin, M. (2001). Dynamic patterns of USPIO enhancement can be observed in macrophages after ischemic brain damage. Magn Reson Med *46*, 1018-1022.

Rausch, M., Hiestand, P., Baumann, D., Cannet, C., and Rudin, M. (2003). MRI-based monitoring of inflammation and tissue damage in acute and chronic relapsing EAE. Magn Reson Med *50*, 309-314.

Rhodes, K.E., Raivich, G., and Fawcett, J.W. (2006). The injury response of oligodendrocyte precursor cells is induced by platelets, macrophages and inflammation-associated cytokines. Neuroscience *140*, 87-100.

Richardson-Burns, S.M., Kleinschmidt-DeMasters, B.K., DeBiasi, R.L., and Tyler, K.L. (2002). Progressive multifocal leukoencephalopathy and apoptosis of infected oligodendrocytes in the central nervous system of patients with and without AIDS. Arch Neurol *59*, 1930-1936.

Richardson, W.D., Kessaris, N., and Pringle, N. (2006). Oligodendrocyte wars. Nat Rev Neurosci *7*, 11-18.

Rivers, L.E., Young, K.M., Rizzi, M., Jamen, F., Psachoulia, K., Wade, A., Kessaris, N., and Richardson, W.D. (2008). PDGFRA/NG2 glia generate myelinating oligodendrocytes and piriform projection neurons in adult mice. Nat Neurosci *11*, 1392-1401.

Rivers, T.M., and Schwentker, F.F. (1935). Encephalomyelitis Accompanied by Myelin Destruction Experimentally Produced in Monkeys. J Exp Med *61*, 689-702.

Rodriguez, M. (2007). Effectors of demyelination and remyelination in the CNS: implications for multiple sclerosis. Brain Pathol *17*, 219-229.

Rosenbluth, J., Nave, K.A., Mierzwa, A., and Schiff, R. (2006). Subtle myelin defects in PLP-null mice. Glia *54*, 172-182.

Saito, M., Iwawaki, T., Taya, C., Yonekawa, H., Noda, M., Inui, Y., Mekada, E., Kimata, Y., Tsuru, A., and Kohno, K. (2001). Diphtheria toxin receptor-mediated conditional and targeted cell ablation in transgenic mice. Nat Biotechnol *19*, 746-750.

Salzer, J.L., Brophy, P.J., and Peles, E. (2008). Molecular domains of myelinated axons in the peripheral nervous system. Glia *56*, 1532-1540.

Schafer, D.P., and Rasband, M.N. (2006). Glial regulation of the axonal membrane at nodes of Ranvier. Current Opinion in Neurobiology *16*, 508-514.

Scheikl, T., Pignolet, B., Mars, L.T., and Liblau, R.S. (2010). Transgenic mouse models of multiple sclerosis. Cell Mol Life Sci *67*, 4011-4034.

Schiffmann, R., and van der Knaap, M.S. (2004). The latest on leukodystrophies. Curr Opin Neurol *17*, 187-192.

Schmierer, K., Scaravilli, F., Altmann, D.R., Barker, G.J., and Miller, D.H. (2004). Magnetization transfer ratio and myelin in postmortem multiple sclerosis brain. Ann Neurol *56*, 407-415.

Schmued, L.C., Stowers, C.C., Scallet, A.C., and Xu, L. (2005). Fluoro-Jade C results in ultra high resolution and contrast labeling of degenerating neurons. Brain Res *1035*, 24-31.

Scholz, J., Klein, M.C., Behrens, T.E., and Johansen-Berg, H. (2009). Training induces changes in white-matter architecture. Nat Neurosci *12*, 1370-1371.

Schweigreiter, R., Roots, B.I., Bandtlow, C.E., and Gould, R.M. (2006). Understanding myelination through studying its evolution. Int Rev Neurobiol *73*, 219-273.

Senchenkov, A., Han, T.Y., Wang, H., Frankel, A.E., Kottke, T.J., Kaufmann, S.H., and Cabot, M.C. (2001). Enhanced ceramide generation and induction of apoptosis in human leukemia cells exposed to DT(388)-granulocyte-macrophage colony-stimulating factor (GM-CSF), a truncated diphtheria toxin fused to human GM-CSF. Blood *98*, 1927-1934.

Serres, S., Anthony, D.C., Jiang, Y., Campbell, S.J., Broom, K.A., Khrapitchev, A., and Sibson, N.R. (2009). Comparison of MRI signatures in pattern I and II multiple sclerosis models. NMR Biomed *22*, 1014-1024.

Setzu, A., Ffrench-Constant, C., and Franklin, R.J. (2004). CNS axons retain their competence for myelination throughout life. Glia *45*, 307-311.

Sherman, D.L., Fabrizi, C., Gillespie, C.S., and Brophy, P.J. (2001). Specific disruption of a schwann cell dystrophin-related protein complex in a demyelinating neuropathy. Neuron *30*, 677-687.

Sherman, D.L., and Brophy, P.J. (2005). Mechanisms of axon ensheathment and myelin growth. Nat Rev Neurosci *6*, 683-690.

Silber, E., and Sharief, M.K. (1999). Axonal degeneration in the pathogenesis of multiple sclerosis. Journal of the Neurological Sciences *170*, 11-18.

Sim, F.J., Zhao, C., Penderis, J., and Franklin, R.J. (2002). The age-related decrease in CNS remyelination efficiency is attributable to an impairment of both oligodendrocyte progenitor recruitment and differentiation. J Neurosci *22*, 2451-2459.

Simons, M., and Trajkovic, K. (2006). Neuron-glia communication in the control of oligodendrocyte function and myelin biogenesis. J Cell Sci *119*, 4381-4389.

Simons, M., and Trotter, J. (2007). Wrapping it up: the cell biology of myelination. Curr Opin Neurobiol *17*, 533-540.

Singh, H., and Jungalwala, F.B. (1979). The turnover of myelin proteins in adult rat brain. Int J Neurosci *9*, 123-131.

Skoff, R.P., Ghandour, M.S., and Knapp, P.E. (1994). Postmitotic oligodendrocytes generated during postnatal cerebral development are derived from proliferation of immature oligodendrocytes. Glia *12*, 12-23.

Smith, K.J., and Lassmann, H. (2002). The role of nitric oxide in multiple sclerosis. Lancet Neurol *1*, 232-241.

Sobottka, B., Harrer, M.D., Ziegler, U., Fischer, K., Wiendl, H., Hünig, T., Becher, B., and Goebels, N. (2009). Collateral Bystander Damage by Myelin-Directed CD8+ T Cells Causes Axonal Loss. The American Journal of Pathology *175*, 1160-1166.

Song, S.K., Sun, S.W., Ramsbottom, M.J., Chang, C., Russell, J., and Cross, A.H. (2002). Dysmyelination revealed through MRI as increased radial (but unchanged axial) diffusion of water. Neuroimage *17*, 1429-1436.

Song, S.K., Sun, S.W., Ju, W.K., Lin, S.J., Cross, A.H., and Neufeld, A.H. (2003). Diffusion tensor imaging detects and differentiates axon and myelin degeneration in mouse optic nerve after retinal ischemia. Neuroimage *20*, 1714-1722.

Song, S.K., Yoshino, J., Le, T.Q., Lin, S.J., Sun, S.W., Cross, A.H., and Armstrong, R.C. (2005). Demyelination increases radial diffusivity in corpus callosum of mouse brain. Neuroimage *26*, 132-140.

Soriano, P. (1999). Generalized lacZ expression with the ROSA26 Cre reporter strain. Nat Genet *21*, 70-71.

Srinivas, S., Watanabe, T., Lin, C.S., William, C.M., Tanabe, Y., Jessell, T.M., and Costantini, F. (2001). Cre reporter strains produced by targeted insertion of EYFP and ECFP into the ROSA26 locus. BMC Dev Biol *1*, 4.

Sriram, S., and Steiner, I. (2005). Experimental allergic encephalomyelitis: a misleading model of multiple sclerosis. Ann Neurol *58*, 939-945.

Stadelmann, C., Ludwin, S., Tabira, T., Guseo, A., Lucchinetti, C.F., Leel-Ossy, L., Ordinario, A.T., Bruck, W., and Lassmann, H. (2005). Tissue preconditioning may explain concentric lesions in Balo's type of multiple sclerosis. Brain *128*, 979-987.

Stecca, B., Southwood, C.M., Gragerov, A., Kelley, K.A., Friedrich, V.L., Jr., and Gow, A. (2000). The evolution of lipophilin genes from invertebrates to tetrapods: DM-20 cannot replace proteolipid protein in CNS myelin. J Neurosci *20*, 4002-4010.

Sternberg, N., and Hamilton, D. (1981). Bacteriophage P1 site-specific recombination : I. Recombination between loxP sites. Journal of Molecular Biology *150*, 467-486.

Stevens, B., Porta, S., Haak, L.L., Gallo, V., and Fields, R.D. (2002). Adenosine: a neuron-glial transmitter promoting myelination in the CNS in response to action potentials. Neuron *36*, 855-868.

Stidworthy, M.F., Genoud, S., Suter, U., Mantei, N., and Franklin, R.J. (2003). Quantifying the early stages of remyelination following cuprizone-induced demyelination. Brain Pathol *13*, 329-339.

Sun, S.W., Liang, H.F., Trinkaus, K., Cross, A.H., Armstrong, R.C., and Song, S.K. (2006). Noninvasive detection of cuprizone induced axonal damage and demyelination in the mouse corpus callosum. Magn Reson Med *55*, 302-308.

Susuki, K., and Rasband, M.N. (2008). Molecular mechanisms of node of Ranvier formation. Current Opinion in Cell Biology *20*, 616-623.

Suter, U., and Scherer, S.S. (2003). Disease mechanisms in inherited neuropathies. Nat Rev Neurosci *4*, 714-726.

Syed, Y.A., Baer, A.S., Lubec, G., Hoeger, H., Widhalm, G., and Kotter, M.R. (2008). Inhibition of oligodendrocyte precursor cell differentiation by myelin-associated proteins. Neurosurg Focus *24*, E5.

Syed, Y.A., Hand, E., Mobius, W., Zhao, C., Hofer, M., Nave, K.A., and Kotter, M.R. (2011). Inhibition of CNS Remyelination by the Presence of Semaphorin 3A. J Neurosci *31*, 3719-3728.

Tachikawa, M., Fukaya, M., Terasaki, T., Ohtsuki, S., and Watanabe, M. (2004). Distinct cellular expressions of creatine synthetic enzyme GAMT and creatine kinases uCK-Mi and CK-B suggest a novel neuron-glial relationship for brain energy homeostasis. Eur J Neurosci *20*, 144-160.

Takahashi, K., Prinz, M., Stagi, M., Chechneva, O., and Neumann, H. (2007). TREM2-transduced myeloid precursors mediate nervous tissue debris clearance and facilitate recovery in an animal model of multiple sclerosis. PLoS Med *4*, e124.

Targett, M.P., Sussman, J., Scolding, N., O'Leary, M.T., Compston, D.A., and Blakemore, W.F. (1996). Failure to achieve remyelination of demyelinated rat axons following transplantation of glial cells obtained from the adult human brain. Neuropathol Appl Neurobiol *22*, 199-206.

Tauber, H., Waehneldt, T.V., and Neuhoff, V. (1980). Myelination in rabbit optic nerves is accelerated by artificial eye opening. Neurosci Lett *16*, 235-238.

Taveggia, C., Zanazzi, G., Petrylak, A., Yano, H., Rosenbluth, J., Einheber, S., Xu, X., Esper, R.M., Loeb, J.A., Shrager, P., Chao, M.V., Falls, D.L., Role, L., and Salzer, J.L. (2005). Neuregulin-1 type III determines the ensheathment fate of axons. Neuron *47*, 681-694.

Taveggia, C., Feltri, M.L., and Wrabetz, L. (2010). Signals to promote myelin formation and repair. Nat Rev Neurol.

Temple, S., and Raff, M.C. (1986). Clonal analysis of oligodendrocyte development in culture: evidence for a developmental clock that counts cell divisions. Cell *44*, 773-779.

Thorburn, J., Frankel, A.E., and Thorburn, A. (2003). Apoptosis by leukemia cell-targeted diphtheria toxin occurs via receptor-independent activation of Fas-associated death domain protein. Clin Cancer Res *9*, 861-865.

Touil, T., Deloire-Grassin, M.S., Vital, C., Petry, K.G., and Brochet, B. (2001). In vivo damage of CNS myelin and axons induced by peroxynitrite. Neuroreport *12*, 3637-3644.

Trapp, B.D., Nishiyama, A., Cheng, D., and Macklin, W. (1997). Differentiation and death of premyelinating oligodendrocytes in developing rodent brain. J Cell Biol *137*, 459-468.

Trapp, B.D., Peterson, J., Ransohoff, R.M., Rudick, R., Mork, S., and Bo, L. (1998). Axonal transection in the lesions of multiple sclerosis. N Engl J Med *338*, 278-285.

Trapp, B.D., Bo, L., Mork, S., and Chang, A. (1999). Pathogenesis of tissue injury in MS lesions. J Neuroimmunol *98*, 49-56.

Trapp, B.D. (2004). Pathogenesis of multiple sclerosis: the eyes only see what the mind is prepared to comprehend. Ann Neurol *55*, 455-457.

Trapp, B.D., and Nave, K.A. (2008). Multiple sclerosis: an immune or neurodegenerative disorder? Annu Rev Neurosci *31*, 247-269.

Trapp, B.D., and Stys, P.K. (2009). Virtual hypoxia and chronic necrosis of demyelinated axons in multiple sclerosis. Lancet Neurol *8*, 280-291.

Truett, G.E., Heeger, P., Mynatt, R.L., Truett, A.A., Walker, J.A., and Warman, M.L. (2000). Preparation of PCR-quality mouse genomic DNA with hot sodium hydroxide and tris (HotSHOT). Biotechniques *29*, 52, 54.

van Waesberghe, J.H., Kamphorst, W., De Groot, C.J., van Walderveen, M.A., Castelijns, J.A., Ravid, R., Lycklama a Nijeholt, G.J., van der Valk, P., Polman, C.H., Thompson, A.J., and Barkhof, F. (1999). Axonal loss in multiple sclerosis lesions: magnetic resonance imaging insights into substrates of disability. Ann Neurol *46*, 747-754.

van Walderveen, M.A., Barkhof, F., Tas, M.W., Polman, C., Frequin, S.T., Hommes, O.R., Thompson, A.J., and Valk, J. (1998). Patterns of brain magnetic resonance abnormalities on T2-weighted spin echo images in clinical subgroups of multiple sclerosis: a large cross-sectional study. Eur Neurol *40*, 91-98.

Vanderlugt, C.L., and Miller, S.D. (2002). Epitope spreading in immune-mediated diseases: implications for immunotherapy. Nat Rev Immunol *2*, 85-95.

Vargas, M.E., and Barres, B.A. (2007). Why is Wallerian degeneration in the CNS so slow? Annu Rev Neurosci *30*, 153-179.

Vargas, M.E., Watanabe, J., Singh, S.J., Robinson, W.H., and Barres, B.A. (2010). Endogenous antibodies promote rapid myelin clearance and effective axon regeneration after nerve injury. Proc Natl Acad Sci U S A *107*, 11993-11998.

Vickers, J.C., King, A.E., Woodhouse, A., Kirkcaldie, M.T., Staal, J.A., McCormack, G.H., Blizzard, C.A., Musgrove, R.E., Mitew, S., Liu, Y., Chuckowree, J.A., Bibari, O., and Dickson, T.C. (2009). Axonopathy and cytoskeletal disruption in degenerative diseases of the central nervous system. Brain Res Bull *80*, 217-223.

Virchow, R. (1846). Ueber das granulierte Aussehen der Wandungen der Gehirnventrikel. Allg Z Psychiat *3*, 242-250.

Wang, S., Sdrulla, A.D., diSibio, G., Bush, G., Nofziger, D., Hicks, C., Weinmaster, G., and Barres, B.A. (1998). Notch receptor activation inhibits oligodendrocyte differentiation. Neuron *21*, 63-75.

Wang, Z., Colognato, H., and Ffrench-Constant, C. (2007). Contrasting effects of mitogenic growth factors on myelination in neuron-oligodendrocyte co-cultures. Glia *55*, 537-545.

Warf, B.C., Fok-Seang, J., and Miller, R.H. (1991). Evidence for the ventral origin of oligodendrocyte precursors in the rat spinal cord. J Neurosci *11*, 2477-2488.

Waxman, S.G. (2006). Ions, energy and axonal injury: towards a molecular neurology of multiple sclerosis. Trends Mol Med *12*, 192-195.

Wegner, M. (2001). Expression of transcription factors during oligodendroglial development. Microsc Res Tech *52*, 746-752.

Westall, F.C. (2006). Molecular mimicry revisited: gut bacteria and multiple sclerosis. J Clin Microbiol *44*, 2099-2104.

Wilkins, A., and Scolding, N. (2008). Protecting axons in multiple sclerosis. Mult Scler *14*, 1013-1025.

Williams, A., Piaton, G., Aigrot, M.S., Belhadi, A., Theaudin, M., Petermann, F., Thomas, J.L., Zalc, B., and Lubetzki, C. (2007). Semaphorin 3A and 3F: key players in myelin repair in multiple sclerosis? Brain *130*, 2554-2565.

Williams, W.C., 2nd, and Gard, A.L. (1997). In vitro death of jimpy oligodendrocytes: correlation with onset of DM-20/PLP expression and resistance to oligodendrogliotrophic factors. J Neurosci Res *50*, 177-189.

Wolff, S.D., and Balaban, R.S. (1994). Magnetization transfer imaging: practical aspects and clinical applications. Radiology *192*, 593-599.

Wolswijk, G. (1998). Chronic stage multiple sclerosis lesions contain a relatively quiescent population of oligodendrocyte precursor cells. J Neurosci *18*, 601-609.

Wolswijk, G. (2002). Oligodendrocyte precursor cells in the demyelinated multiple sclerosis spinal cord. Brain *125*, 338-349.

Woodruff, R.H., and Franklin, R.J. (1999). Demyelination and remyelination of the caudal cerebellar peduncle of adult rats following stereotaxic injections of lysolecithin, ethidium bromide, and complement/anti-galactocerebroside: a comparative study. Glia *25*, 216-228.

Yakovlev, P.I., and Lecours, A.R. (1967). The Myelogenetic Cycles of Regional Maturation of the Brain. In: A. Minkowski, Editor, Regional Development of the Brain in Early Life. Blackwell, Oxford, 3–70.

Yamaizumi, M., Mekada, E., Uchida, T., and Okada, Y. (1978). One molecule of diphtheria toxin fragment A introduced into a cell can kill the cell. Cell *15*, 245-250.

Yin, X., Crawford, T.O., Griffin, J.W., Tu, P., Lee, V.M., Li, C., Roder, J., and Trapp, B.D. (1998). Myelin-associated glycoprotein is a myelin signal that modulates the caliber of myelinated axons. J Neurosci *18*, 1953-1962.

Yool, D.A., Klugmann, M., McLaughlin, M., Vouyiouklis, D.A., Dimou, L., Barrie, J.A., McCulloch, M.C., Nave, K.A., and Griffiths, I.R. (2001). Myelin proteolipid proteins promote the interaction of oligodendrocytes and axons. J Neurosci Res *63*, 151-164.

Yoshida, M., and Colman, D.R. (1996). Parallel evolution and coexpression of the proteolipid proteins and protein zero in vertebrate myelin. Neuron *16*, 1115-1126.

Zalc, B., Goujet, D., and Colman, D. (2008). The origin of the myelination program in vertebrates. Curr Biol *18*, R511-512.

Zawadzka, M., Rivers, L.E., Fancy, S.P., Zhao, C., Tripathi, R., Jamen, F., Young, K., Goncharevich, A., Pohl, H., Rizzi, M., Rowitch, D.H., Kessaris, N., Suter, U., Richardson, W.D., and Franklin, R.J. (2010). CNS-resident glial progenitor/stem cells produce Schwann cells as well as oligodendrocytes during repair of CNS demyelination. Cell Stem Cell *6*, 578-590.

Zhao, C., Li, W.W., and Franklin, R.J. (2006). Differences in the early inflammatory responses to toxin-induced demyelination are associated with the age-related decline in CNS remyelination. Neurobiol Aging *27*, 1298-1307.

Zivadinov, R. (2007). Can imaging techniques measure neuroprotection and remyelination in multiple sclerosis? Neurology *68*, S72-82; discussion S91-76.

List of figures and tables

List of abbreviations

All abbreviations are also defied in the text upon their first appearance and in the figure legends

ac	anterior commissure
APP	amyloid precursor protein
BBB	blood-brain barrier
bs	brain stem
cb	cerebellum
cc	corpus callosum
CNPase	2'3'-cyclic nucleotide 3'-phosphodiesterase
CNS	central nervous system
Cre	causes recombination protein of bacteriophage P1
CreERT2	fusion protein (Cre and modified estrogen receptor binding domain (ERT2))
Cx32	connexin 32
DT-A	diphtheria toxin fragment A
DTI	diffusion tensor imaging
EAE	experimental autoimmune encephalomyelitis
EF-2	elongation factor 2
experimental mice	TAM-treated, *PLP:CreER/DT-A* double-transgenic mice
FA	fractional anisotropy in DTI
FADD	Fas-associated death domain
fx	frontal cortex
GFAP	glial fibrillary acidic protein
IdU	iodo-deoxyuridine, a thymidine analogue
i.p.	intraperitoneal
i.v.	intravenous
Kv	voltage-gated K^+ channel
$\lambda_{\parallel}$	axial diffusitivity in DTI
$\lambda_{\perp}$	radial diffusitivity in DTI
LFB	luxol fast blue
MAG	myelin-associated glycoprotein
mb	midbrain
MBP	myelin basic protein
MHC	major histocompartibility complex molecule
MOG	myelin oligodendrocyte glycoprotein
MRI	magnetic resonance imaging
MS	multiple sclerosis
MTI	magnetisation transfer imaging

MTR	magnetisation transfer ratio
Nav	voltage-gated Na^+ channel
NF(-M)	neurofilament (M)
NFR	nuclear fast red
NRG	neuregulin
ob	olfactory bulb
OPC	oligodendrocyte precursor cell
PCR	polymerase chain reaction
PDGF-A	platelet-derived growth factor A
PLP	proteolipid protein
PMP22	peripheral myelin protein 22
PNS	peripheral nervous system
PSA-NCAM	polysialated neural cell adhesion molecule
P0	myelin protein zero
ROI	region of interest
SMI32	antibody against non-phosphorylated neurofilament
spc gm/wm	spinal cord grey/white matter
st	striatum
SVZ	subventricular zone
TAM	tamoxifen
TNF	tumour necrosis factor
T2	transverse relaxation time
qT2	quantitative T2 MRI
ΔT2	difference in T2 values between pre- and postUSPIO acquisition
USPIO	ultra small particles of iron oxide
YFP	yellow fluorescent protein

Curriculum vitae

Personal details

name, forename	Pohl, Hartmut Bernd Frederik
nationality	German
birth	December 8, 1977 in Aachen, Germany
marital status	single
current address	Heidwiesen 6, 8051 Zürich, Switzerland; hartmut.pohl@8knut.de

Education

since 07.2005	PhD thesis in the lab of Prof. Dr. U. Suter at the Institute of Cell Biology topic: Characterisation of a Novel Mouse Model for Demyelination part of ZNZ - Neuroscience Zurich Centre graduate school
10.2001-10.2004	Major studies in biology at the ETH Zürich, branch of experimental biology Diploma thesis in the lab of Prof. Dr. U. Suter at the Institute of Cell Biology topic: Functional Studies on Myotubularin-Related Protein 2 Diploma exams in: Cell Biology, Immunology, Microbiology, Anatomy & Physiology, Genetics
10.1998-9.2001	Basic studies in biology at the Ruhr-University Bochum with acquisition of the Vordiplom in biology
1988-1997	High school Schiller-Schule in Bochum with certificate Abitur

Extra-curricular activities

05.2004-12.2004	Scientific under-assistant at the Institute of Cell Biology, ETH Zürich; genotyping and maintenance of laboratory mice
02.2001-04.2002	Part-time employee in field service at Krupp Uhde, Dortmund, Process Department; build up and operation of an chlorine alkali-electrolysis mini-plant-system
1998-2005	Free-lance assistant for the Institute of Material Testing, Ruhr University Bochum and the Euro-Labor GmbH for Damage Analysis and Material Inspection, Bochum; in field sample collection and administration
1997-1998	Community service in the evangelic parish Thomascenter, Bochum
occasionally	Free-lance photographer and author for web-based and print freeski journals; photographic awards: 1st place 2009's powderguide.com photo contest; 2nd place 2010's F-Stop Adventure Sports photo contest; 3rd place 2010's powderguide.com photo contest, category "avalanche"

Acknowledgements

This work would not have been possible without manifold help.

I first want to thank Ueli Suter for initiating and giving me the chance to perform this work, for his supervision, and for providing excellent research conditions. His support was a reliable factor throughout my thesis.

I deeply and lovingly thank Cristina Porcheri. It was the greatest of pleasures to work with her on this project, enjoy together exciting times and ease the hard ones. And it will be.

I also want to thank Markus Rudin for introducing me into the world of MRI physics, his constructive discussions and for being the co-referee of my thesis.

Furthermore, I would like to thank Thomas Mueggler for the excellent collaboration on the MRI project. And for the fun doing it.

I would like to thank Robin Franklin for his enthusiasm, his believe and his input into the project and Dieter Riethmacher for not only providing transgenic mice but also being so curious about what I did to them.

Markus Kulstrunk and Lukas Bachmann –two bright and driven young researchers– deserve my thanks for their collaboration, their enjoyment of it, and the fun and motivation supervising them included.

Cristof Baltes and David Ratering not only tolerated my lack of physical knowledge, they also didn't skip any opportunity to fool me. Thank you for a great collaboration.

A just finite number of people deserve my thanks for precious input, motivation, and being always good company: Ned Mantei for breeding some mice, solving uncounted experimental problems in the blink of an eye, proof-reading the manuscript; Axel Niemann for his scientific input, motivation and humor as well as the help with the mice; Simon Braun for input and proof-reading; Malgorzata Zawadzka for the introduction into surgery and the great collaboration; Mike Peacock for solving miraculous EM problems; Frank Heppner for his introduction into the wonders of pathology; Klaus-Armin Nave for his interest in and his input into the project; Gianluca Civenni; Marcel Ruegg; Dominik Herzog; Konstanze Wagner; Nina Huber; Páris Sidiropoulus; Tina Thurnherr; Yves Benninger; Jorge Pereira; Suzanna Atanasoski; Lukas Sommer; João Relvas; Frédéric Lebrun-Julien; Elisa Tinelli; and all members of the Suter-, Sommer-, Relvas- and Jessberger-group for input and fruitful discussions in- and outside of the field of biology.

Last but not least I would like to thank my parents, Anette and Michael, for whose support I am very grateful.